INVESTIGATION OF COMBINED BIOLOGICAL ROLES OF NEURAMINIDASE 1 AND GM3 SYNTHASE ENZYMES IN GLYCOLIPID METABOLISM

A Thesis Submitted to
The Graduate School of
İzmir Institute of Technology
in Partial Fulfillment of the Requirements for the Degree of

MASTER OF SCIENCE

in Molecular Biology and Genetics

by
Melike CAN

July 2020
İZMİR

ACKNOWLEDGMENTS

First of all, I would like to express my deepest regards and gratitude to my supervisor Prof. Dr. Volkan SEYRANTEPE for his guidance, motivation, support, extensive knowledge in my research and thesis studies.

I am grateful to Prof. Dr. Yiğit UYANIKGİL for his support during histological analysis.

I would like to thank to The Scientific and Technological Research Council of Turkey (TUBITAK) (117Z259) for financial support of the Project and providing me scholarship.

I am also grateful to my co-workers Selin ATEŞ, Berkay DAĞALP and Orhan Kerim İNCİ for their support and kindness during my thesis work. I am grateful to my supportive friends, Tuğçe ŞENGÜL, Hande BASIRLI, Deniz AK for their help, assistance, support and kindness during my researches and thesis work. I especially thank to Seçil AKYILDIZ DEMİR and Zehra Timur KEVSER for her assistance and help during my undergraduate and graduate studies. I am also thankful to undergraduate members of the Seyrantepe Laboratory for their sincere help and kindness.

At last but not least, I thank to my family, my father Adnan CAN, my mother Nilgün CAN, my grandmother Seyide TOKER and my brother Cemal Anıl CAN for their sincere love, motivation, belief and support throughout all my life and education. I am also grateful to Güven ÖZGÜR for his love, understanding, motivation and endless support.

ABSTRACT

INVESTIGATION OF COMBINED BIOLOGICAL ROLES OF NEURAMINIDASE 1 AND GM3 SYNTHASE ENZYMES IN GLYCOLIPID METABOLISM

Gangliosides are sialic acid-containing glycosphingolipids, and commonly expressed in nervous system. GM3 Synthase is responsible for production of GM3 ganglioside known as precursor of a- and b- series gangliosides. Sialidases catalyze removing of sialic acid residues from sialoglycoconjugates and classified based on subcellular localization. Lysosomal Neu1 sialidase is responsible for catabolism of glycolipids, glycoproteins and oligosaccharides. Mutations of lysosomal Neu1 sialidase cause sialidosis and Neu1-/- mice mimic symptoms seen in patients. Glycosphingolipid accumulation in visceral organs of sialidosis patients was notified previously, and it was also reported the GM3 ganglioside as substrate of lysosomal sialidase *in vitro*. However, effect of Neu1 sialidase in the case of complex ganglioside deficiency in brain remains unclear. In the concept of research, we aimed to understand biological role of lysosomal Neu1 sialidase alone and combined with GM3S in ganglioside metabolism *in vivo*. In accordance with this purpose, cortex, cerebellum and thalamus tissues of 2- and 5-month old Neu1-/-GM3S-/-, Neu1-/- and GM3S-/- mice were compared with age-matched control group using molecular biological, histological, immunohistochemistry and behavioral analyses. Alterations in ganglioside metabolism, oligosaccharide pattern and cellular processes (ER-oxidative stress, apoptosis), structural abnormalities, glycoconjugate accumulation, loss of neurons and oligodendrocytes in addition to age dependent behavioral impairments in motor function, memory and muscle strength were demonstrated in single and double knock-out mice. In regard of these results, we have concluded that altered glycosphingolipid metabolism with accumulated secondary metabolites like oligosaccharides affect cellular processes and brain pathology resulting in behavioral abnormalities in age dependent and region specific manner.

ÖZET

NÖROMİNİDAZ 1 VE GM3 SENTAZ ENZİMLERİNİN GLİKOLİPİT METABOLİZMASINDAKİ BİRLEŞİK BİYOLOJİK ROLÜNÜN ARAŞTIRILMASI

Gangliositler, sinir sisteminde yaygın olarak ifade edilen sialik asit içeren glikosifingolipitlerdir. GM3 Synthase a- ve b-serisi gangliositlerin üretimi için öncü olan GM3 gangliositinin üretiminden sorumludur. Sialidazlar, sialoglikokonjugatlardan sialik asit kalıntılarının uzaklaştırılmasını katalizlerler ve hücresel lokalizasyonlarına göre sınıflandırırlar. Lizozomal Neu1 sialidaz glikolipit, glikoprotein ve oligosakkaritlerin katabolizmasından sorumludur. Neu1 sialidaz mutasyonları, sialidoz hastalığına sebep olur ve Neu1 enzim eksikliğine sahip fareler hastalarda görülen semptomları taklit eder. Hastaların Neu1 sialidaz eksikliğine bağlı olarak iç organlarında glikosfingolipit birikimi önceki çalışmalarda gösterilmiş ve *in vitro* olarak lizozomal sialidaz substratının GM3 gangliositi olduğu bildirilmiştir. Fakat Neu1 sialidazının beyinde kompleks gangliositlerin eksikliğindeki rolü bilinmemektedir. Bu araştırmamız kapsamında, lizozomal Neu1 sialidazın tek başına ve GM3S ile birlikte beyindeki glikosfingolipit metabolizması üzerindeki biyolojik etkisini *in vivo* olarak anlamayı amaçladık. Bu amaç doğrultusunda, 2 ve 5 aylık Neu1-/-GM3S-/-, Neu1-/- ve GM3S-/- fare gruplarının korteks, beyincik ve talamus dokuları yaş eşleniği kontrol grubu ile moleküler biyolojik, histolojik, immunohistokimyasal ve davranış deneyleri yapılarak karşılaştırıldı. Glikolipit metabolizması, oligosakkarit paterni, hücresel süreçlerdeki (ER-oksidatif stres ve apoptoz) değişimler, yapısal bozukluklar, glikokonjügat birikimi, nöron ve oligodendrosit sayılarında azalma ve bunlara ek olarak motor fonksiyonunda, hafıza ve kas gücünde hasarlar gibi yaşa bağlı davranışsal bozukluklar tek ve çift gen eksikliğine sahip fare modellerinde gösterilmiştir. Bu sonuçlar doğrultusunda, glikolipit metabolizmasındaki değişiklikler ile birlikte oligosakkarit gibi sekonder metabolitlerin birikimi yaşa ve bölgeye bağlı çeşitli hücresel süreçleri ve beyin patolojisini etkileyip davranışlar bozukluklara sebep olduğu gösterilmiştir.

Dedicated to my precious family…

TABLE OF CONTENTS

LIST OF FIGURES

Figure **Page**

Figure **Page**

Figure **Page**

Figure **Page**

Figure **Page**

Figure **Page**

LIST OF TABLES

Table **Page**

CHAPTER 1

INTRODUCTION

1.1. Glycolipids

Glycolipids are localized at cell membrane and amphiphilic components of the cell membrane (Malhotra, 2012). Glycolipids includes hydrophilic sugar head group and hydrophobic lipid part anchoring into cell membrane. The hydrophobic part of glycolipids can vary such as acyl glycerol, sphingolipid, ceramide, and phenyl phosphate (Malhotra, 2012). The gylcosyl derivatives of lipids, glycolipids, affect the membrane features including fluidity and lipid raft formation (Brandenburg and Holst 2015), (Malhotra, 2012). Furthermore, gangliosides have biological roles such as cell – cell recognition, adhesion, signaling (Brandenburg and Holst 2015).

1.2. Glycosphingolipids

Sphingolipids are glycolipids composed of sphingosine core groups and unsaturated hydrophobic hydrocarbon part (Carter et al. 1947). Sphingolipids are synthesized from endoplasmic reticulum (ER) (Iqbal et al. 2017) and contribute to cellular functions such as signal transduction and cell recognition (Borodzicz et.al. 2015).

Glycosphingolipids are sphingolipids and they include ceramide as hydrophobic lipid moiety linked to sugar residue (Malhotra, 2012). Ceramides can be derived from GlcCer or GalCer that are glucosylceramide or galactosyl ceramide separately. Glycosphingolipids are localized on the outer part of the cell membrane and have significant role for the development, differentiation of nervous system (Olsen and Færgeman 2017). Glycosphingolipids are highly concentrated in the tissues related with central nervous system such as brain (Coet et al. 1998). These lipids are categorized depending on the carbohydrate moiety such as ganglio-, globo-, lacto/neolacto-, and asialo-series (Furukawa et al. 2014).

1.3. Gangliosides

Gangliosides are group of acidic glycosphingolipids and these complex gangliosides includes sialic acid which refers to NANA (Olsen and Færgeman 2017). Therefore, these complex lipids are known as sialylated glycosphingolipids and from the 10-20% of total lipid amount (Xu et al.2010). They are amphipathic molecules consisting of ceramide hydrophobic tail and hydrophilic carbohydrate head group. Similar to glycolipids, they are structural part of plasma membrane and localized at membrane domains such as lipid rafts and they also interact sphingolipids and cholesterol localized at plasma membrane (Sandhoff et al. 2013).

Gangliosides are expressed in most tissues, and they have important functions such as regulation of growth / hormone receptor, signal transduction, cell - cell recognition, adhesion, protein trafficking (Xu et al. 2010). Importantly, they are widely enriched in both glial and neuronal membranes of nervous system, therefore they are essential for differentiation function and development of neurons (Yao et al. 2014).

1.3.1. Production of Gangliosides

Synthesis of ganglioside starts in the Endoplasmic Reticulum (ER) and transferred to the Golgi apparatus for the carbohydrate chain addition (Yu et al. 2011). Complex sphingolipids are produced from ceramide with distinct pathways and ceramide production occurs by de novo synthesis in ER (Olsen and Færgeman 2017). Synthesized ceramide in the ER is delivered to Golgi apparatus and glucosylceramide (GluCer) is produced from the ceramide. When galactose is added to this Glucosylceramide, lactosylceramide (LacCer), an intermediate for the other glycosphingolipid production, is produced (Olsen and Færgeman 2017). Glycosphingolipids are produced when sugar and other chemical groups are added to LacCer with galactosyltransferases, sialyltransferases, N-acetylgalactosamine transferases and GalCer sulfotransferases located in Golgi apparatus (Palmano et al. 2015). Gangliosides are also subgroup of glycosphingolipids and their head groups are produced with several combinations of glucose, galactose, N-acetylglucosamine and sialic acid residues producing diversity among gangliosides (Schengrund 2015).

Glycosyltransferases and galactosyltransferases play role in the ganglioside production. Except GM4 ganglioside (derived from galactosylceramide), nearly all of gangliosides are produced from Lactosylceramide (LacCer). Lactosylceramide synthase (B4Galgt6) is responsible for the lactosylceramide (LacCer) formation (Schengrund, 2015). Lactosylceramide is pioneer for the 0- series of gangliosides that refers to GA2, GA1, GM1b and GD1c in the ganglioside pathway.

GM3 synthase enzyme add a sialic acid residue to LacCer and thereby GM3 ganglioside is produced. GM3 ganglioside is essential for the production of a- series of gangliosides (GM2, GM1, GD1a, GT1a).

GD3 ganglioside which is precursor for the production of b- series (GD2, GD1b, GT1b, GQ1b) gangliosides. b- series (GD2, GD1b, GT1b, GQ1b) are produced with the GD3 synthase enzyme activity with addition of one sialic acid to GM3 ganglioside (Figure 1.1).

STIII enzyme supplies the addition of one sialic acid to GD3 ganglioside. Therefore,STIII catalyzes the production of GT3 from the GD3 gnaglioside. GT3 gnaglioside which is an intermediate for the c- series (GT2, GT1c, GQ1c, GP1c) ganglioside production (Olsen and Færgeman 2017).

N-acetlyglucoseamine residues are added to LacCer, GM3, GD3 and GT3 gangliosides by the β1–4Nacetylgalactosaminyltransferase enzyme (Galgt1) for the production of GA2, GM2, GD2, GT2 gangliosides separately (Figure 1.1) The downstream gangliosides (GA1, GM1, GD1b, and GT1c) are produced with the addition of galactose group by Galactosyltransferase enzyme (B3Galgt4) (Yu et al. 2011).

Sialyltransferase IV (STIV) catalyzes the addition of one sialic acid residue to GA1, GM1, GD1b, and GT1c gangliosides for GM1b, GD1a, GT1b, and GQ1c gangliosides production while Sialyltransferase V (STV) enzyme is responsible for the one sialic acid residue to GM1b, GD1a, GT1b, and GQ1c for GD1c, GT1a, GQ1b, and GP1c gangliosides production (Yu et al. 2011).

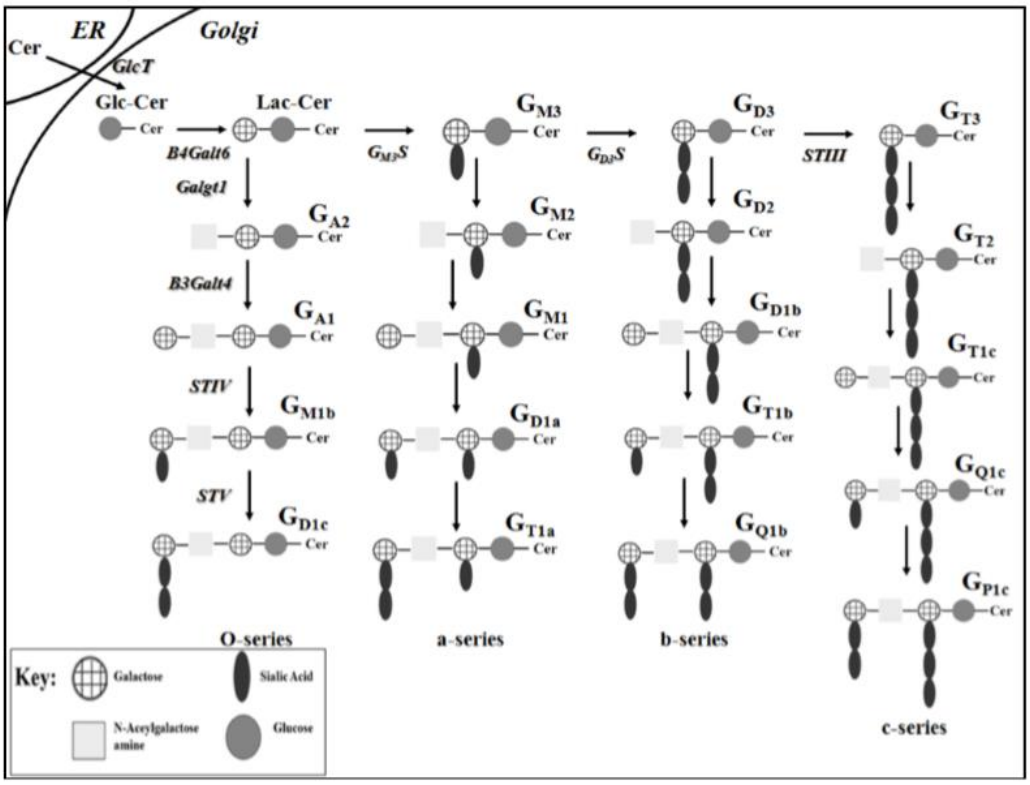

Figure 1.1. The production pathway of gangliosides in human. Ceramide is produced in ER and delivered to Golgi apparatus. GlcCer synthase catalyzes the production of GlcCer from the ceramide. When galactose is added to this Glucosylceramide, lactosylceramide (LacCer), an intermediate for the other glycosphingolipid production, is produced. LacCer, GM3S, GD3S and STIII supply the synthesis of o-, a-, b- and c- series of gangliosides. Monosaccharides are added by Galgt and B3Galgt4 in a stepwise manner and STIV and STV sialylate the terminal Gal residues of gangliosides (by courtesy of Schengrund, 2015 & Olsen and Færgeman 2017).

1.3.2. Degradation of Gangliosides

There is a balance in the production and degradation of gangliosides in a cell. Gangliosides are transferred to lysosomes or acidic part of the cell with endocytosis and they are degraded with help of enzymes, lipids (negatively charged) and activator proteins (Kolter 2012). There are several lysosomal exohydrolases and proteins which are responsible for sequential removal of carbohydrate and sialic acid parts of gangliosides. For instance, galactose residues are removed by β-Galactosidase (β-Gal), glucose residues by β-Glucosidase (GCase), and N-acetylgalactoseamine groups by βHexosaminidase a and b (Hexa, Hexb) (Xu et al. 2010). Sialic acid residues on

gangliosides are also removed by the activity of sialidases (Figure 1.2). Sialidases are enzymes and catalyze the hydrolysis of terminal sialic acid residues of oligosaccharides, glycoproteins and glycolipids (Figure 1.2).

There are four mammalian sialidases and each sialidase shows specificity for the distinct gangliosides (Miyagi et al. 2012).

The production and degradation pathway of gangliosides are different from each other. This difference is derived from the enzymes. Enzymes which are functional for the anabolism of gangliosides are membrane bound while enzymes that responsible for the degradation of gangliosides are soluble in lysosomes. Therefore, activator proteins play role in the catabolism of gangliosides but not in anabolism of gangliosides (Xu et al. 2010).

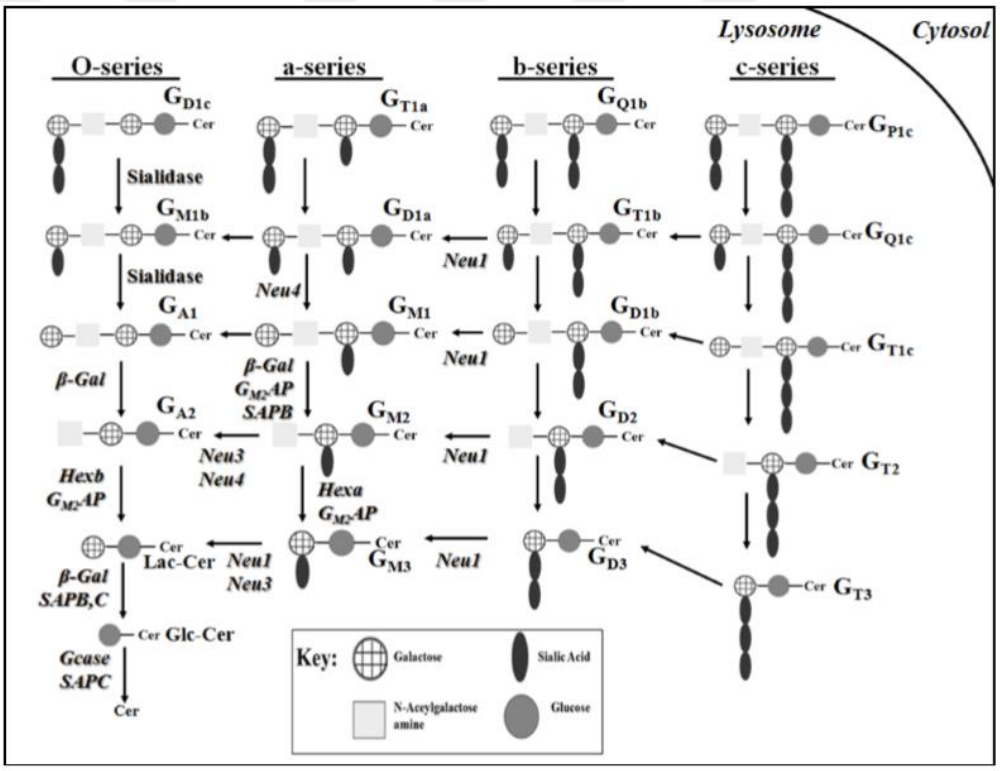

Figure 1.2. The degradation pathway of gangliosides in humans. Gangliosides are transferred to lysosomes or acidic part of the cell with endocytosis and they are degraded by several hydrolases. Sialidases removes the sialic acid parts from the gangliosides. Galactose residues are removed by β-Galactosidase (β-Gal), glucose residues by β-Glucosidase (GCase), and N-acetylgalactoseamine groups by βHexosaminidase a and b (Hexa, Hexb) (by courtesy of Kolter and Sandhoff 2010 & Xu et al. 2010).

1.4. GM3 Synthase (ST3GAL5) Enzyme

GM3 synthase (lactosylceramidealpha-2,3sialyltransferase) enzyme catalyzes the production of complex gangliosides from Lactosylceramide (LacCer) (Simpson et al. 2004). Primary, GM3 synthase enzyme is responsible for the production of GM3 ganglioside, precursor of a -series ganglioside production, from the Lactosylceramide (LacCer) (Olsen and Færgeman 2017). GM3 synthase is the first biosynthetic enzyme for the a-, b-, and c- series gangliosides since GM3 ganglioside is not only essential for a-series ganglioside but also production of GD3 which is precursor for b- series gangliosides (Figure 1.3). However, GM3 synthase enzyme deficiency does not shown any effect for the production of o- series (asialo) ganglioside because the precursor of o-series is LacCer, and GM3 synthase enzyme deficiency does not cause any problem for the production of LacCer ganglioside (Yamashita et al. 2003).

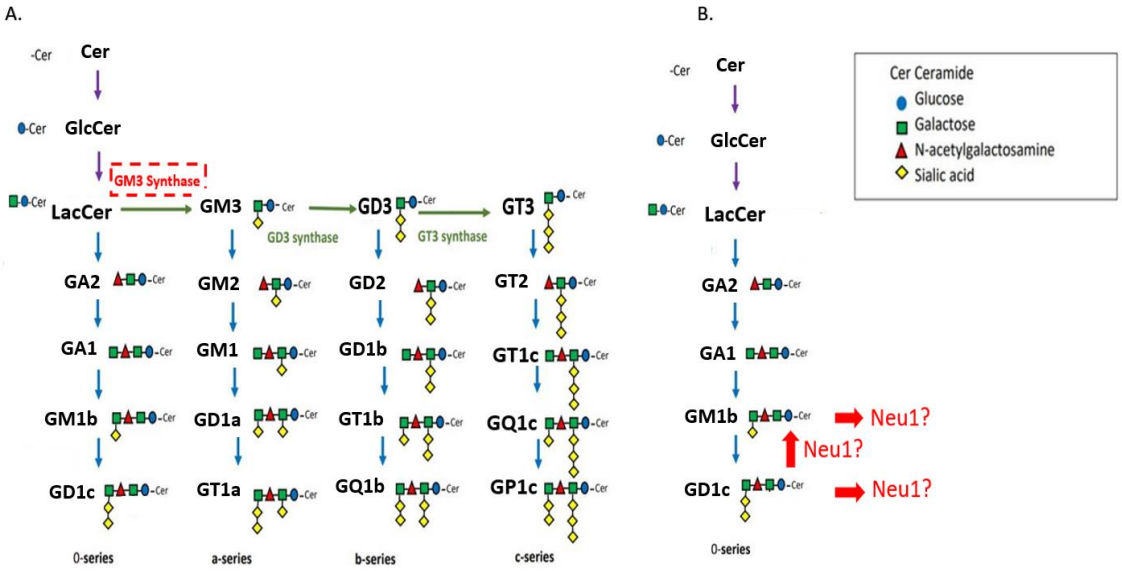

Figure 1.3. Glycosphingolipid synthetic pathway and GM3S role. GlcCer synthase responsible for production of GLcCer from Ceramide. (A) GM3, precursor of a- and b- series gangliosides, is produced by GM3 Synthase enzyme. (B) Potential involment of Neu1 sialidase in the case GM3S deficiency (by courtesy of Daniela et al. 2019).

GM3 ganglioside includes simple oligosaccharide composed of glucose, galactose and sialic acid components (Yamashita et al. 2003). GM3 ganglioside is widely expressed in most tissues and almost all of complex gangliosides are derived from GM3 ganglioside.

GM3 ganglioside plays role in the several processes such as cell death, cell adhesion, mobility, embryogenesis, oncogenesis, cell differentiation and proliferation (Prokazova, et al. 2009). Therefore, the absence of GM3 ganglioside not only affect the complex ganglioside production, but also cause the failure in the various cellular events and processes. GM3 ganglioside are localized at the plasma membrane and form the microdomains (lipid rafts) similar to other gangliosides, but generally GM3 ganglioside constitutes clusters and spread on the human peripheral blood lymphocytes, and the primary ganglioside for monocytes and lymphocytes is the GM3 ganglioside (Kiguchi et al. 1990). Clusters formed by GM3 gangliosides interact with several signal molecules and related receptors, so these clusters regulate the signaling pathways in the cell (Kiguchi et al. 1990). On the other hand, GM3 ganglioside regulates the cell population growth and proliferation. For instance, GM3 ganglioside prolongs the G1 phase for the cell cycle, so it prevents the cell growth (Prokazova, et al. 2009). GM3 ganglioside inhibits the tumor cells by disrupting EGF receptor (its activation is related with many tumor) phosphorylation and dimerization (Prokazova, et al. 2009). On the other hand, GM3 ganglioside participates in the regulation of inflammation, insulin resistance and apoptosis by affecting the tumor necrosis factor- α (TNF-α) expression. GM3 ganglioside is involved in cell adhesion and differentiation processes by increasing the interaction between cells and extracellular matrix, and induction of human polypotent leukemia cell differentiation to monocyte phenotype respectively (Nakamura et al. 1991).

1.4.1. GM3 Synthase Enzyme Deficiency

Simpson et al. 2004 were identified an autosomal recessive infantile onset symptomatic epilepsy syndrome in the eight individuals. Surprisingly, a nonsense mutation which cause the premature termination of GM3 synthase enzyme was characterized in the all examined affected individuals. Symptoms as epilepsy seizure stars in the age of 2 weeks to 3 months in children. The plasma glycosphingolipid analysis by biochemical methods showed that GM3 ganglioside and all derivatives were absent in the individuals affected from the epilepsy syndrome, whereas lactosylceramide and o- series gangliosides were elevated in the eight individuals (Simpson et al. 2004). The eight surviving affected individuals not only showed the epilepsy seizures, but also

developmental problems, intellectual disability, hearing loss and blindness depending on the GM3 synthase enzyme deficiency was indicated (Simpson et al. 2004).

Two children affected from the early-onset refractory epilepsy was shown by Fragaki et al. 2012. The respiratory chain (RC) dysfunction, psychomotor delay, developmental problems, and blindness were shown in affected children. Exome sequencing was revealed the nonsense mutation in the GM3 synthase gene resulted in complete lack of GM3 and its derived products (Fragaki et al. 2012). The decreasing level of mitochondrial membrane potential gave rise to apoptosis in the fibroblasts of affected children compared to control groups depending on the GM3 synthase enzyme deficiency (Fragaki et al. 2012). These results implied that GM3 synthase deficiency is related with epilepsy syndrome as well as respiratory chain (RC) dysfunction.

Phenotypic spectrum depending on GM3 synthase deficiency was shown by Gordon-Lipkin et al. 2018. GM3S deficient patients showed the profound intellectual disability (ID), choreoathetosis, deafness, regression, vision problems and skin abnormalities. Therefore, it was noticed that GM3 synthase deficiency leads to neurodevelopmental disorder (Gordon-Lipkin et al. 2018).

Plasma glycosphingolipid analysis were performed by Aoki et al. 2019, and it was clearly showed that there was accumulation of precursors and alternative glycosphingolipids such as LacCer, Gb3Cer, Gb4Cer due to deficiency of GM3S gene in patients (Aoki et al. 2019).

1.4.2. Mice Models of GM3 Synthase Enzyme Deficiency

Mutant mice, GM3S-/-, were established by Yamashita et al. 2003. Mutant mice could not produce the GM3 ganglioside due to the GM3 synthase deficiency. Although the absence of GM3 and other complex gangliosides (a- and b- series of gangliosides) in the mutant mice, GM3S-/- mice viable without major problems. Mutant mice showed normal life span with fertile ability and there were no significant difference in body weights compared to wild type mice. Brain ganglioside analysis with Thin Layer Chromatography showed the absence of -a and -b series gangliosides such as GM1a, GD1a, GD1a, GD1b and GT1b in GM3S-/- mice (Figure 1.4). However, -o series gangliosides (GM1b and GD1α), that do not require GM3 synthase gene activity, expressed in GM3S-/- mice in order to compensate the absence of -a and -b series

gangliosides (Figure 1.4). Electrospray – ionization tandem mass spectrometry results was also confirmed the expression of -o series gangliosides GM1b, GD1α and also GD1c in GM3S gene deficient mice brain (Yamashita et al. 2003). Surprisingly, GM3S-/- mice displayed enhanced sensitivity to insulin and these mutant mice were avoided from the high fat diet induced insulin resistance (Yamashita et al. 2003). These results revealed that insulin signaling pathway is regulated by GM3 ganglioside negatively, and this makes it therapeutic agent for diabetes (Type 2) (Yamashita et al. 2003).

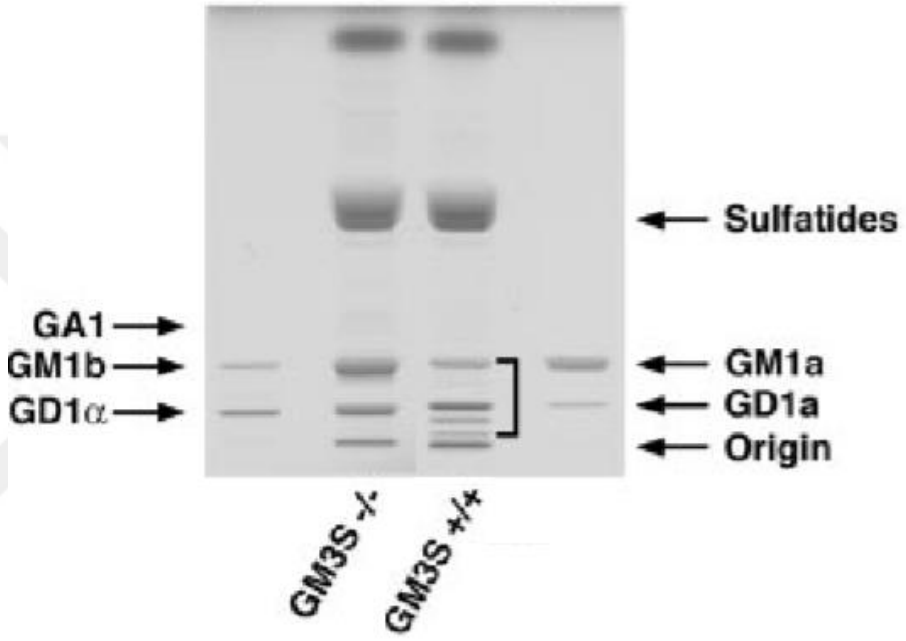

Figure 1.4. Gangliosides isolated from brain of GM3S-/- and GM3S+/+ mice. Major gangliosides such as GM1a, GD1a, GD1b and GT1b are present in wild-type mice. -o series gangliosides (GM1b and GD1α) are shown in GM3S-/- mice (by courtesy of Yamashita et al. 2003).

In GM3 synthase null mice, deformation of hair cell in Corti organ resulted in hear disability was illustrated (Yoshikawa et al. 2009). Thin layer chromatography of acidic gangliosides isolated from inner ear of the age of 6 – 8-week mice indicated highly expressed o- series of gangliosides such as GM1b, GD1α in order to compensate the absence of a- and b- series of gangliosides. Neutral gangliosides were also analyzed and the expression of lactosylceramide (LacCer) was shown in only GM3S-/- mice, indicating blockage in the LacCer to GM3 conversion, while no expression was identified in GM3S+/+ and GM3S+/- mice for LacCer. Although the presence of hearing loss, there

was no any disability in motor functions according to rotarod test results (Yoshikawa et al. 2009).

Several gangliosides including GD1a (-a series) and GT1b (-b series) are essential gangliosides for the axon-myelin interactions and myelination process of neurons (Schnaar 2010). GM3S deficient mice did not have expression of -a and -b series gangliosides, although -o series gangliosides such as GM1b and GD1α are accumulated in GM3S-/- mice. Interestingly, GM3S synthase deficient mice did not have obvious axon-myelin defects although GD1a and GT1b are absent in GM3S knock-out mice (Schnaar 2010). It was suggested that cisGM1 (GM1b) and GD1α prevents the significant demyelination and axon-myelin defects in GM3S-/- mice (Schnaar 2010).

The absence of GM3 synthase gene in mice caused some neuropsychological symptoms such as hyperactivity and anxiety. GM3S-/- mice at 6-weeks of age showed anxiety and higher motor activity compared to control group (Niimi et al. 2011).

GM3 ganglioside is a regulator for the inflammation and it prevents the immune responses. Cartilage damage and bone destruction was notified depending on the inflammation response in GM3S knock-out mice, thereby rheumatoid arthritis known as autoimmune disease was shown in GM3S-/-mice (Geboes et al. 2009). Significantly elevated inflammation level resulted in cartilage problems and bone destruction was displayed in the age of 4 -month-old GM3S-/- mice (Sasazawa et al. 2014). The cartilage explants from 4 -month-old GM3S-/- mice demonstrated higher level of apoptosis compared to control groups, thereby showing regulator role of GM3 ganglioside for apoptosis (Sasazawa et al. 2014).

The GM3 role in visual function in mice was investigated by Hiraoka et al. 2019. The ganglioside profile isolated from retinas of ST3GAL5-/- (GM3S-/-) mice demonstrated lack of GM3 ganglioside and -a and -b series gangliosides, but accumulation of LacCer, precursor of GM3 ganglioside, and -o series gangliosides (GM1b and GD1α) were observed in ST3GAL5-/- mice (Hiraoka et al. 2019). Although visual impairment is seen in GM3S deficient humans, optic nerve atrophy and visual problem was not seen in older ST3GAL5-/- mice eyes (Hiraoka et al. 2019).

1.4. Sialidases

Sialidases (Neuraminidases) are glycohydrolytic enzymes that catalyze the removing of α-glycosidically linked sialic acid residues from the oligosaccharides, glycoproteins, glycolipids, gangliosides (Saito and Sugiyama 2002) These sialidases have important functions including cell proliferation, cell adhesion, differentiation and receptor alterations in addition to degradation of glycoconjugates such as gangliosides. (Miyagi et al. 2012).

There are four mammalian sialidases and these sialidases are encoded by various genes such as Neu1, Neu1, Neu3 and Neu4 (Table 1.1). Sialidases are classified depending on the subcellular localization. Subcellular localization can be lysosomal (Neu1) (Miyagi and Tsuiki 1985), cytosolic (Neu2) (Seyrantepe et al. 2004), plasma membrane associated (Neu3) (Miyagi 1990) or mitochondrial (Neu4) (Yamaguchi et al. 2005). In addition to subcellular localization, substrate specificity and immunological features of sialidases are different from each other (Miyagi 1990).

Neu1 sialidase is located in the lysosomes and responsible for the degradation, catabolism of sialoglycoconjugates in lysosomes (Frisch et al. 1979). Substrates for the Neu1 sialidase is oligosaccharides and glycopeptides (Schneider et al. 1991).

Neu2 sialidase (Neuraminidase 2) is localized in the cytosol and it has affinity for the gangliosides, oligosaccharides and glycoproteins. It was noted that Neu2 shows its activity for the GM3 ganglioside (Miyagi and Yamaguchi 2012).

Neu3 sialidase (Neuraminidase 3) is located at plasma membrane and it is an integral membrane protein. Ganglioside oligosaccharide chains are modulated by Neu3 sialidase and these alterations on oligosaccharide chains affect the cell adhesion, differentiation, apoptosis, carcinogenesis and some signaling pathway as insulin signaling (Miyagi and Yamaguchi 2012). This sialidase has activity for the gangliosides such as GM1, GD1a, de-sialylates, GM2 and GM3 gangliosides (Miyagi and Yamaguchi 2012).

Neu4 sialidase (Neuraminidase 4) is found in the inner and outer membranes of mitochondria (Yamaguchi et al. 2005) and lysosomal lumen (Seyrantepe et al. 2004). It has affinity for the oligosaccharides and glycoproteins. Mitochondrial associated Neu4 play role in the apoptosis, neural differentiation. This sialidase shows its activity for GM2 and GD1a (Seyrantepe et al. 2008).

Table 1.1. Properties of human sialidases (by courtesy of Momti et al. 2002).

	NEU1	NEU2	NEU3	NEU4
Cellular Localization	Lysosome	Cytosol Nucleus	Plasma membrane	Lysosome Intracellular membrane Mitochondria
Substrate Preference	Oligosaccharides 4MU-Neu5Ac[1]	Glycoproteins Oligosaccharides Gangliosides 4MU-Neu5Ac	Gangliosides	Glycoproteins Oligosaccharides Gangliosides 4MU-Neu5Ac
Optimal pH	4.4-4.6	6.0-6.5	4.6-4.8	4.4-4.5
Deduced Functions/ Processes Involved	Lysosomal catabolism Immune response	Myogenesis	Tumorigenesis Neuronal differentiation	Lysosomal catabolism Neuronal differentiation
Genomic Location	6p21.31	2p37.1	11q13.4	2p37.3

1.5.1. Neu1 (Neuraminidase 1) Sialidase

Sialidase Neu1 (Neuraminidase 1) is localized in the lysosome of the cell. In the 1990s, the human Neu1 gene was established and it was clarified that Neu1 gene encodes a protein including 145 aminoacids (Pshezhetsky et al. 1997). Neu1 gene was found on chromosome 6 (6p21.3) in human (Pshezhetsky et al. 1997), whereas it is located on the chromosome 17 in the mouse (Frisch et al. 1979). Although the human Neu1 gene is expressed in whole tissues, it is widely expressed in the pancreas and also there is lesser expression in brain (Bonten et al. 1996). The expression of the Neu1 gene is variable in the mouse but it is most commonly expressed in the pancreas, kidney later in the brain, spinal cord and other tissues such as heart, liver, spleen, lung (Igdoura et al. 1998).

Neu1 sialidase is responsible for the degradation, catabolism of sialoglycoconjugates in lysosomes (Frisch et al. 1979). Substrates for the Neu1 sialidase is oligosaccharides and glycopeptides. However, it was reported that Neu1 sialidase may assigned in the catabolism of glycolipids (Schneider et al. 1991).

Neu1 sialidase enzyme forms a complex with βgalactosidase (β-Gal) and lysosomal protective protein Cathepsin A (PPCA) (Horst et al. 1989). The protective protein Cathepsin A supplies the glycosidase stabilization and the deficiency of PPCA activity causes the galactosialidosis known as a lysosomal storage disorder (D'Azzo et al. 1996).

Neu1 sialidase enzyme has regulator effect on the immune response in addition to catabolism of sialoglycoconjugates. Surprisingly, it was noted that of IFN-γ expression is prevented in the case of deficiency of Neu1 sialidase activity (Nan et al. 2007). Additionally, Neu1 sialidase activity supplies the production of Th2 cytokines, Toll like receptor activation (Chen et al. 2014). In another process, it was reported that complex formed by PPCA and Neu1 have a task for tropoelastin secretion, and Neu1 sialidase in the complex supplies the releasing of tropoelastin for the elastic fibers formation (Hinek et al. 2006). The negative correlation between Neu1 sialidase activity and metastatic capacity of cancer cells was also implied previously (Uemura et al. 2009). Together, the lower Neu1 sialidase activity resulted in higher levels of GM3 ganglioside in mouse carcinoma cells (Miyagi and Yamaguchi 2012). It was also reported that lysosomal substrate is GM3 ganglioside *in vitro* (Fingerhut et al. 1992), however in a recent study it was shown that GM3 ganglioside accumulation does not occur in all cell types in the case of Neu1 deficiency (Aerts et al. 2019). Additionally, it was claimed that Neu3 and Neu4 sialidases have more potential role for GM3 ganglioside catabolism in the mouse brain (Pan et al. 2016). However, the effect of Neu1 deficiency on brain gangliosides in brain remains unclear (Breiden and Sandhoff 2020).

1.6. Lysosomal Storage Diseases

Lysosomal storage diseases (LSDs) are rare hereditary metabolic disorders due to several gene mutations. These mutations are inherited in autosomal recessive manner, but X-linked inheritance is also seen (Platt et al. 2012). Especially, impairment in lysosomal degradation pathway of biomolecules causes lysosomal storage disorders (Plomp et al. 2009). Deficiency of several enzymes in lysosomes due to gene mutations lead impairment of lysosomal degradation pathway. These enzymes may have hydrolysis activity or can be a protein that plays role in post- translational modification, hydrolase activation or transportation of a lysosomal protein (Neufeld 1991; Tardy et al. 2004). Due to absence of several enzymes located in lysosomes, accumulation of noncatabolized substrates or biomolecules including glycoproteins, glycosaminoglycans, gangliosides, sphingolipids, glycosphingolipids and other lipids in the lysosomes was shown and this abnormal accumulation causes the cellular toxicity (Ferreira and Gahl 2017).

Accumulation of substrates reflects the storage and this storage is progressive. Storage affects distinct systems and cell types such as reticuloendothelial system, nervous system, eye, muscle, etc. (Boustany 2013). Patients who suffer from lysosomal storage disorders can show mild or severe phenotype depending on accumulation. Actually, enzyme activity determines the accumulated level of substrates. If enzyme activity decreases dramatically, more substance accumulates and severe phenotype is seen in earlier ages (Conzelmann and Sandhoff 1983). Structural and histological alterations are seen in patients suffering from the lysosomal storage disorders owing to progressive noncatabolized substrate accumulation. Structural alterations can be vacuole formation, and these vacuoles include noncatabolized biomolecules. For instance, storage bodies is seen in Tay-Sachs disease which is a lysosomal storage disorder (Tourtellotte 1965). Additionally, secondary changes are also observed in the lysosomal storage disorders in the case of lysosomal hydrolase deficiency. Intermediate metabolites such as oligosaccharides, glycoaminoacids may accumulates in urines of patients and intermediate metabolite accumulation is used as diagnosis for patients (Xia et al. 20013).

1.6.1. Sialidosis

The deficiency of Neu1 sialidase causes a systematic disease known as sialidosis. Sialidosis is an autosomal recessive lysosomal storage disorder. The accumulation of sialylated oligosaccharides in tissues and extraction of accumulated substance in urines or body fluids is mostly common indicator of the sialidosis disease (Pelt et al. 1988). There two clinical variants of the sialidosis depending on severity and age of onset (Seyrantepe et al. 2003). Type I and Type II are the clinical variants of this disease.

Type I refers to mild form (cherry- red- spot myoclonus) and symptoms are observed in the second or third decade of life. Myoclonus and progressive vision impairment are the common symptoms of Type I sialidosis (d'Azzo et al. 2015). Patients may remain intellectually normal, but the voluntary movement problems, tremors, generalized seizures, vacuolated lymphocytes in peripheral blood and swollen lysosomes in the Kupffer cells of liver are observed in the Type I patients (d'Azzo et al. 2015). The accumulation of oligosaccharides in neurons of central nervous system (CNS) was notified in the brain biopsy of Type I sialidosis patients (Sekijima et al. 2013).

Type II sialidosis is the severe variant of the disease and its onset at birth or early infancy. The distinct mutations (more than 30 mutations) such as nonsense, missense mutations, deletions or insertions cause the severe type of sialidosis (Seyrantepe et al. 2003). Several lipids such as GM3, GD3, GM4 and LM1 accumulates in the visceral organs of patients, but accumulation of these glycolipids has not been detected the brains of patients (Breiden and Sandhoff 2020). Mental retardation, neurological problems, coarse face, spleen and liver enlargement, vertebral deformities, hearing loss are the known symptoms of this clinical variant (d'Azzo et al. 2015). Life span of patients may show diversity depending on the type and number of mutations on Neu1 gene.

1.6.2. Mice Models of Neu1 (Neuraminidase I) Sialidase Deficiency

Mice nullizygous at Neu1 locus was created by d'Azzo at al., 2002 in order to enlight the roles of neuraminidase 1 in physiological pathways. These mice mimics the manifestations seen in the patients suffering from early onset of sialidosis (Type II), and complete loss of Neu1 gene in mice caused the several symptoms including nephropathy, neurological impairment, edema, spleen enlargement, urinary extraction of oligosaccharides, deformity of spine and hematopoiesis (d'Azzo et al. 2002). 1-month-old Neu1-/- mice had smaller size compared to age matched WT mice. Ballooned epithelial cells are seen in eyes of 5 -month-old Neu1-/-mice and vacuolation is observed in epithelial cells of kidney sections according to H&E staining results (Figure 1.5). Additionally, H&E histological analysis revealed the presence of ballooning of Kupffer cells in liver sections of 5 -month-old Neu1-/- mice and vacuolation of apical epithelial cells of the intestinal villi in 3 weeks old Neu1-/- mice (d'Azzo et al. 2002). Life span was between the 8 and 12 months in Neu1-/- mice and mice stopped the producing offspring at the age of 10 weeks (d'Azzo et al. 2002).

In the Neu1-/- brain, it was noted that extensive vacuolization in the epithelial cells (de Geest et al. 2002). The mostly affected cells were microglia and macrophages resulted in neurodegeneration in the especially dendrite gyrus and hippocampus region of the Neu1-/- mice. Storage of microglia and macrophages (indicator of neuroinflammation) in brain parenchyma, dendrite gyrus impairments were also seen in 5-month-old sialidosis mice (de Geest et al. 2002).

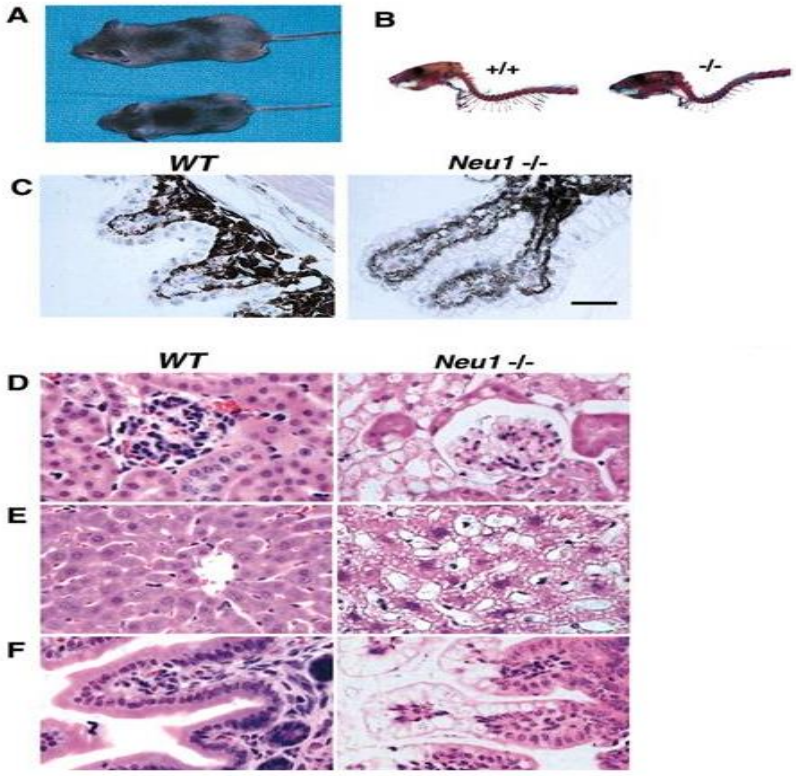

Figure 1.5. Clinical and histopathological phenotype of Neu1-/- mice. 1 -month-old Neu1-/- mice are smaller compared to age matched WT mice (A). Curvature cervical spine is shown in 5 -month-old Neu1-/- mice with skeletal staining while no curvature cervical spine is observed in age matched WT littermates (B). Ballooned epithelial cells are seen in eyes of 5 -month-old Neu1-/-mice (C). Vacuolation is observed in epithelial cells of kidney sections of 5 -month-old Neu1-/- mice by using H&E staining (D). Ballooning of Kupffer cells in liver sections of 5 -month-old Neu1-/- mice by using H&E staining (E). Vacuolation of apical epithelial cells of the intestinal villi is detected in 3 weeks old Neu1-/- mice by using H&E staining (by courtesy of d'Azzo et al. 2002).

The deficiency of Neu1 gene causes the accumulation of sialylated lysosomal protein known as LAMP-1 which leads to lysosomal exocytosis (Yogalingam et al. 2008). In order to understand the role of LAMP-1 for the exocytosis, LAMP-1 was silenced and it was implied that lysosomal exocytosis returned to the normal levels. Therefore, it was proven that LAMP-1 is associated with the exocytosis. The regulation effect of Neu1 gene on the LAMP-1 was also showed that Neu1 gene regulates the lysosomal exocytosis negatively since deficiency of Neu1 leads to enhanced lysosomal exocytosis (Yogalingam et al. 2008). Surprisingly, increased level of lysosomal exocytosis due to lack of Neu1

gene gave rise to hematopoiesis and degradation of cell adhesion molecules, so it is clear that the phenotypic alterations in sialidosis can be affected by the exacerbated cellular processes (lysosomal exocytosis) instead of impairment of processes.

Muscle atrophy seen in Type II sialidosis patients was also shown in the Neu1-/- mice owing to alteration in the connective tissues. Interestingly, muscle atrophy was explained by the excessive lysosomal exocytosis derived from the highly sialylated LAMP-1. Infiltration and degeneration of muscle fibers happened by the excessive level of lysosomal exocytosis in Neu1-/- mice at 4 months of age (Zanoteli et al. 2010). In addition to muscle degeneration, exacerbated lysosomal exocytosis provoked the hearing loss by causing impairment in the sound transduction in Neu1-/- mice (Wu et al. 2010). Surprisingly, Annunziata et al. 2013 indicated Alzheimer's disease like amyloidogenic process in Neu1-/- mice. The accumulation of oversialylated amyloid precursor protein in lysosomes and the releasing of accumulated Aβ-peptides by exacerbated lysosomal exocytosis was shown in Neu1-/- mice (Annunziata et al. 2013). Additionally, in Neu1-/- mice, the reduction of accumulated β-amyloid plaques with cerebral injection of Neu1 was considered that Neu1 may have therapeutic effect for Alzheimer's disease (Annunziata et al. 2013). In macrophages, phagocytosis regulation by Neu1 has been described and the exogenous Neu1 gene reduced the sialylated proteins and repaired phagocytic activity of macrophages (Seyrantepe et al.2010).

When CathAS190A–Neo mice with secondary Neu1 deficiency were fed with high fat diet (HFD), these mice groups showed glucose intolerance and insulin resistance (Dridi et al. 2013). Although production of insulin in CathAS190A–Neo mice is normal, reduction in insulin sensitivity was demonstrated in this mice groups. Additionally, impairment in the insulin signaling pathway was demonstrated in fibroblasts derived from patients, implying Neu1 role in the insulin signaling pathway (Dridi et al. 2013). It was implied that the insulin receptor kinase (IRK) remains to oversialylated when the Neu1 is absent, therefore insulin tyrosine kinase (IRK) is a target of Neu1 (Dridi et al. 2013).

1.7. The Aim of The Study

GM3 Synthase is enzyme for production GM3 ganglioside which is the first biosynthetic enzyme for a- and b-series gangliosides (Olsen and Færgeman 2017). Sialidases, neuraminidases, are also enzymes which supply the removing of sialic acid

residues from sialoglycoconjugates (Saito and Sugiyama 2002). Neu1 sialidase located in lysosomes is responsible for the degradation and catabolism of sialoglycoconjugates (Frisch and Neufeld 1979), and this enzyme forms a complex with βgalactosidase (β-Gal) and lysosomal protective protein Cathepsin A (PPCA) (Horst et al. 1989). The accumulation of glycolipids such as GM3, GD3, GM4 and LM1 in visceral organs of sialidosis patients due to Neu1 sialidase deficiency was notified previously (Breiden and Sandhoff. 2020), and it was also reported the GM3 ganglioside as substrate of lysosomal sialidase *in vitro* (Fingerhut et al. 1992). However, the effect of Neu1 deficiency on complex gangliosides, and glycolipid metabolism *in vivo,* remains unknown. In this thesis study, we aimed to understand the biological role of lysosomal Neu1 sialidase alone and combined with GM3S in glycosphingolipid and gangliosides including sialic acid residues *in vivo*. Newly generated Neu1-/-GM3S-/- mice model and existing Neu1-/- mice were compared to existing WT and single gene deficient counterparts and thereby effects of lysosomal Neu1 sialidase and GM3S enzyme on glycosphingolipid metabolism was goaled to understood in brain. In accordance with this purpose, molecular biological, histopathological and behavioral analysis were carried out. All in all, analyses allow us further investigation of lysosomal sialidase (Neu1) role and combined biological roles of Neu1 and GM3 synthase enzymes in glycosphingolipid metabolism, cellular events and behavioral tests.

CHAPTER 2

MATERIALS AND METHODS

2.1. Animals

GM3S gene knockout mice (GM3S-/-) were donated by Prof. Dr. Roger Sandhoff (Technical University of Applied Sciences in Mannheim, Germany), while Neu1 gene knockout mice (Neu1-/-) were present in the laboratory of Dr. Alessandra d'Azzo (Genetics Department of St. Jude Children's Research Hospital, ABD) and donated by her to our laboratory. The Neu-/- mice were brought to Turkey. Mice were placed in Izmir Institute of Technology Animal Research Center. Breeding and housing of mice were applied in cages which have maximum five mice. Their maintenance were supplied at constant temperature and humidity with 12- hour light:dark cycle. In cages, water and food was present and there was no any restriction to get water and food, so feeding was ad libitum. Animal experiments were approved by the Institutional Animal Care and Use Committee of Izmir Institute of Technology, then all experiments were applied in accordance with the Turkish Institute of Animal Health guide that includes the usage procedure of animals as laboratory animals.

Two female mice (Neu1+/-) were crossed with a male mouse (GM3S-/-), and heterozygous female and male mice (Neu1+/-GM3S+/-) were obtained (Figure 2.1). The obtained 8 heterozygous female and 4 heterozygous male mice were used in order to obtain female and male WT, Neu1-/-, GM3S-/-, and Neu1-/-GM3S-/- mice. Additionally, obtained WT female and male mice from heterozygous breedings were also crossed in order to obtain only WT offspring. The Neu1-/- mice were obtained by the crossing of female Neu1+/-GM3S+/+ mice and male Neu1+/-GM3S+/+ mice of F2 generation because Neu1-/- mice were infertile (d'Azzo et al. 2002). Female Neu1+/+GM3S-/- mice was also crossed with male Neu1+/+GM3S-/- mice to get only GM3S gene deficient (GM3S-/-) mice. Lastly, the double knock-out (Neu1-/-GM3S-/-) mice was generated by the crossing of female Neu1+/-GM3S-/- mice with male Neu1+/-GM3S-/- mice.

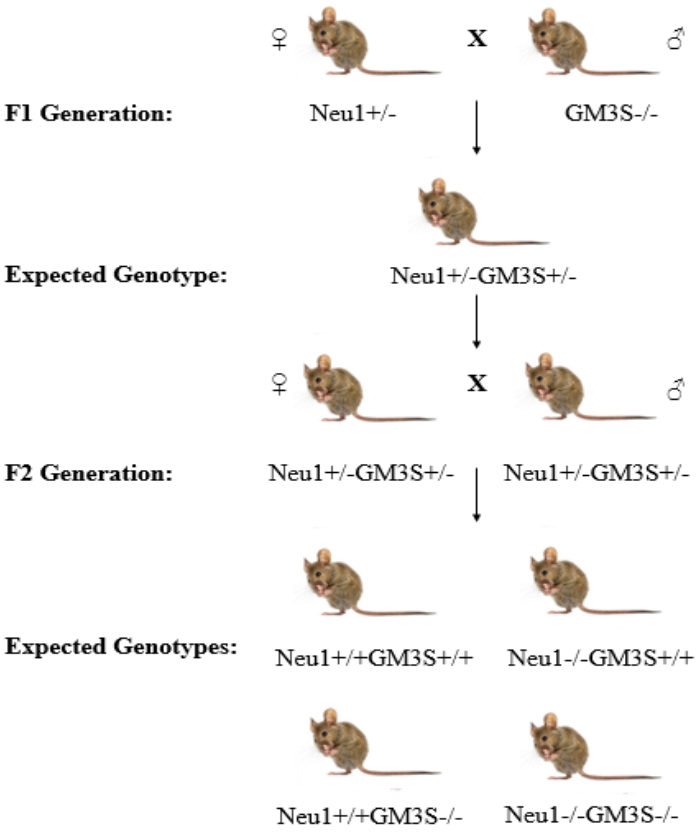

Figure 2.1. Representative crossing scheme of Neu1 and GM3S mice.

2.2. Mouse Genotyping

Mouse genotyping was done after mice were weaned from their parents at 1-month-old age. Mouse tails were used for DNA isolation to determine the genotypes of weaned mice. DNAs that are taken from mice were incubated in shaking incubator (70rpm) at 55ºC for overnight in Eppendorf tubes consisting of 500 µl Lysis Buffer (10% 1M Tris pH 7.6, 2.5% 0.2M EDTA, 20% SDS, 4% 5M NaCl) and 12 µl Proteinase K (25µg/µl, Sigma- Aldrich, Germany). Following day samples were centrifugated at 13000 rpm for 10 minutes. After centrifugation process, supernatant parts of samples were transferred into new Eppendorf tubes and equal volume of 100% isopropanol was added to samples for precipitation. Samples were shaked for several times to precipitate DNAs. Then, precipitated DNAs were taken with help of tip and transferred into new Eppendorf tubes including 500 µl of 70% ethanol for purification. Samples were centrifugated at 15000 rpm for 1 minutes and supernatant parts of samples were removed. Remaining ethanol was air-dried by incubating samples at room temperature for 10 – 15 minutes.

After removal of ethanol, 100 µl of ultrapure water was added to samples to dissolve DNAs and samples were incubated in incubator at 55ºC for 1 hour.

2.2.1. Genotyping of Mice for Neu1 Allele

Isolated DNAs were used for genotyping of Neu1 allele with PCR protocol. About 100 ng of DNAs were used for PCR. For PCR protocol, reaction mix was total 50 µl and reaction mix includes 0.4 µM of each forward primer (Table 2.2), 0.4 µM reverse primer (Table 2.2), 0.4 mM dNTP, 10X PCR buffer including 2mM $MgCI_2$ (GeneDireX), 1.25 units of Taq polymerase (GeneDireX). The PCR conditions for Neu1 allele were as follows: 3 minutes at 94℃; 30 seconds at 94℃ (30 cycles), 30 seconds at 58.1℃ (30 cycles); 2 minutes at 72℃; and 10 minutes at 72℃.

Table 2.1. Primer sequences and product sizes used for genotyping of Neu1 allele.

Gene	Primer	Primer Sequence	Product Size
Neu1	MNTG-1 Forward	5'-GACAGGGATCGCCGGGAGCTATGG-3'	WT Allele 180 bp KO Allele 400 bp
	MNTG-2 Forward	5'-CACCAGGCTGAAGTCATCCTCTGC-3'	
	LacZ Reverse	5'-GATAGGTTACGTTGGTGTAGATGGGCG -3'	

2.2.2. Genotyping of Mice for GM3S Allele

PCR reaction was performed for genotyping of GM3S alleles with about 100 ng genomic DNA. Reaction mixture was 25 µl for WT (wild type) allele genotyping and mixture consists of 0.4 µM forward primer (Table 2.3), 0.4 µM reverse primer (Table 2.3), 0.8 mM dNTP, 3 mM $MgCI_2$, 10X PCR buffer including 2mM $MgCI_2$ (GeneDireX), 5 units of Taq polymerase (GeneDireX). The PCR conditions for GM3S WT allele were as follows: 5 minutes at 95℃; 30 seconds at 95℃ (30 cycles), 45 seconds at 56℃ (30 cycles); 1 minutes at 72℃; and 5 minutes at 72℃.

Reaction mixture was 50 µl for KO (knock-out) allele genotyping and mixture consists of 0.4 µM forward primer, 0.4µM reverse primer, 0.4 mM dNTP,10X PCR buffer including 2mM $MgCI_2$ (GeneDireX), 2.5 units of Taq polymerase (GeneDireX). The PCR

conditions for GM3S KO allele were as follows: 3 minutes at 94℃; 30 seconds at 94℃ (30 cycles), 1 minutes at 56℃ (30 cycles); 2 minutes at 72℃; and 5 minutes at 72℃.

Table 2.2. Primer sequences and product sizes used for genotyping of GM3S allele.

Gene	Primer	Primer Sequence	Product Size
GM3S WT Allele	GM3S Forward (WT1)	5'-AGCTCAGAGCTATGCTCAGGA-3'	WT Allele 400 bp
	GM3S Reverse (WT2)	5'-TCACACATCGAACTGGTTGAG-3'	
GM3S KO Allele	GM3S Forward (KO3)	5'-GAGCCTGTGCCACACATCT-3'	KO Allele 907 bp
	GM3S Reverse (KO4)	5'-TCGCCTTCTTGACGAGTTCTTCTGAG-3'	

2.3. Body Weight Measurement

In order to understand the body weight changes depending on the genotypes, body weight measurement was done for each mouse. Each mouse was put on a beaker and beaker including mouse was placed on a balance. Weight of each mouse was recorded by balance. Beaker mass was also weighed, and its mass was used as a blank in order to record the exact weight of each mouse. Weight measurement for each mice group was done for fortnightly. 15 independent mice for each group was used.

2.4. Tissue Handling

Brain dissection and fixation was done for the 2- and 5-month-old WT, Neu1-/-, GM3S-/- and Neu1-/-GM3S-/- mice. Brain samples were used in biochemical and histological analysis.

2.4.1. Brain Dissection

Brain samples were collected by brain dissection for biochemical analyzes. 2- and 5-month-old WT, Neu1-/-, GM3S-/- and Neu1-/-GM3S-/- mice were placed to CO_2

cabinet and scarified in it. Brain were removed and brain sections were separated as cortex, cerebellum and thalamus with dissector blade. Dissected brains were snap frozen with liquid nitrogen, then samples were placed in the -80^{o}C freezer until used.

2.4.2. Fixation

Fixed brains were used for histological analysis. Firstly, mice were anesthetized with ksilazol and basilazin chemicals by intraperitoneal injection. After the mice became pale, they lay on their back and immobilized. Then, mice were fixed with tape and an incision was made from abdomen. Rib cage was cut and thoracic cavity was opened. After the thoracic cavity was opened, heart was allowed to exposed and right atrium was cut with sharp scissors. Needle was placed in the left ventricle and 8–10 ml of 0.9% NaCI solution (pH 7.4) was flowed through circulation system. NaCI solution flowing tube was closed after the blood of mice were drained. 8-10 ml of 4% paraformaldehyde dissolved in 1XPBS was prepared freshly and given to mice until the all organs fixed. Afterwards, brains were excised, put into Falcons containing 4%paraformaldeyde solution and incubated at +4^{o}C for 16 hours. On the following day, sucrose gradient was done for each brain. Sucrose gradient started with 10% sucrose and continued with 20%, and 30% sucrose solution. Each concentrated sucrose solution was prepared by using 1XPBS (pH 7.6) and brains were incubated with 10% and 20% concentrated sucrose solutions for 2 hours at +4 ^{o}C. Brain of each sample was waited for 16 hours in 30% concentrated sucrose solution at +4 ^{o}C. After sucrose gradient was completed, samples were embedded in boxes containing OCT and samples were frozen quickly by using dry ice.

Samples were stored in -80^{o}C freezer until required. For histological analysis, coronal sections with a thickness of 10 μm were taken by using Leica Cryostat (CM1850-UV, Leica, Wetzlar, Germany) at -20°C. Adhesive-coated slides were used for each section. Collected adhesive-coated slides were ready for histological and immunohistochemistry analysis, so these slides were also stored in 80^{o}C freezer until used (Schneider Gasser et al. 2006; Risher et al. 2014).

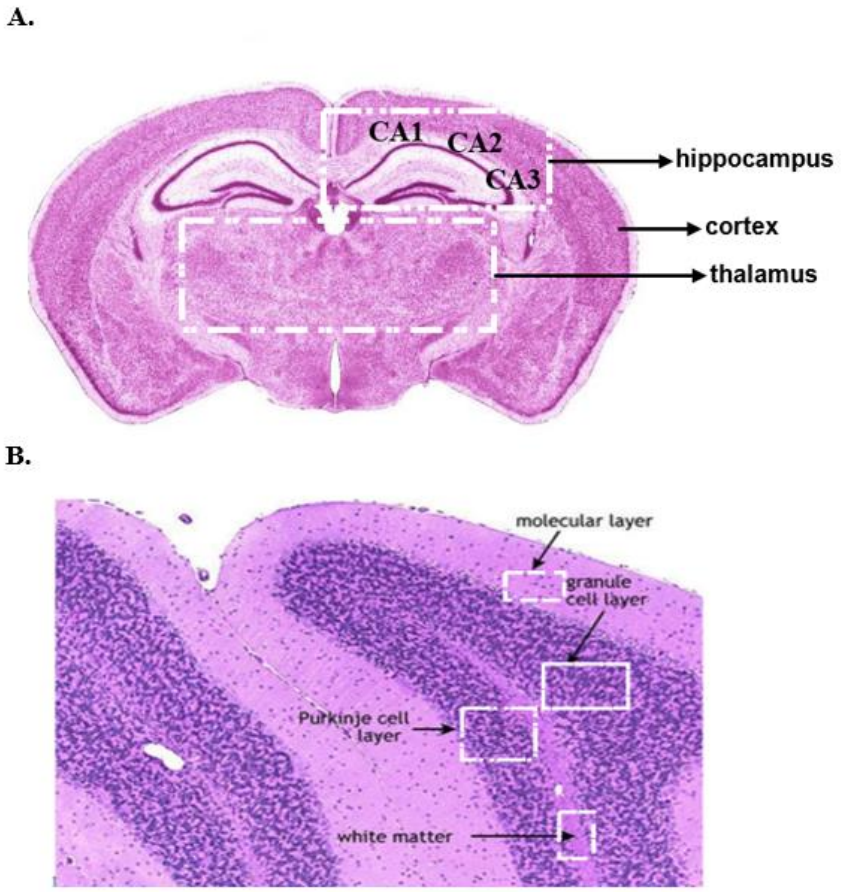

Figure 2.2. Mouse brain coronal sections for Hippocampus, Cortex, Thalamus (A) and Cerebellum (B) tissues (by courtesy of Woods et al. 2013).

2.5. Thin Layer Chromatography Analysis

Thin layer chromatography was performed for 2- and 5-month-old WT, Neu1-/-, GM3S-/- and Neu1-/-GM3S-/- mice groups in order to analyze the ganglioside patterns in different brain regions (cortex and cerebellum). Three independent mice for each genotype were used for TLC analysis.

2.5.1. Neutral and Acidic Ganglioside Isolation from Brain

50mg of cortex and 30mg of cerebellum brain regions were weighed with a balance and neutral and acidic ganglioside isolation were done from these brain regions (Sandhoff et al. 2002). Brain samples were put into borosilicate glass tubes and 2 ml water

was added to each sample. Homogenization of samples were done by using ultra turax homogenizer (IKA T10, Sigma, Darmstadt, Germany) for 45 seconds at 6000rpm. Samples were then sonicated with a sonication machine (Bandelin-sonopuls, Berlin, Germany) for three times (4 x 1.5 minutes). Sonicated samples were placed to Reacti-Therm Heating module (Thermo, Massachusetts, USA) including 55°C of water and then dried with help of N_2 flow for 30 minutes. After water evaporation was completed, 3 ml of acetone was added to samples and vortexed properly. Then, samples were centrifugated at 2000rpm for 5 minutes and supernatants consisting of membrane lipids and phospholipids were discarded. This process was repeated for three times. 1.5 ml of chloroform:methanol:water solution (10:10:1) was added to pellet parts and centrifugated at 2000 rpm for 5 minutes. Obtained supernatant parts were collected into clean neutral tubes with glass Pasteur pipettes. The same procedure was done twice and 2ml of chloroform:methanol:water (30:60:8) was added to collected supernatants. Afterwards, samples were vortexed and centrifugated for 5 minutes at 2000 rpm. Similar to previous step, supernatants were collected to previous neutral tubes consisting of supernatant parts. This step was performed for two times and the supernatants were put into the same neutral tube. That's way, neutral and acidic gangliosides were isolated form the brain regions. Neutral gangliosides were separated from acidic gangliosides for thin layer chromatography process.

DEAE Sephadex A-25 were utilized for acidic and neutral ganglioside separation and it was prepared by addition of 10ml of chloroform: methanol:0.8M sodium acetate (30:60:8) to 1gr of DEAE Sephadex A-25 resin (GE Health Care, Little Chalfont, United Kingdom). Prepared resin were incubated for 5 minutes at room temperature and centrifugated at 2000 rpm for 1 minute. After centrifugation, supernatant part was taken from the resin and resin was washed for several times with previous prepared solution. Prepared resin was incubated for 16 hours in 10ml of chloroform: methanol:0.8M sodium acetate (30:60:8). Before usage, supernatant was discarded, and resin was washed with 10ml of chloroform:methanol:water (30:60:8) for several times. Columns were prepared by using both glass woolen and resin. Firstly, glass woolen was placed into Pasteur pipette to close the tip of pipette and resin was poured to Pasteur pipettes. Resin as loaded to all samples with the same volume (2cm) and prepared columns were washed for 8 – 10 times with 1ml of chloroform:methanol:water (10:10:1) and 1ml of chloroform:methanol:water (30:60:8) solution. Then, clean neutral glass tubes were placed under the prepared columns in order to collect the neutral gangliosides. Collected total gangliosides were

added to columns and 4ml of 100% methanol. Liquids flowing tubes were collected as neutral gangliosides. Isolated neutral gangliosides were evaporated by N_2 flow after the samples were placed into Reacti-Therm Heating module (Thermo, Massachusetts, USA) in 55°C of water. Evaporated samples were kept at +4°C for the Thin Layer Chromatography. Columns were then put on the top of new neutral tubes and columns were washed with 5ml of 500 mM potassium acetate dissolved in methanol. Collected liquid parts in new neutral tubes were used for further process to isolate the acidic gangliosides. Superclean LC-18 column (Supelco, Sigma, Darmstadt, Germany) was used for isolation of acidic gangliosides and LC-18 columns were put onto Chromabond Vacuum manifold (Macherey-Nagel, Düren, Germany) which adjust to 5Hg. 2ml of methanol and 2ml of 500 mM potassium acetate dissolved in methanol were added to columns one by one for equilibration process. Previously collected liquid parts including acidic gangliosides were added to columns. 10ml of distilled water was added to each column to wash columns and flowing liquid part was discarded. Afterwards, clean neutral tubes were placed under the columns. Elution was performed by the addition of 4ml methanol and 4ml chloroform:methanol (1:1) to columns with the constant 5Hg vacuum. Liquid flowing neutral tubes was acidic gangliosides and these tubes were placed into Reacti-Therm Heating module (Thermo, Massachusetts, USA) in 55°C water and samples were evaporated with N_2 flow. Evaporated samples were kept in the +4^{o}C for Thin Layer Chromatography.

2.5.2.Thin Layer Chromatography

Isolated samples were runned on silica plates (Merck, New Jersey, USA) to separate them according to their weights. Running solution was prepared before usage and its ingredients were Chloroform:methanol: 0.2% CaCl2(30:65:8). Prepared running solution was poured into TLC tanks and TLC tank was closed properly to prevent any air intake. TLC tank including running solution was incubated at room temperature for 2 hours. Silica plates (20cm x 20 cm and 10cm x 10cm) were placed to 100°C oven and incubated for 30 minutes inside oven. Then, acidic and neutral gangliosides were dissolved in 100 µl of chloroform:methanol:water (10:10:1) solution separately. 45µl of acidic and 20µl of neutral ganglioside samples were loaded to silica plates by using

Linomat 5 (Camag, Muttenz, Switzerland) machine. Loaded samples were dried and placed into TLC tank, then samples were run on the silica plate for 10cm.

2.5.3. Orcinol Staining of Plates and Visualization

Orcinol solution (0.05g orcinol/10ml acetone/0.5ml sulfuric acid) was prepared before staining of silica plate and prepared solution was incubated at room temperature for cooling. Then, silica plates were dyed with orcinol solution and plates were placed onto TLC plate heater (Camag, Muttenz, Switzerland) at 120°C. Plates were waited until the bands became visible. HP scanner was used to scan silica plates. Band intensities were determined by ImageJ program and statistical analysis was performed with GraphPad Prism.

2.6. DNA Isolation and Agarose Gel Electrophoresis

Brain sections (cortex, cerebellum and thalamus) of three independent 2- and 5-month-old WT, Neu1-/-, GM3S-/- and Neu1-/-GM3S-/- mice were used for DNA isolation and agarose gel electrophoresis protocol (Huang et al. 1997).

Firstly, lysis buffer including 10 mM Tris–HCl, pH 8.0, 100 mM NaCl, 25 mM EDTA, 100 µg/ml proteinase K, 0.5%SDS were added to brain sections taken from each genotype, and samples were incubated in water bath at 40^{o}C for overnight. Then, DNA isolation was applied depending on phenol-chloroform method. Equal volume of phenol:chloroform:isoamly alcohol (25:24:1) was added to samples after incubation process. Samples were centrifugated at 13000 rpm and room temperature for 10 minutes. Then, supernatant was transferred into new tube and the same procedure was repeated for two times and obtained supernatants were collected to the same Eppendorf tube. The same volume of chloroform was added to Eppendorf tube including supernatants and centrifugated at 13000 rpm and room temperature for 10 minutes. Then, supernatant part was taken into new Eppendorf tube. This procedure was repeated once time and the supernatant was added to previous supernatant part again. Following reagents as 3M NaOAc (0,1 x sample volume) and 100% ethanol [2,5 x (sample + NaOAc volume)] were added to supernatant part and samples were incubated at -80 ^{o}C for 1 hour. Samples were

taken from -80 ºC at the end of the 1 hour and centrifugated at 13000 rpm and 4 ºC for 10 minutes. Supernatant parts were removed and 150 µl of 70% ethanol was added to pellet (DNAs) parts for purification. Again, samples were centrifugated at 13000 rpm and 4 ºC for 10 minutes and supernatant part was removed. Remaining ethanol was air dried for 10 – 15 minutes. DNAs were dissolved in 100 µl of TE including 0.1 M Tris–HCl, pH 8.0, 10 mM EDTA. DNA concentration were determined with NanoDrop spectrophotometer (ND-1000) and DNAs were prepared as 2000ng. 2% concentrated agarose gel including ethidium bromide (0.4µg/ml) was prepared and samples were run on gels at 50 volt for 3 hours. Fragmented DNAs were observed under UV.

2.7. Real Time PCR

RNA analysis was done by Real Time PCR. The cortex, cerebellum and thalamus tissues of 2- and 5-month-old WT, Neu1-/-, GM3S-/- and Neu1-/-GM3S-/- mice were used for real time PCR analysis. Real time PCR procedure was performed with RNA isolation, cDNA synthesis form RNA and RT-PCR protocols. Three independent mice for each genotype were used for Real Time PCR analysis.

2.7.1. RNA Isolation

Brain sections (cortex, cerebellum and thalamus) of 2- and 5-months old WT, Neu1-/-, GM3S-/- and Neu1-/-GM3S-/- mice were used and 50 mg of cortex sections, 35 mg of cerebellum and 25 mg of thalamus section were weighed for RNA isolation. 500 µl, 250 µl and 100 µl of GeneZol (GeneAid) were added to 2ml Eppendorf tubes including cortex, cerebellum and thalamus respectively according to manufacturer's instructions. Then, samples were homogenized by using RNase free beads in tissue homogenizator (Retsch MM100). Samples were transferred into new 1.5 ml Eppendorf tubes. 100 µl chloroform was added to samples and tubes were mixed inversely for 10 seconds. Samples were centrifugated at 15000xg and 4 ºC for 15 minutes for phase separation. Colorless aqueous part of samples including RNAs were taken into new clean 1.5 ml Eppendorf tubes after centrifugation. One volume of 100% isopropanol were added to samples and samples were incubated at room temperature for 10 minutes for precipitation

of RNAs. Then samples were centrifugated for 10 minutes at 15000xg at +4°C to obtain RNAs as pellet form. After centrifugation, supernatant parts were removed and 1ml of 70% ethanol were put into Eppendorf tubes including RNAs in order to wash pellet parts. Centrifugation at 15000xg and 4 °C for 5 minutes were done, supernatant part was removed and RNA pellets were air dried at 4 °C for 5 – 10 minutes. 30 µl RNase free water was added to RNA pellets to dissolve the RNAs and samples were put into water bath (55 °C) along 10 minutes. RNA concentrations were determined with NanoDrop Spectrophotometer (ND-1000).

2.7.2. cDNA Synthesis

cDNA conversion from isolated RNAs were done by using Evo Script Universal cDNA Master (Roche Life Science), and manufacturer's instructions were applied. Reaction mixture volume was 20 µl and cDNA was synthesized at a concentration 50ng/µl for each sample. cDNA synthesis mixture includes 1X reaction buffer, 2 µl of 10X Enzyme Mix, water and RNA depending on nanodrop results. cDNA conversion conditions were as following; 15 minutes at 42˚C; 5 minutes at 85˚C, 15 minutes at 65˚C.

After cDNA conversion, PCR protocol was applied for housekeeping GAPDH gene in order to confirm whether all RNAs obtained from distinct samples were converted to cDNA successfully. For GAPDH PCR protocol, total volume of mixture was 25 µl and its ingredients were 0.8 mM of GAPDH primers, 10 mM of each dNTPs, 1X reaction buffer including $MgCl_2$, 1.75 units DNA polymerase (GeneDireX) and 50 ng concentrated cDNA for each sample. PCR reaction conditions for GAPDH gene were as follows: 2 minutes at 95˚C; 20 seconds at 95˚C (30 seconds), 15 seconds at 65˚C (30 seconds), 22 seconds at 72˚C, and 3 minutes at 72˚C. 1% concentrated agarose gel was prepared and PCR products were loaded to agarose gel and run at 100 volt for 20 minutes.

2.7.3. RT-PCR

Gene expression analysis based on RNA level were done by using RT-PCR protocol. Genes related with ER stress (ATF6, Calnexin and XBP1), oxidative stress (SOD2, catalase and TTase1) and apoptosis (Bax, Bak, Bcl-XL and Bcl-2) were analyzed.

RT-PCR protocol was done with Roche LightCycler® 96 System by using Roche LightCycler 480 SYBR Green I Master Mix.

Table 2.3. Primers sequences and PCR product sizes used in RT-PCR.

Gene	Primer Sequences	PCR Product (bp)
ATF6	F:5'- TGGAAGTGGGAAGATCGGGA-3', R: 5'-AGGACAGAGAAACAAGCTCGG-3'	354
Calnexin	F:5'- ATTGCCAACCCCAAGTGTGA-3', R: 5'-TCCAGCATCTGCAGCACTAC-3'	362
XBP1	F:5'- TCCGCAGCACTCAGACTATG-3', R:5'-GACTCTCTGTCTCAGAGGGGA-3'	360
SOD2	F:5'- GTGTCTGTGGGAGTCCAAGG-3', R: 5'-CCCCAGTCATAGTGCTGCAA-3'	339
Catalase	F:5'- TTCGTCCCGAGTCTCTCCAT-3', R: 5'-GAGGCCAAACCTTGGTCAGA-3'	351
TTase1	F:5'- CTGCAAGATCCAGTCTGGGAA-3', R: 5'-CTCTGCCTGCCACCCCTTTTAT-3'	322
Bcl-2	F:5'- CGCAGAGATGTCCAGTCAGC-3', R: 5'-TATGCACCCAGAGTGATGCAG-3'	369
Bcl-XL	F:5'- TCAGCCACCATTGCTACCAG-3', R: 5'-GTCTGAGGCCACACACATCA-3'	356
Bax	F:5'- AGGATGCGTCCACCAAGAAG-3', R: 5'-CTTGGATCCAGACAAGCAGC-3'	306
GAPDH	F:5'- CCCCTTCATTGACCTCAACTAC-3', R:5'-ATGCATTGCTGACAATCTTGAG-3'	347

Total volume of reaction mixture was 20µl and it includes and 50ng cDNA, 0.4 µM each primer (Table 2.3) and 1X Roche LightCycler 480 SYBR Green I Master Mix. Reaction conditions were as following; 10 minutes at 95˚C; 20 seconds at 95˚C (45 cycles), 15 seconds at 60˚C, 22 seconds at 72˚C. GAPDH is a housekeeping gene, so GAPDH expression level was used for normalization. Gene expression ratio was calculated for each sample. Experiments were repeated at three times for each genotype and the average of three independent mice results were used for statistical analysis. For statistical analysis, two-way ANOVA on GraphPad Prism was utilized.

2.8. Western Blot

Protein analysis was done by Western blot analysis. Firstly, proteins were isolated from different brain sections (cortex, cerebellum and thalamus) of 2 and 5-month-old WT, Neu1-/-, GM3S-/- and Neu1-/-GM3S-/- mice. Then, protein concentrations were evaluated with Bradford assay. Lastly, SDS-PAGE gel electrophoresis was done for western blot analysis. Three independent mice for each genotype were used for Western Blot analysis.

2.8.1. Protein Isolation

Protein isolation was done form cortex, cerebellum and thalamus regions of 2 and 5-month-old WT, Neu1-/-, GM3S-/- and Neu1-/-GM3S-/- mice groups. Protein lysis buffer (1% TritonX100, 50mMHepes, 150mM NaCl, 10%Glycerol, 50mM Tris-Base, 1%PMSF, 1% protease inhibitor) was used to obtain protein lysates form brain regions. 500 µl protein lysis buffer were used for cortex and cerebellum brain regions while 100µl lysis buffer was utilized for thalamus brain region. Protein lysis buffer was added to brain regions and homogenized with mini homogenizator. After homogenization, incubation on ice for was done for 1 hour and samples were mixed with vortex machine for every 10 minutes in order to supply homogenization of samples properly. After 1-hour incubation was completed, samples were centrifugated at 14000 rpm (0^oC) for 15 minutes and supernatants including proteins were transferred into new clear Eppendorf tubes.

2.8.2. Bradford Assay and Protein Preparation

In order to determine the protein concentrations of different samples, Bradford Assay was done. Firstly, obtained proteins were diluted as 1:80 with distilled water (2µl isolated protein + 158µl dH_2O). Protein lysis buffer was also diluted as 1:80 with distilled water and it was used as blank for isolated proteins. Different concentrated BSA solutions (20, 40, 80 and 100 µg/ml) were prepared in order to obtain a standard curve which supply the calculation of protein concentration of distinct samples.

50µl diluted samples and different concentrated BSA solution were added to 96 well plate and 200µl Bradford reagent (SERVA Electrophoresis GmbH, Heidelberg, Germany) was added to samples. Then, plate was incubated for 10 minutes at room temperature. Absorbance levels of each sample were evaluated at 595nm with i-Mark Microplate Absorbance Reader (Bio-Rad Labotories, California, USA). Absorbance values that obtained from different concentrated BSA solutions were used to plot a standard curve. Equation obtained from standard curve was also used for protein concentration calculations. Protein concentration of each sample was equalized (20µg) by using this equation.

Protein were prepared according to obtained absorbance values from Bradford Assay. For each sample 20µg concentrated proteins were prepared with addition of calculated water and protein amounts to Eppendorf tubes. Then, 4:1 loading buffer (40% Glycerol, 240mM Tris-HCl pH 6.8, 8%SDS, 0.04%Bromophenol Blue, 5% β-mercaptoethanol) was added to each sample and samples were boiled at 95^0C for 10 minutes. Boiled samples were used for SDS-PAGE gel electrophoresis.

2.8.3. SDS-PAGE Gel Electrophoresis

Resolving and stacking gels were used for SDS-PAGE gel electrophoresis. Resolving gel (10%) refers to lower gel and its ingredients are 3 ml Lower buffer (1.5 M Tris-HCl), 4 ml Acrylamide (30%), 5 ml Water, 60µl SDS (10%), 60µl APS (10%) and 6 µl TEMED. All ingredients were mixed in a falcon tube and it was poured into gap between glasses which are compressed to each other with casting frames. Polymerization of lower gel was supplied with incubation at room temperature. After that, stacking gel refers to upper gel and its ingredients are 1.5 ml Upper Buffer (1M Tris-HCl), 1 ml Acrylamide (30%), 3.5 ml Water, 60µl SDS (10%), 60µl APS (10%) and 6 µl TEMED. All ingredients were mixed in a falcon tube and prepared stacking gel was poured to top of polymerized resolving gel and well-forming comb was placed to stacking gel. Gels were incubated at room temperature for polymerization of stacking gel. After gel polymerization, well forming comb was taken from stacking gel and glass was removed from casting frames. Glass was put into cell buffer dam and running buffer (0.25M Tris-Base, 1.92M Glycine, 1%SDS) was poured into both inner and outer chamber of tank as being required level. Prepared proteins were loaded into wells and run at 120V for ~1.5

hours. Then, proteins on gel were transferred onto nitrocellulose membrane (Bio-Rad). Transfer process was done with sandwich method by using transfer cassettes. Transfer cassettes were placed into tank and transfer buffer (48mM Tris-Base, 39mM Glycine, 20%Methanol, pH 9.2) was added to tank. Transfer process was done at constant ampere (25mA) for 1.5 hour. After transfer process, blots were blocked by using 5%milk in PBST (0.005%Tween20) for 1 hour at room temperature and washed with PBS-Tween for 3 times (5 minutes for each time). Then, blots were incubated in primary antibodies such as Fas-Ligand (1:1000, Cell Signaling Technology), Caspase 3 (1:1000, Cell Signaling Technology), Caspase 9 (1:1000, Cell Signaling Technology), and BiP (1:1000, Cell Signaling Technology) at 4^0C for overnight according to manufacturer's instructions.. β-actin was used as internal control since it is a housekeeping gene and all blots was also incubated in primary antibody of β-actin (1:1000, Cell Signaling Technology) for 1 hour at room temperature according to manufacturer's instructions. All primary antibodies were diluted in Red Solution (5%BSA, 0.02% NaAzide, Phenol Red, in PBS-T pH 7.5). After primary antibody incubation, blots were washed 3 times for 5 minutes in PBS-Tween solution and incubated in HRP-conjugated secondary antibody (Jackson ImmunoResearch Lab) for 1hour at room temperature. Blots were washed 3 times for 5 minutes with PBS-Tween. Visualization of proteins was done with (Bio-Rad, ChemiDoc XRS+) after the LuminataTM Forte Western HRP Substrate (Millipore) addition to blots. Band intensities were determined with ImageJ program and statistical analysis was done with two-way ANOVA on GraphPad Prism.

2.9. Histological Analysis

Histological analysis was performed for cortex, cerebellum, thalamus and hippocampus sections of 2- and 5-month-old WT, Neu1-/-, GM3S-/- and Neu1-/-GM3S-/- mice (Figure 2.1). Fixed brains were used for histological analysis.

10um cryosections were taken from the fixed brains of distinct genotypes by Leica Cryostat (CM1850-UV) and cryosection were mounted onto HistoBond slides, then slides were stored at -80ºC in order to use them for histological and immunohistochemical analysis. Manufacturer's instructions were done for all histological and immunohistochemical analysis.

2.9.1. Hematoxylin – Eosin (H&E) Staining

Hematoxylin – Eosin staining was applied to understand the presence of abnormalities in tissue morphology. Slides stored in -80^{o}C were incubated on ice for 15 minutes and slides were placed to humidified chamber, then slides incubated in incubator at 55^{o}C for 15 minutes. Samples on slides were washed with 1XPBS for 3minutes and distilled water for 2 minutes in chalet. Slides were dried with Kim Wipes (KimTech, Irving, Texas, USA). ~20µl of Hematoxylin (Merck, Darmstadt, Germany) reagent was added to each brain sample and incubated for 3 minutes at room temperature. Samples were washed with distilled water for 2 minutes and then tap water for 3 minutes in chalet. Samples were waited in chalet including 1% HCI in 70% ethanol for 30 seconds. Samples were then washed with tap water for 3 minutes and distilled water for 2 minutes. ~20µl of Eosin (Merck, Darmstadt, Germany) reagent was added to each brain sample on slides and incubated for 30 seconds at room temperature. Samples on slides were washed twice with 95% ethanol and 100% ethanol for 2 minutes separately. Slides were air-dried with Kim Wipes (KimTech, Irving, Texas, USA), then mounted with mounting medium Richard-Allan Scientific CytosealXYL (Thermofisher, UK). Slides were observed to understand the morphological changes depending on ganglioside pattern by using light microscope (Olympus BX53).

2.9.2. Cresyl - Echt Violet Staining

In order to study the structure of neurons and abnormalities, Cresyl Echt Violet staining was performed for prepared slides. Slides stored in -80^{o}C were incubated on ice for 15 minutes. slides were then placed to humidified chamber and incubated in incubator at 55^{o}C for 15 minutes. Samples were washed for 5 minutes with 1XPBS in chalet and dried with Kim Wipes (KimTech, Irving, Texas, USA). ~20µl of Cresyl Echt Violet solution (ScyTek Laboratories, Utah, USA) was added to each brain sample and incubated for 5 minutes at room temperature. Afterwards, samples were placed to different chalets including distilled water, 100% ethanol, 100% ethanol and xylene in order and samples were waited in each solution for 5 seconds. Slides were dried with Kim Wipes (KimTech, Irving, Texas, USA), then mounted with mounting medium mounting medium Richard-Allan Scientific CytosealXYL (Thermofisher, UK). Slides were

analyzed to evaluate the neuron structure changes by using light microscope (Olympus BX53).

2.9.3 Periodic acid-Schiff Stain (PAS) Staining

Periodic Acid Schiff (PAS) staining was performed for samples to show the glycosphingolipid accumulation depending on genotype and age. Slides in -80^{o}C were incubated on ice for 15 minutes and slides were placed to humidified chamber, then incubated in incubator at 55^{o}C for 15 minutes. Samples on slides were washed with 1XPBS for 5 minutes in chalet and slides were transferred to a chalet including Carnoy's solution including ethanol, chloroform and acetic acid (6:3:1), then incubated for 10 minutes. Afterwards, ~20µl of 5% Periodic Acid (Merck, Darmstadt, Germany) solution was added to each brain sample and incubated for 5 minutes at room temperature. After 5 minutes, samples were washed with tap water for 3 minutes and distilled water for 2 minutes in chalets. Slides were dried with Kim Wipes (KimTech, Irving, Texas, USA) and ~20µl of Schiff (Merck, Darmstadt, Germany) solution was added to each brain sample on slides and incubated at room temperature for 12 minutes. After Schiff solution, tap water for 5 minutes and distilled water for 2 minutes were used for washing process. The slides were dried with Kim Wipes (KimTech, Irving, Texas, USA) again and then each brain sample was incubated with ~20µl of Hematoxylin (Merck, Darmstadt, Germany) solution in chalet at room temperature for 1.5 minutes. Slides were washed with tap water for 5 minutes. After all steps, each slide was incubated for 1 minute in each chalet including 70% ethanol, 95% ethanol, 100% ethanol and xylene solutions. Slides were dried with Kim Wipes (KimTech, Irving, Texas, USA), then mounted with mounting medium mounting medium Richard-Allan Scientific CytosealXYL (Thermofisher, UK). In order to show glycosphingolipid accumulation depending on genotype and age slides were analyzed by using light microscope (Olympus BX53).

2.9.4. Luxol – Fast Staining

Luxol – Fast staining is used to show the demyelination and this staining was performed to understand the de/myelination process in distinct aged and genotyped mice

groups. Slides in -80ºC were incubated on ice for 15 minutes and slides were placed to humidified chamber, then incubated in incubator at 55ºC for 15 minutes. Samples on slides were washed with 1XPBS for 5 minutes in chalet and slides were transferred to a chalet consisting of ice-cold acetone, then slides were incubated in this chalet for 10 minutes. After these steps, slides were washed with 1XPBS for 5 minutes in chalet. Each brain sample was incubated with ~50µl of Luxol Fast Blue (ScyTek Laboratories, Utah, USA) reagent in chalet at 60ºC for 2 hours. Slides were washed with distilled water for 5 minutes and then slides were placed to chalets including 0.05% Lithium Carbonate Solution (ScyTek Laboratories, Utah, USA) and incubated twice in 0.05% Lithium Carbonate Solution for 10 seconds. Distilled water for two times along 5 seconds was used for washing process. ~20 µl of 0.1% Cresyl Echt Violet (ScyTek Laboratories, Utah, USA) was added to each brain sample on slides and incubated for 3 minutes at room temperature. Lastly, slides were washed with distilled water and 100% ethanol for three times and 5 seconds. Slides were dried with Kim Wipes (KimTech, Irving, Texas, USA), then mounted with mounting medium Richard-Allan Scientific CytosealXYL (Thermofisher, UK). In order to show de/myelination depending on genotype and age slides were analyzed by using light microscope (Olympus BX53).

2.10. Immunohistochemistry Analysis

Fixed brains of 5-month-old WT, Neu1-/-, GM3S-/- and Neu1-/-GM3S-/- were utilized for immunohistochemistry analysis such as CNPase, NeuN, and TUNEL methods. Three independent mice for each genotype were used for Immunohistochemistry analysis.

2.10.1. Anti-CNPase Staining

The oligodendrocytes presence was detected by Anti-CNPase staining for different mice groups by using primary antibody anti-CNPase (Cell Signaling Technology, The Netherlands) and secondary antibody anti-rabbit Alexa Fluor®-488 (Abcam, Cambridge, UK).

Slides stored at -80 ^{o}C were placed on ice for 15 minutes and then incubated at 55 ^{o}C incubator for 15 minutes. Slides were incubated in %4 PFA dissolved in 1X PBS for 10 minutes in order to fix the brains on slides. Then, slides were washed with 1X PBS for 5 minutes and this process was applied for three times. Slides were put in chalet including %100 cold methanol and incubated for 10 minutes. After methanol incubation is completed, slides were washed with 1X PBS for 5 minutes and liquid blocker PAP pen (Sigma-Aldrich, Germany) was used to determine the edges of each brain on slide. Blocking solution (%0.3 Triton X-100, %4 BSA, 0.3M Glycine, %10 Goat serum in 1X PBS) was added to each brain section to prevent the non-specific banding and each sample was incubated with blocking solution for 1 hour at room temperature. Primary antibody anti-CNPase (Cell Signaling Technology, The Netherlands) was diluted in blocking buffer (1:100) and prepared primary antibody was added to each brain section after blocking process. Slides were placed in humidified chamber and incubated with primary CNPase antibody at 4^{0}C for overnight. On the following day, slides were washed three times for 5 minutes by using 1X PBS. The secondary antibody anti-rabbit Alexa Fluor®-488 (Abcam, Cambridge, UK) was prepared in blocking solution (1:500). Secondary antibody was added to brain sections and incubated for 1 hour at room temperature in dark. After secondary antibody incubation, slides were washed three times with 1X PBS for 5 minutes and Fluoroshield mounting medium DAPI (Abcam, Cambridge, UK) was used to stain nucleus of the cell. Lastly, slides were covered with coverslips. Images were observed with fluorescent microscope (Olympus BX53). Image J program was used to colocalize the green and blue fluorescence. Statistical analysis was done with GraphPad Prism.

2.10.2. Anti-NeuN Staining

Anti- NeuN staining was performed in order to analyze the neurons on distinct mice groups by using primary antibody anti-NeuN (Cell Signaling Technology, The Netherlands) and secondary antibody anti-rabbit Alexa Fluor®-568 (Abcam, Cambridge, UK).

Slides in -80^{o}C were incubated on ice for 15 minutes and slides were placed to humidified chamber, then incubated in incubator at 55^{o}C for 15 minutes. Slides were washed by using 1X PBS for 10 minutes and then they were incubated in cold acetone

for in order to supply the permeabilization of brain sections. Slides were washed twice by 1X PBS for 5 minutes. Liquid blocker PAP pen (Sigma-Aldrich, Germany) was used to determine the edges of each brain on slide. Blocking solution (%0.3 Triton X-100, %4 BSA, 0.3M Glycine, %10Goat serum in 1X PBS) was added to each sample to prevent the non-specific banding and slides were incubated at room temperature for 1 hour. After blocking was completed, primary antibody anti-NeuN (Cell Signaling Technology, The Netherlands) was diluted in blocking buffer (1:50) and added to each sample. Slides were placed in humidified chamber and incubated at 4^0C for overnight. On the following day, slides were washed three times along 5 minutes with 1X PBS and secondary antibody anti-rabbit Alexa Fluor®-568 (Abcam, Cambridge, UK) was prepared in blocking solution (1:500). The prepared secondary antibody was added to samples and incubated at room temperature for 1 hour in dark. After 1 hour secondary antibody incubation, slides were washed three times with 1X PBS along 5 minutes. Fluoroshield mounting medium DAPI (Abcam, Cambridge, UK) was used to stain nucleus of the cell and slides were covered with coverslips. Images were taken by using fluorescent microscope (Olympus BX53). Image J program was used to colocalize the red and blue fluorescence. Statistical analysis was done by using GraphPad Prism.

2.10.3. In Situ Apoptosis Analysis (TUNEL)

Promega-Dead End® Fluorometric Tunel Systems kit was used for the TUNEL analysis to detect the apoptosis depending on the genotype. Selected slides for each genotype were put on ice and incubated at 55 ^{o}C for 15 minutes separately. Slides were washed with PBS (137 mM NaCI, 268 mM KCI, 1.47 Mm K_2HPO_4, 8.1 mM Na_2HPO_4) pH 7.4 for 5 minutes at room temperature. Then slides were fixed with %4 PFA in PBS for 15 minutes at room temperature, and slides were washed with PBS for 5 minutes at room temperature. Liquid blocker PAP pen (Sigma-Aldrich, Germany) was used to determine the edges of each brain on slide. 20 µg/ml Proteinase K solution in PBS was prepared from the stock solution (10mg/ml dissolved in 100mM Tris-HCI (pH 8) and 50 mM EDTA) for permeabilization of brain sections. Proteinase K solution was added to each brain section and incubated for 20 minutes at room temperature. After incubation, slides were washed with PBS for 5 minutes at room temperature and %4 PFA in PBS was used to fix brain sections. Fixation was applied for 5 minutes at room temperature. Then,

slides were washed with PBS for 5 minutes at room temperature. For positive control, DNase I treatment was done. Firstly, DNase buffer (40 mM TrisHCI (pH 7.9), 10 mM NaCI, 6 mM $MgCI_2$, 10 mM $CaCI_2$) was prepared and added to selected brain for positive control. Brain section was incubated with DNase buffer for 5 minutes at room temperature. Then, DNase I (5u/ml) in DNase I buffer was prepared and added to brain section. Brain section was incubated with DNase for 10 minutes at room temperature and washed three times with distilled water for 2 minutes. Equilibration buffer was added to each slide and slides were incubated for 10 minutes at room temperature. rTdT incubation buffer (Equilibration buffer, Nucleotide Mix, rTdT Enzyme) was prepared. 10 µl rTdT incubation buffer (9 µl Equilibration buffer, 1 µl Nucleotide Mix, 0,2 µl rTdT Enzyme) was used for each brain section. For negative control, distilled water was used instead of rTdT enzyme in rTdT incubation buffer. Slides were placed in humidified chamber and 10 µl rTdT incubation buffer was added to each brain section and slides were incubated at 37°C for 60 minutes in dark. 20X SSC solution (reaction stop solution) was diluted to 2X SSC with water and added to each brain in order to stop the reaction. Slides were incubated with 2X SSC solution for 5 minutes at room temperature. Then, slides were washed three times with PBS for 5 minutes. Propidium Iodide (PI) was used to stain the cell nucleus. Propidium Iodide (1 µg/ml) was prepared from stock PI solution (Sigma-Aldrich, Germany) by using PBS. Prepared PI solution was added to each brain section and incubated 15 minutes at room temperature in dark. Then, slides were washed three times by using distilled water for 5 minutes. Lastly, Propidium Iodide (PI) mounting medium (Sigma-Aldrich, Germany) was added to slides and slides were covered with coverslips. Fluorescent microscope (Olympus BX53) was used to take the image on slides. Image J program was used for colocalization of green and red fluorescence and further analysis. Statistical analysis was done by using GraphPad Prism.

2.11. Behavioral Test

Several behavioral tests were performed for 2- and 5-month-old WT, Neu1-/-, GM3S-/-, and Neu1-/-GM3S mice in order to understand the effects of glycosphingolipid metabolism changes on different brain regions and neurons. Six independent mice for each genotype were used for behavioral analysis.

2.11.1. Rotarod Test

Motor neuron function and activity was evaluated with Rotarod Test. Mice groups were trained before the experiment and it was learnt to walk on the rod for each mice group. Rod (Pan-Lab Harvard Apparatus, Barcelona, Spain) had an accelerating speed from 4 rpm to 40 rpm and experiment was performed along 3 minutes and each mouse was walked on the rod for three times. The duration time on the rod and speed of rod during falling down of mice were recorded for each mice group in order to evaluate the motor neuron functions and coordination of mice groups (Nampoothiri et al. 2017). Statistical analysis was performed by using GraphPad Prism.

2.11.2. Grip Strength Measurement Test

Limb Grip Strength Test was used as behavioral test for each mice group to evaluate the nerve-muscle functions and muscle strength of different genotyped mice depending on the differentiation in ganglioside pattern. Grip Strength Meter (IITC Life Science, USA) was used for limb grip test and the indicator of apparatus was zerod before experiment. Each mouse was held from the tail and it is provided that the front legs are at the same height as the bar level. After mice were held to T-shaped bar with front legs, mice were moved as horizontal by holding from the tails. Mice should hold to bar with front legs during movement and mice were pulled with the constant velocity and force until mice released the bar (Nampoothiri et al. 2017). Force value of each mouse was recorded during experiment. Mice that use the back legs or only one front leg was eliminated from experiment. Test was repeated for three times for each mouse to reach the best performance. GraphPad Prism software program was used for statistical analysis.

2.11.3. Passive Avoidance

Passive avoidance was used to elucidate the damages in hippocampus brain region depending on the age and ganglioside pattern changes. Test platform was divided into two regions that are dark and bright. The region lit by light was larger than the dark regions. These two sections are separated from each other by a vertical movable door.

Experiment continued for three days and consisting of introduction, training and test sections. Introduction section is the first day of the experiment and each mouse was placed in the bright room with its face facing the movable door and held for 1 minute. After 1 minute was completed, door opened automatically, and the mouse was allowed to recognize the dark and bright region. When the mouse entered the dark part, the door closed automatically and after 10 seconds, the mouse was removed from the device and placed in its cage. On the day of training day, the mouse was put into the bright region and waited for 1 minute as day of introduction. After 1 minute, door opened automatically. As soon as four feet of the mouse were in the dark compartment, door closed automatically. After the door closed, the mouse was exposed to an electric shock of 0.2 mA for 2 seconds. After 10 seconds, the mouse was taken from the apparatus and put into its cage. On the day of test section, the mouse was placed to the bright room and waited for 1 minute. Door opened automatically after 1 minute. Passage time to dark region was recorded with ShutAvoidv1.8 (Harvard Apparatus). If mice did not enter the dark region at the end of the 300 seconds, door closed automatically, and experiment was over (Yamanaka et al. 1994 & Liu et al. 1997). Passage time to dark region was used as data for analysis and statistical analysis was done with GraphPad Prism.

2.11.4. Open Field Test

Open field Test was performed for each mice group in order to determine the anxiety behaviors and locomotor activities of mice. The square white platform made from plastic matter was used for open field test. Dimension of square platform was 45 cm (length) x 45 cm (width) x 40 cm (height). There were two floor part of platform which are white and black. White platform was used for black colored mice groups while black platform was preferred for white colored mice groups. The square platform was cleaned by using 95% ethanol before experiment. The platform was air-dried to remove all the 95% ethanol. Mice groups were transferred to test room and mice groups were waited for 30 minutes before experiment so that mice got used to test room (Seibenhener and Wooten 2015). After 30 minutes, each mouse was placed to square platform from the corner of the platform and mice movements was free for 5 minutes. Movements of mice was recorded by a software program (Panlab/Harvard Apparatus) and camera which was located at the top of the platform. The center and corners of platform were determined

and software program recorded the mice movements such as total distance and, time percentage at center and periphery to understand the locomotor activities and anxiety behaviors. After 5 minutes, each mouse was taken from the platform and placed to their cages. Results obtained from SMART Video software was analyzed with GraphPad Prism.

2.12. Analysis of Urinary Oligosaccharides by TLC

Urines were collected from 2 and 5-month-old WT, Neu1-/-, GM3S-/- and Neu1-/-GM3S-/- mice groups by using metabolic cages (Techniplas). Three independent mice for each genotype were used for urinary oligosaccharides by thin layer chromatography. Mice were put into these metabolic cages including water and food and mice groups were waited for overnight to obtain urines. The collected urines were placed into -20^{o}C freezer and urinary samples were kept into freezer until the oligosaccharide analysis was done. Creatine amount in urines were determined by using creatine Assay Kit (Cat No ab204537, Abcam, Cambridge, United Kingdom) and creatine values of urine samples were used for normalization of distinct samples according to manufacturer's instructions. Firstly, samples taken from -20^{0}C were centrifugated at 13000 rpm for 10 minutes and supernatant part was used for further steps. Urine samples were diluted (1:50) with distilled water. Standard solution found in Creatine Assay Kit was also diluted serially with distilled water in order to plot a creatine standard curve. 50 µl of each sample and different concentrated standard solutions were put into 96 well plate and 50 µl creatine detection reagent was added to each sample. Then, samples in 96 well plate was incubated for 30 minutes at room temperature. Absorbance values of distinct samples were measured at 490 nm by using i-Mark Microplate Absorbance Reader (Bio-Rad Laboratories, California, USA). Standard curve was plotted according to absorbance values of different concentrated standard solutions and equation was found. Equation was used for equalization of creatine amount (500ng) in each sample. Samples including 500 ng creatine were prepared with addition of water and urine that have 15 µl final volume. Prepared samples and 0,5 mg/ml of sugar standards (D+ Lactose Monohydrate, D+ Mannose, D+ Glucose, Sucrose, Galactose, D+ Xylose and D+ Raffinose Pentahydrate (Sigma-Aldrich, Darmstadt, Germany) were loaded to 20 cm x 20 cm silica TLC plates (Merck, New Jersey, USA) by using Linomat 5 (Camag, Muttenz, Switzerland) machine.

For tank preparation, 37,5 ml butanol, 18,75 distilled water and 18,75 acetic acid were put into TLC tank and tank was closed properly. Solution was incubated for 2 hours. Then, silica plates were placed into tank and samples were run on silica plate for 3 hours.

Orcinol solution (0.05g orcinol/10ml acetone/0.5ml sulfuric acid) was prepared before staining of silica plate and prepared solution was incubated at room temperature for cooling. Then, silica plates were dyed with orcinol solution and plates were placed onto TLC plate heater (Camag, Muttenz, Switzerland) at 120°C. Plates were waited until the bands became visible. HP scanner was used to scan silica plates. Band intensities were determined by ImageJ program and statistical analysis was performed with GraphPad Prism.

2.13. Statistical Analysis

Two age groups and four genotypes were used for all experiments except immunohistochemistry analysis (IHC). Only 5-month-old mice groups were used for immunohistochemistry analysis and 1-way-Anavo was performed for IHC results. 2-way-Anova was used for other all experiments to determine p values in order to understand the significant conditions depending on age and distinct genotypes. GraphPad program supplied the calculation of p-values with 2- and 1-way-Anova tests. Errors in graphs were reported as means ± SE.

CHAPTER 3

RESULTS

3.1. Genotyping of Mice for Neu1 and GM3S Alleles

Wild type and mutant alleles were determined for Neu1 and GM3S genes by using Polymerase Chain Reaction (PCR). According to amplified bands of Neu1 and GM3S genes, mice were determined +/+, +/-, and -/- for both Neu1 (Figure 3.1) and GM3S (Figure 3.2 A and Figure 3.2 B) genes. The mice groups as WT, Neu1-/-, GM3S-/-, and Neu1-/-GM3S-/- were determined.

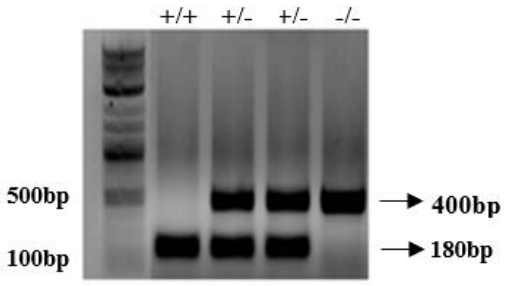

Figure 3.1. Genotyping of Neu1 alleles from the mice tails by using PCR protocol. Amplified 180 bp represent the mutant allele and 400 bp shows the wild type allele of Neu1 gene.

Neu1 PCR reaction was applied with Neu1 specific primers such as MNTG-1, MNTG-2 and LacZ primers. Amplified 180 bp and 400 bp referred to WT and KO allele for Neu1 gene, respectively (Figure 3.1).

GM3S PCR reaction was applied for the WT and KO allele separately as indicated in Figure 3.2. GM3S WT1 and WT2 primers were the primers for the GM3S WT PCR. Amplified 400 bp with GM3S WT PCR was indicator of WT allele for GM3S gene (Figure 3.2 A). The KO3 and KO4 primers were used in GM3S KO PCR. The amplified 907 bp with GM3S KO PCR represented the presence of KO allele for GM3S gene (Figure 3.2 B).

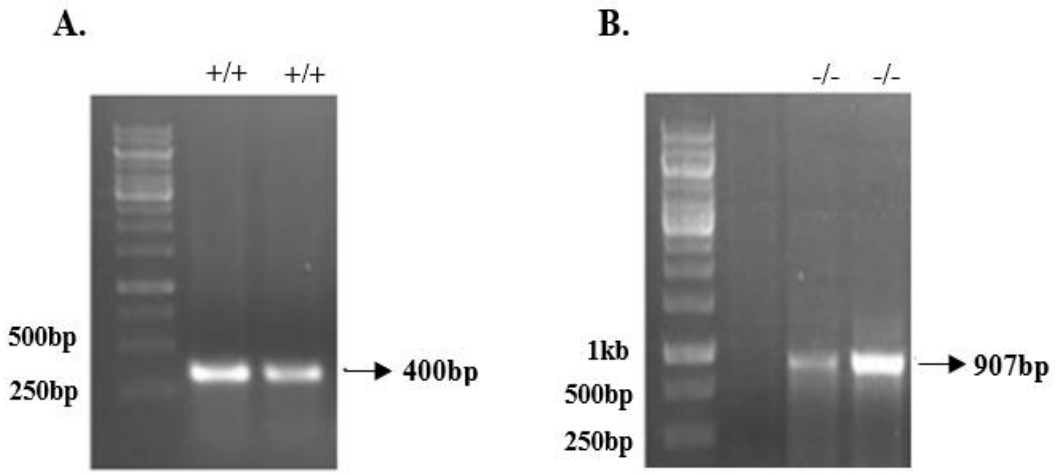

Figure 3.2. Genotyping of GM3S alleles from the mice tails by using PCR protocol. Amplified 400 bp refers to wild type allele (A), 907 bp represent the mutant allele (B) for GM3S gene.

WT, GM3S-/- mice groups could produce their offspring, however the Neu1-/- mice could not produce offspring since Neu1-/- mice were infertile (d'Azzo et al. 2002). In order to obtain Neu1-/- mice, Neu1+/- female and Neu1+/- male were crossed. On the other hand, Neu1+/-GM3S-/- female and Neu1+/-GM3S-/- male were crossed in order to get Neu-/-GM3S-/- mice.

3.2 Body Weight Measurement

Body weight of both female and male mice groups consisting of WT, Neu1-/-, GM3S-/- and Neu1-/-GM3S-/- mice were measured for fortnightly from 6 weeks to 20 weeks (Figure 3.3 A and C). 20 weeks was determined as end point for measurement since Neu1-/-GM3S-/- double deficient mice lived a maximum of 5 month (20 weeks).

WT mice had more body weight than Neu1-/- and Neu1-/-GM3S-/- mice from the 6 to 20 weeks for both female and male mice. On the other hand, the most weight loss was exhibited in the Neu1-/-GM3S-/- double gene deficient mice for both female and male mice (Figure 3.3 A and C).

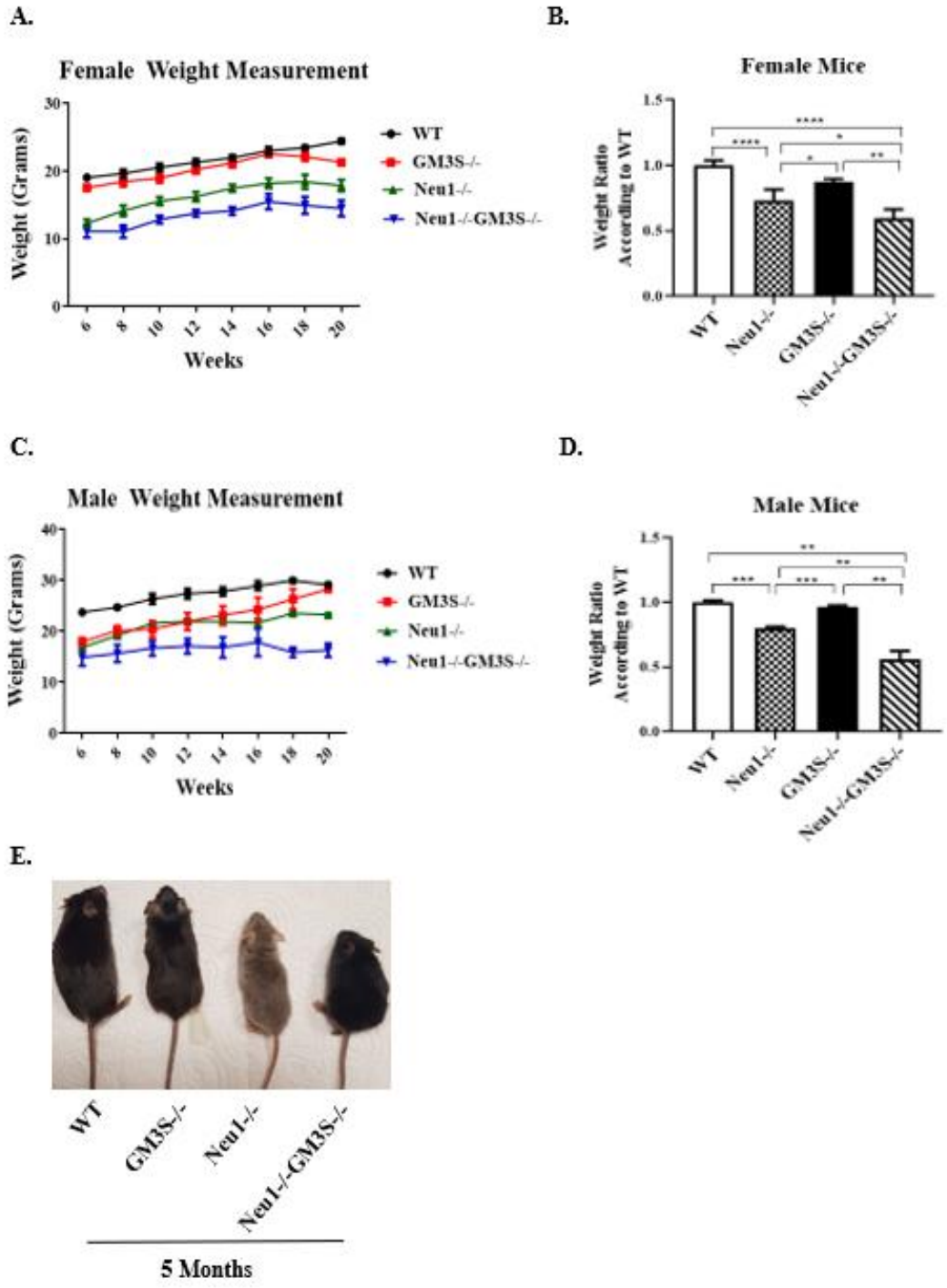

Figure 3.3. Female (A) and male (C) weight measurement of WT, Neu1-/-, GM3S-/- and Neu1-/-GM3S-/- mice for fortnightly from 6 weeks to 20 weeks. The weight ratios of female (B) and male (D) mice to WT mice at 20 weeks. Gross appearance of 5 -month-old WT, Neu1-/-, GM3S-/- and Neu1-/-GM3S-/- male mouse (E). 1-way-Anova analysis was used to determine p values by using GraphPad. Data were reported as means SEM (n=12 independent mice for each mice group, (*p<0,05, **p<0,025, ***p<0,001, ****p<0,0001).

The weight ratios of female and male mice to WT mice at 20 weeks were calculated (Figure 3.3 B and D). 20 weeks old body weight ratio of WT and GM3S-/- female and male mice did not showed significant difference. However, 20 weeks old body weight ratio of female Neu1-/- mice had less weight than age matched female WT mice as approximately 1.3-fold and GM3S-/- mice as approximately 1.1-fold (Figure 3.3 B). Especially, 20 weeks old body weight ratio of female Neu1-/-GM3S-/- mice showed more dramatic weight loss compared with age matched female WT, Neu1-/- and GM3S-/- mice as approximately 1.6, 1,2 and 1,4-fold, respectively (Figure 3.3 B).

20 weeks old body weight ratio of male Neu1-/- mice had also less weight than age matched male WT littermates as approximately 1.25-fold and GM3S-/- littermates as approximately 1.2-fold (Figure 3.3 D). The dramatic weight loss in the 20 weeks old body weight ratio of male Neu1-/-GM3S-/- mice was demonstrated compared to age matched male WT, Neu1-/- and GM3S-/- mice as approximately 1.8, 1,4 and 1,7-fold, respectively (Figure 3.3 D).

Gross appearance of 5 -month-old male mice was indicated in Figure 3.3 E. The differences of male mice was clear and there was no significant difference between the length of WT and GM3S-/- mouse. However, the length of Neu1-/- mouse was smaller than that of WT and GM3S-/- mouse. Especially, male Neu1-/-GM3S-/- mouse showed the smallest length compared to age matched male WT, GM3S-/- and Neu1-/- mouse. The most prominent feature of Neu1-/-GM3S-/- mouse was that it was round (Figure 3.3 E).

3.3. Thin Layer Chromatography Analysis of Brain Gangliosides

Thin layer chromatography was performed to understand the effect of lysosomal sialidase, Neu1, on the ganglioside synthesis and degradation pathway. The cortex and cerebellum brain tissues of 2- and 5-month-old WT, Neu1-/-, GM3S-/- and Neu1-/-GM3S-/- mice groups were used for thin layer chromatography analysis. The differentiation of acidic (Figure 3.4 and 3.9) and neutral gangliosides (Figure 3.7 and 3.12) for both cortex and cerebellum tissues depending on the genotype and age were determined with TLC analysis.

Acidic gangliosides (GM1, GD1a, GD1b, GM1b, GD1α and GT1b) which are isolated from cortex tissue of 2- and 5-month-old WT, Neu1-/-, GM3S-/- and Neu1-/-GM3S-/- mice were analyzed by using thin layer chromatography (Figure 3.4, 3.5 and 3.6).

Thin layer chromatography results of cortex tissue showed that -a series (GM1 and GD1a) (Figure 3.5 A and B) and -b series (GD1b and GT1b) (Figure 3.5 C and F) gangliosides did not indicate different pattern in both 2- and 5-month-old WT and Neu1-/- mice. However, these gangliosides were absent in the 2- and 5-month-old GM3S-/- and Neu1-/-GM3S-/- mice groups owing to lack of GM3 Synthase enzyme which is responsible for production of -a and -b series gangliosides besides GM3 ganglioside.

GM1b and GD1α, -o series gangliosides, compensatory expressed in the cortex tissue of 2- and 5-month-old GM3S-/- and Neu1-/-GM3S-/- mice due to blockage of GM3 synthesis in these mice groups (Figure 3.6 A and B). The GM1b and GD1α gangliosides exhibited a significant decrease in the 2-month-old Neu1-/-GM3S-/- compared to age matched GM3S-/- mice. However, this significant decrease was not determined for the 5-month-old GM3S-/- and Neu1-/-GM3S-/- mice in the cortex tissue (Figure 3.6 A and B).

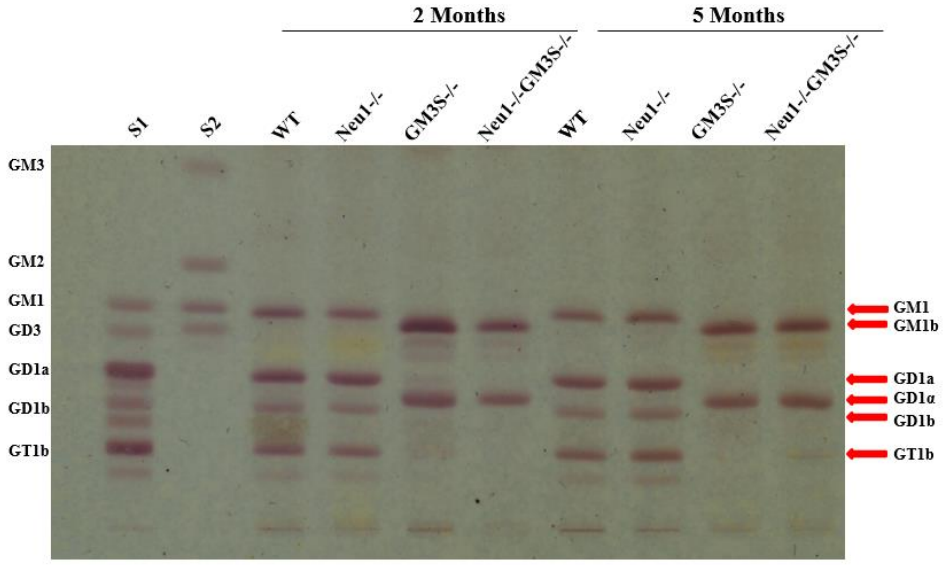

Figure 3.4. The thin layer chromatography and orcinol staining for acidic gangliosides isolated from cortex tissue of 2- and 5-month-old WT, Neu1-/-, GM3S-/- and Neu1-/-GM3S-/- mice (S1, standard for total ganglioside; S2, mixed ganglioside standard, GM3, GM2, GM1 and GD3).

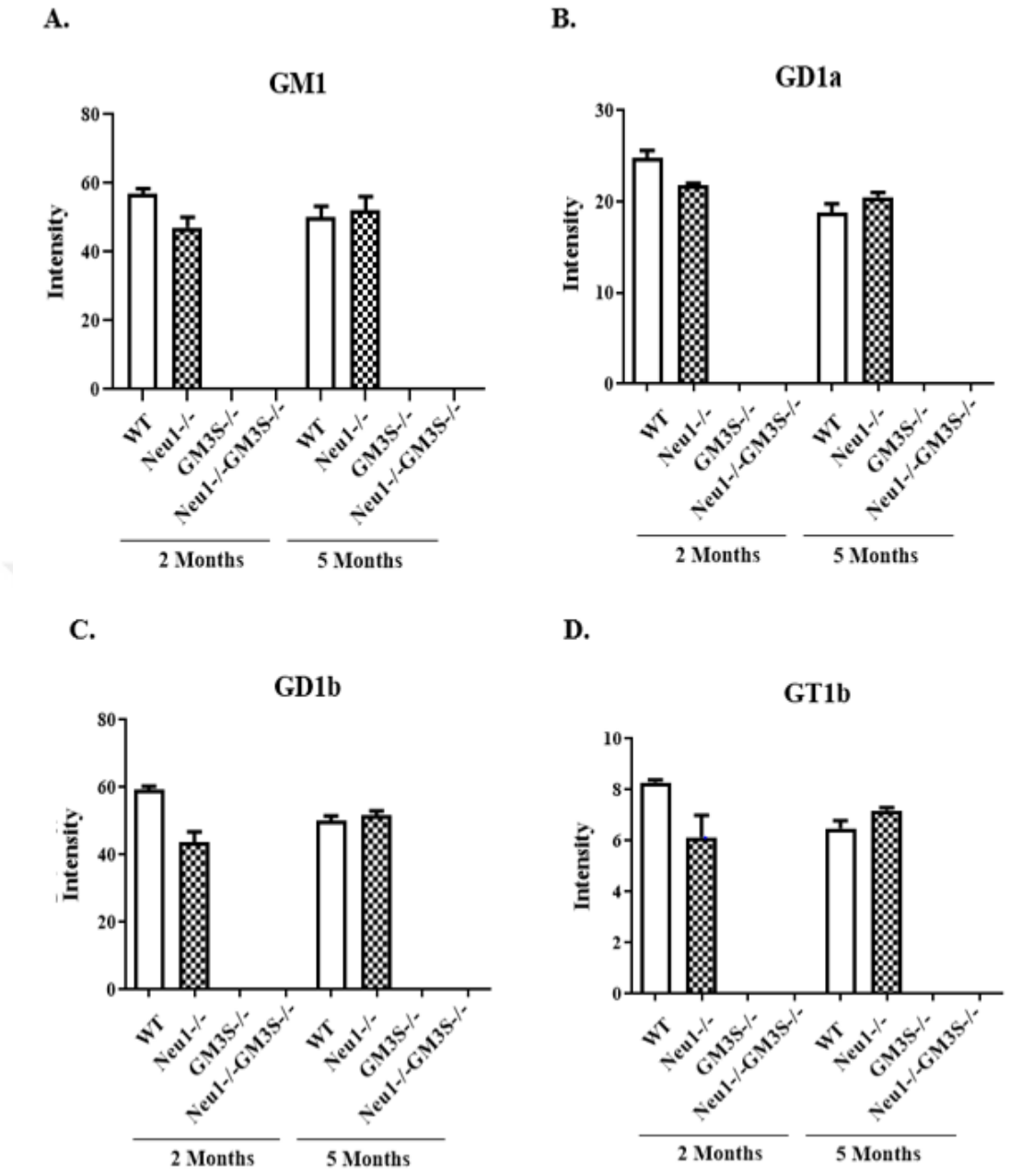

Figure 3.5. Intensity analysis of -a series GM1 (A) and GD1a (B); and -b series GD1b (C) and GT1b (D) gangliosides from cortex tissue of 2- and 5-month-old WT, Neu1-/-, GM3S-/- and Neu1-/-GM3S-/- mice. Band intensity of each ganglioside was detected with ImageJ and 2-way-Anova analysis was used to determine p values by using GraphPad. Data were reported as means SEM (n=3, ****p<0,0001).

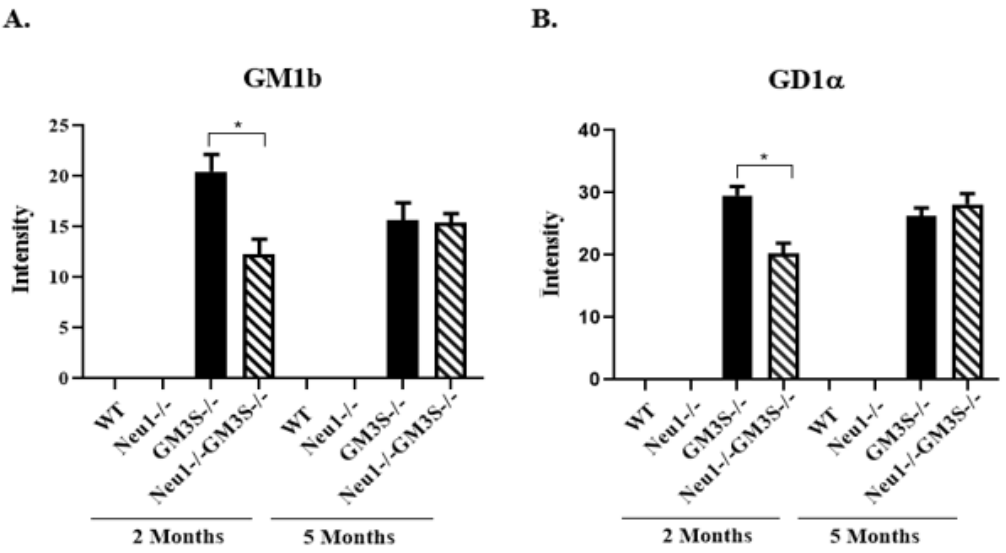

Figure 3.6. Intensity analysis of -o series GM1b (A) and GD1α (B) gangliosides from cortex tissue of 2- and 5-month-old WT, Neu1-/-, GM3S-/- and Neu1-/-GM3S-/- mice. Band intensity of each ganglioside was detected with ImageJ and 2-way-Anova analysis was used to determine p values by using GraphPad. Data were reported as means SEM (n=3, *p<0,05).

In cortex tissue, Lactosylceramide (LacCer), an intermediate for other glycosphingolipids production, was analyzed with Thin Layer Chromatography (TLC). There was no significant change between WT and Neu1-/- mice for both age groups (Figure 3.7 and 3.8 A). However, LacCer showed a significant increase level in both 2- and 5-month-old GM3S-/- and Neu1-/- GM3S-/- mice compared to aged matched WT and Neu1-/- mice (Figure 3.8 A). Accumulation of LacCer in 2- and 5-month-old GM3S-/- mice reflected blockage in the conversion of LacCer intermediate to GM3 ganglioside due to deficiency of GM3S gene. The accumulation of LacCer in Neu1-/-GM3S-/- mice at any ages resulted from GM3S gene deficient.

Lactosylceramide is also pioneer for the o- series of gangliosides that refers to GA2, GA1, GM1b and GD1c in the ganglioside pathway (Schengrund 2015). GA2 is a neutral ganglioside which is produced from the LacCer intermediate with the Galgt1 activation. GA1 ganglioside is also neutral ganglioside synthesized from the GA2 ganglioside. The expression levels of GA2 and GA1 gangliosides were compared in the distinct mice littermates for the cortex tissue (Figure 3.8 B and C). It was shown that 2- and 5-month-old GM3S-/- and Neu1-/-GM3S-/- mice had higher level of GA2 and GA1 neutral gangliosides while no expression was observed in WT and Neu1-/- littermates at any ages (Figure 3.8 B and C).

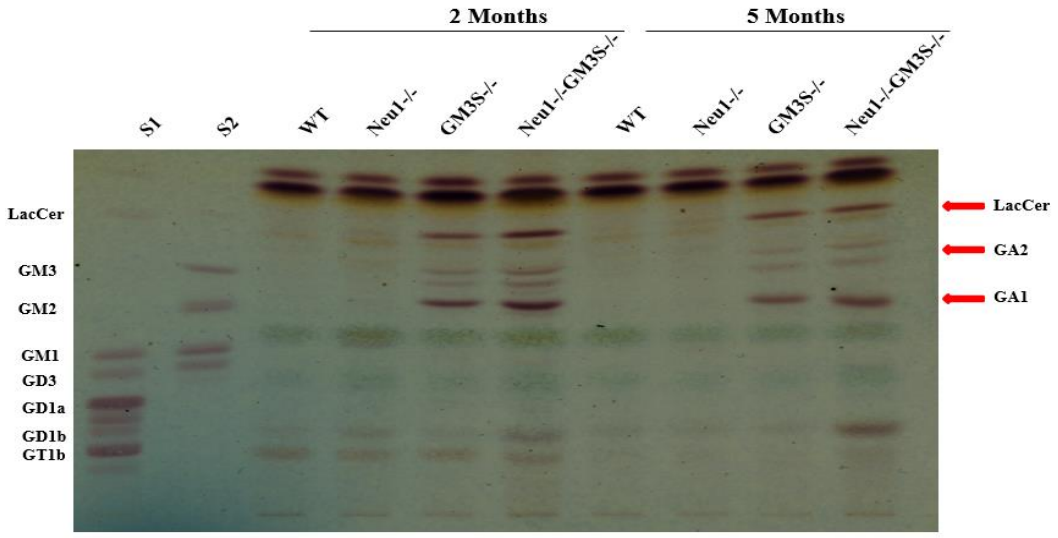

Figure 3.7. The thin layer chromatography and orcinol staining for neutral gangliosides isolated from cortex tissue of 2- and 5-month-old WT, Neu1-/-, GM3S-/- and Neu1-/-GM3S-/- mice (S1, standard for total ganglioside; S2, mixed ganglioside standard, GM3, GM2, GM1 and GD3).

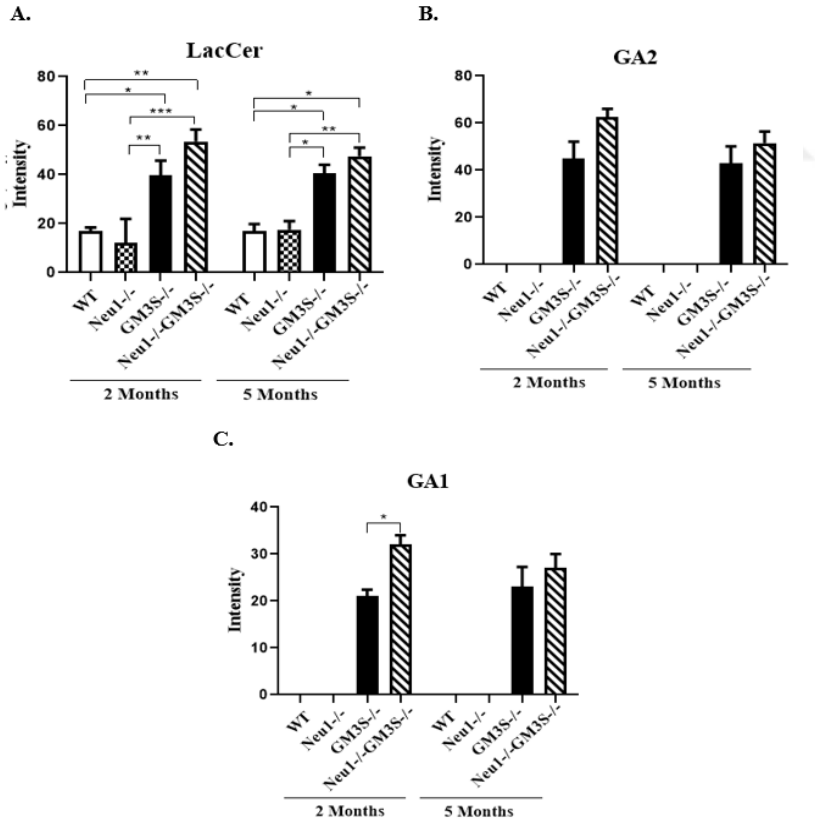

Figure 3.8. Intensity analysis of -o series LacCer (A), GA2 (B) and GA1 (C) gangliosides from cortex tissue of 2- and 5-month-old WT, Neu1-/-, GM3S-/-, Neu1-/-GM3S-/- mice. Band intensity of each ganglioside was detected with ImageJ and 2-way-Anova analysis was used to determine p values by using GraphPad. Data were reported as means SEM (n=3, *p<0,05, ****p<0,0001).

Thin layer chromatography results of cerebellum tissue indicated that -a series (GM1 and GD1a) (Figure 3.10 A and B) and -b series (GD1b and GT1b) (Figure 3.10 C and D) gangliosides were similarly expressed in both 2- and 5-month-old WT and Neu1-/- mice.

The expression of -a series (GD1a and GM1) and -b series (GT1b and GD1b) gangliosides were lack in the both ages of GM3S-/- and Neu1-/-GM3S-/- littermates since GM3 ganglioside, precursor of -a and -b series gangliosides, could not be produced in both GM3S-/- and Neu1-/-GM3S-/- mice groups in the cerebellum tissue due to deficiency of GM3S enzyme deficiency in GM3S-/- and Neu1-/-GM3S-/- mice (Figure 3.9 and 3.10).

On the other hand, -o series gangliosides such as GM1b, GalNAc-GM1b and GD1α (Figure 3.11 A, B and C) were significantly expressed in cerebellum tissue of 2- and 5-month-old GM3S-/- and Neu1-/-GM3S-/- mice although these gangliosides could not be expressed in the both ages of WT and Neu1-/- mice. The reason of highly -o series ganglioside expression in the GM3S-/- and Neu1-/-GM3S-/- mice is due to the absence of -a and -b series gangliosides.

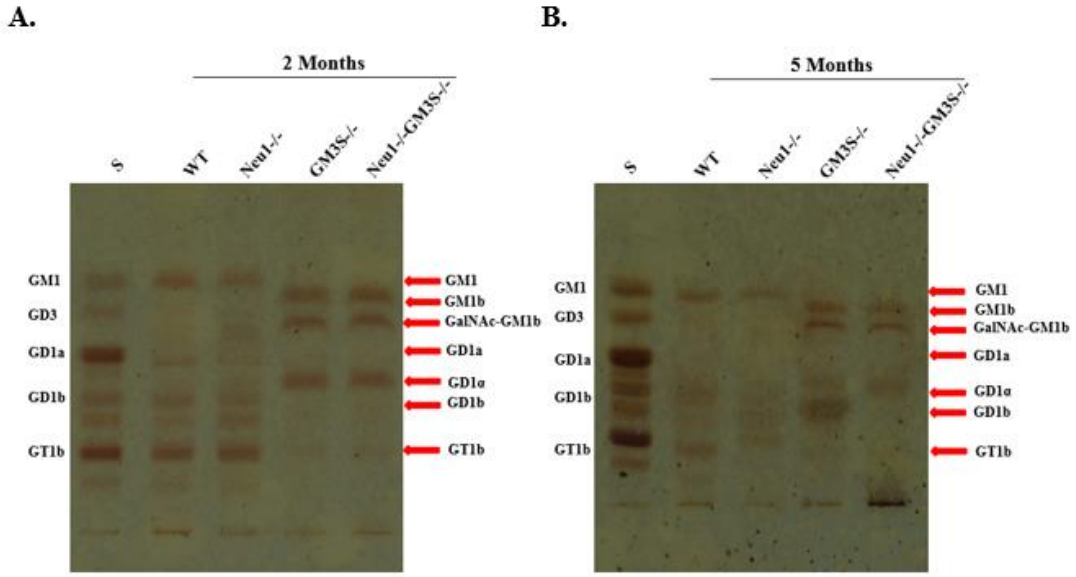

Figure 3.9. The thin layer chromatography and orcinol staining for acidic gangliosides isolated from cerebellum tissue of 2- (A) and 5- (B) month-old WT,Neu1-/- , GM3S-/- and Neu1-/-GM3S-/- mice (S, standard for total ganglioside).

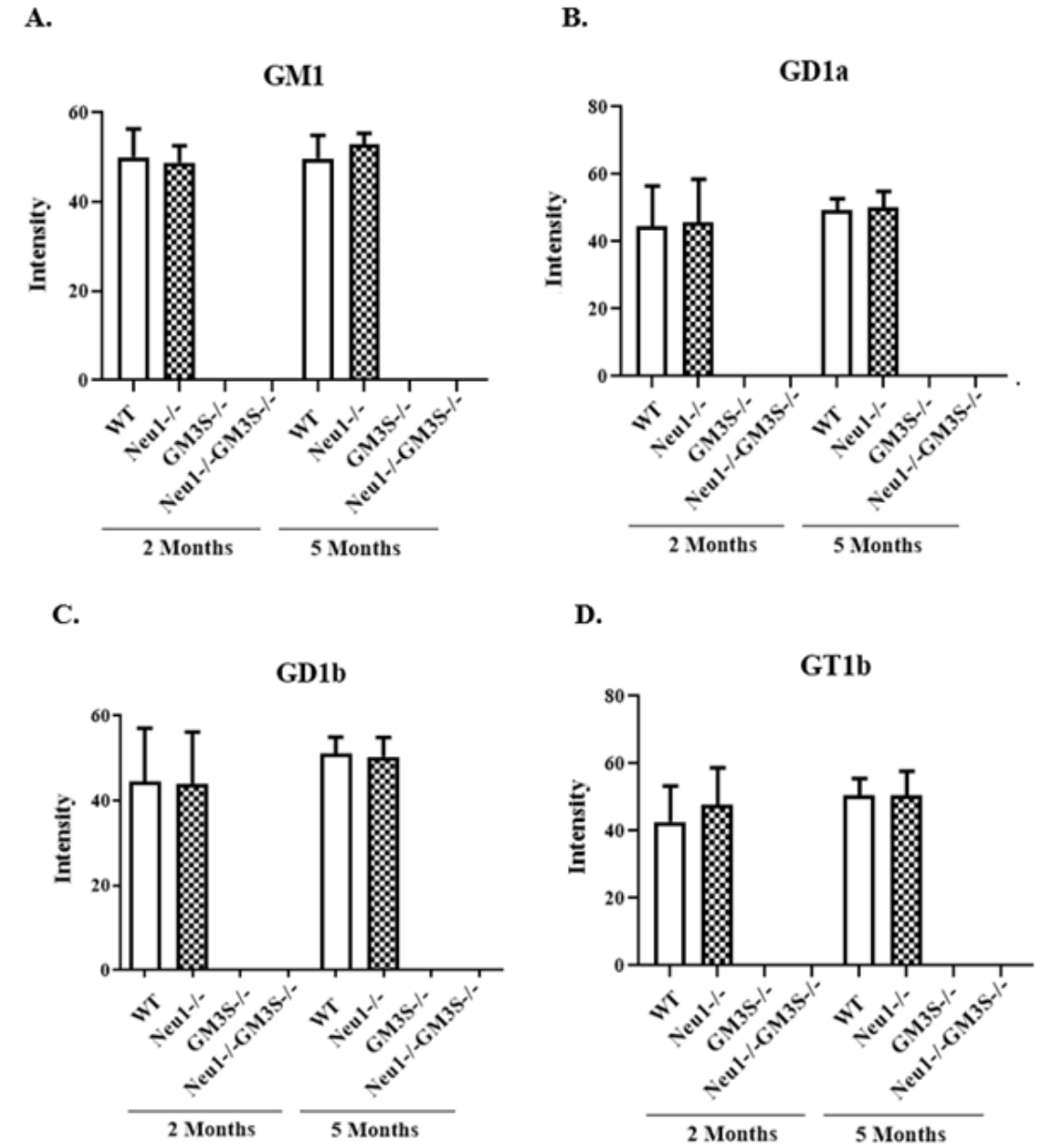

Figure 3.10. Intensity analysis of -a series GM1 (A) and GD1a (B); and GD1b (C) and GT1b (D) gangliosides from cerebellum tissue of 2- and 5-month-old WT, Neu1-/-, GM3S-/- and Neu1-/-GM3S-/- mice. Band intensity of each ganglioside was detected with ImageJ and 2-way-Anova analysis was used to determine p values by using GraphPad. Data were reported as means SEM (n=3).

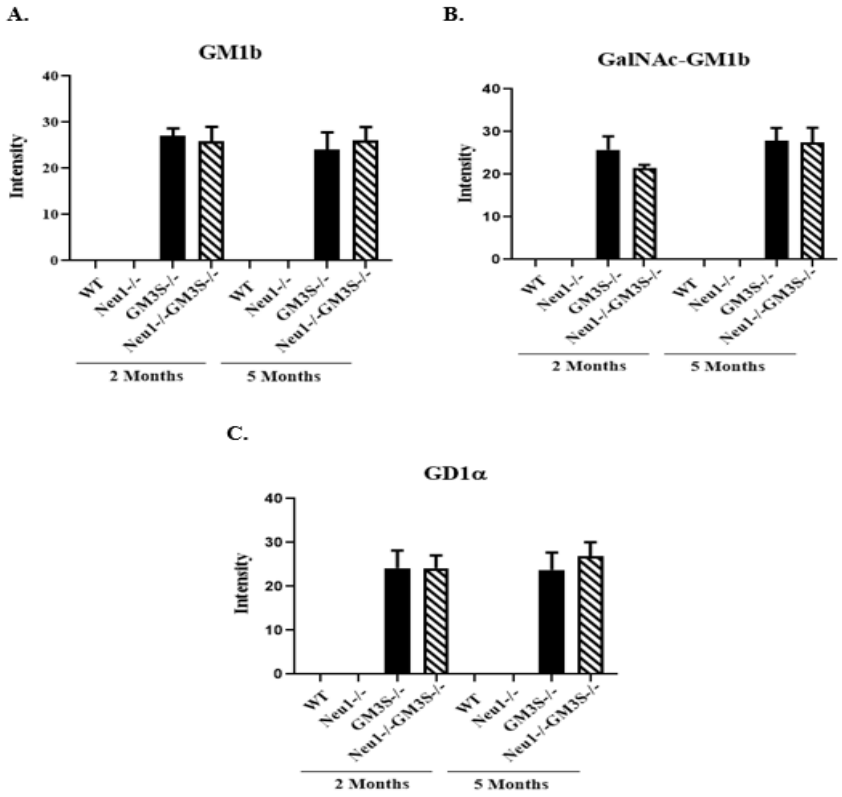

Figure 3.11. Intensity analysis of -o series GM1b (A), GalNAc-GM1b (B) and GD1α (C) gangliosides from cerebellum tissue of 2- and 5-month-old WT, Neu1-/-, GM3S-/- and Neu1-/-GM3S-/- mice. Band intensity of each ganglioside was detected with ImageJ and 2-way-Anova analysis was used to determine p values by using GraphPad. Data were reported as means SEM (n=3).

Lactosylceramide (LacCer) did not show different expression pattern in WT and Neu1-/- mice for cerebellum tissue. Its expression in WT and Neu1-/- mice at any ages showed slight expression (Figure 3.12 and 3.13 A). Especially, GM3S-/- and Neu1-/-GM3S-/- mice had higher expression level of LacCer intermediate due lack of GM3S enzyme for both age groups (Figure 3.13 A).

GA2 and GA1 gangliosides, neutral -o series gangliosides, absent in the cerebellum tissue of WT and Neu1-/- mice (Figure 3.13 B and C). The expression of GA2 and GA1 gangliosides were shown at 2 and 5 months of age GM3S-/- and Neu1-/-GM3S-/- littermates. There was slightly increase in the GA2 level in older GM3S-/- and Neu1-/-GM3S-/- mice compared to their young counterparts. Additionally, the significant increase in the GA1 ganglioside was observed in the 5-month-old GM3S-/- and Neu1-/-GM3S-/- mice compared to their young counterparts (Figure 3.13 C). This result represented the accumulation of neutral GA2 and GA1 gangliosides in age dependent manner for cerebellum tissue of GM3S-/- and Neu1-/-GM3S-/- mice.

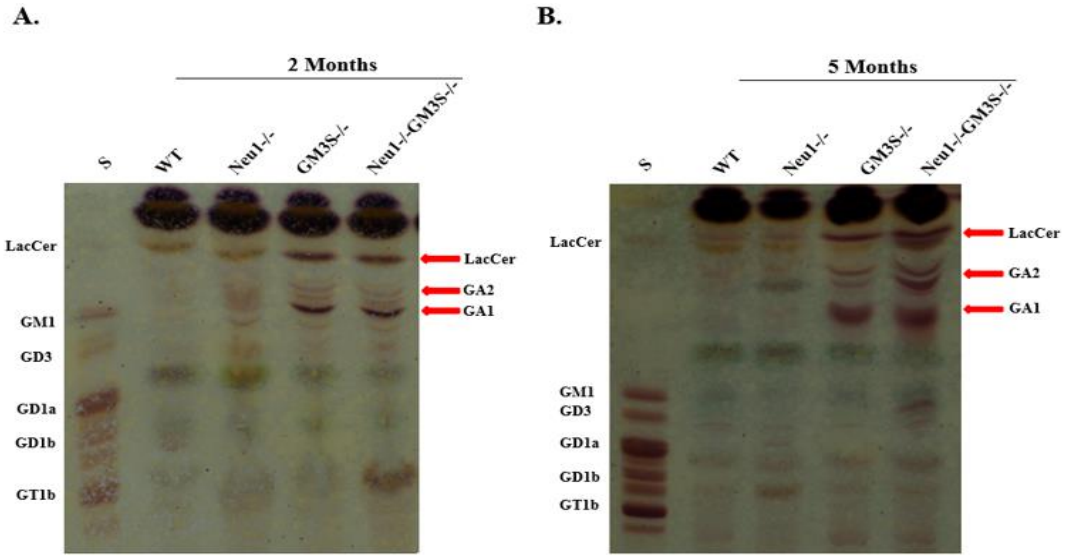

Figure 3.12. The thin layer chromatography and orcinol staining for neutral gangliosides isolated from cerebellum tissue of 2- (A) and 5- (B) month-old WT, Neu1-/-, GM3S-/- and Neu1-/-GM3S-/- mice (S, standard for total ganglioside).

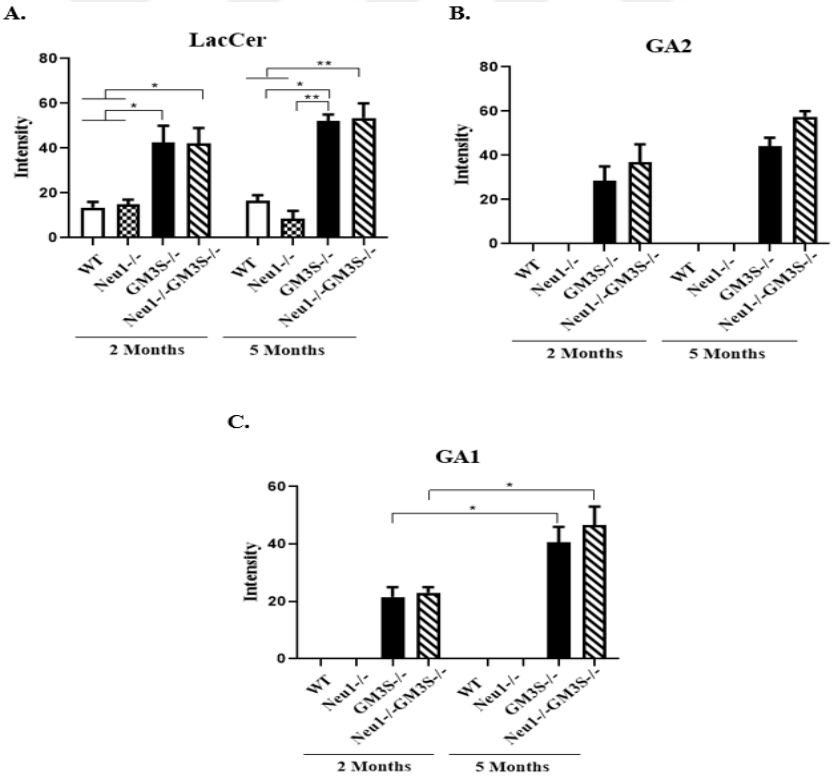

Figure 3.13. Intensity analysis of -o series LacCer (A), GA2 (B) and GA1 (C) gangliosides from cerebellum tissue of 2- and 5-month-old WT, Neu1-/-, GM3S-/- and Neu1-/-GM3S-/- mice. Band intensity of each ganglioside was detected with ImageJ and 2-way-Anova analysis was used to determine p values by using GraphPad. Data were reported as means SEM (n=3, *p<0,05, **p<0,01).

3.4. DNA Isolation and Gel Electrophoresis

DNA isolation and agarose gel electrophoresis was applied in order to determine the apoptosis depending on age and genotype. The small and fragmented DNAs except genomic DNA are indicator of the apoptosis. 2- and 5-month-old WT, Neu1-/-, GM3S-/- and Neu1-/-GM3S-/- mice were used for DNA isolation and gel electrophoresis, and cortex, cerebellum and thalamus tissues of all differently genotyped mice were analyzed

According to results of DNA isolation and agarose gel electrophoresis, there was no extra band in the 2 -month-old Neu1-/-, GM3S-/- and Neu1-/-GM3S-/- mice compared with age matched WT mice in the cortex tissue (Figure 3.14 A). However, 5 -month-old GM3S-/- and Neu1-/-GM3S-/- mice had an extra band which was not seen in the age matched WT and Neu1-/- mice. This extra band in 5 -month-old Neu1-/-GM3S-/- mice could be derived from the deficiency of GM3S gene since this band was also observed in the 5-month-old GM3S-/- mice. However, extra band was not be seen in the Neu1-/- mice (Figure 3.14 A).

In the cerebellum tissue, extra bands were only seen in the 2 -month-old Neu1-/-GM3S-/- mice although there was no any fragmented DNA in other 2 -month-old WT, Neu1-/- and GM3S-/- littermates. On the other hand, fragmented DNAs which may be indicator of apoptosis were not be observed in the 5-month-old mice groups (Figure 3.14 B).

Thalamus tissue analysis of 2- and 5-month-old mice demonstrated that there were extra bands, fragmented DNAs, in the both 2 and 5-month-old mice which had single gene deficient (Neu1-/- and GM3S-/-) mice and double gene deficient (Neu1-/-GM3S-/-) mice compared to aged-matched control groups (Figure 3.14 C).

The fragmented DNAs and smears except the genomic DNAs were more clearly observed in the thalamus tissue compared to other cortex and cerebellum tissues (Figure 3.14). According to previous studies, observed fragmented DNAs can be associated with apoptosis and also these bands may be signs of the apoptosis in differently genotyped mice.

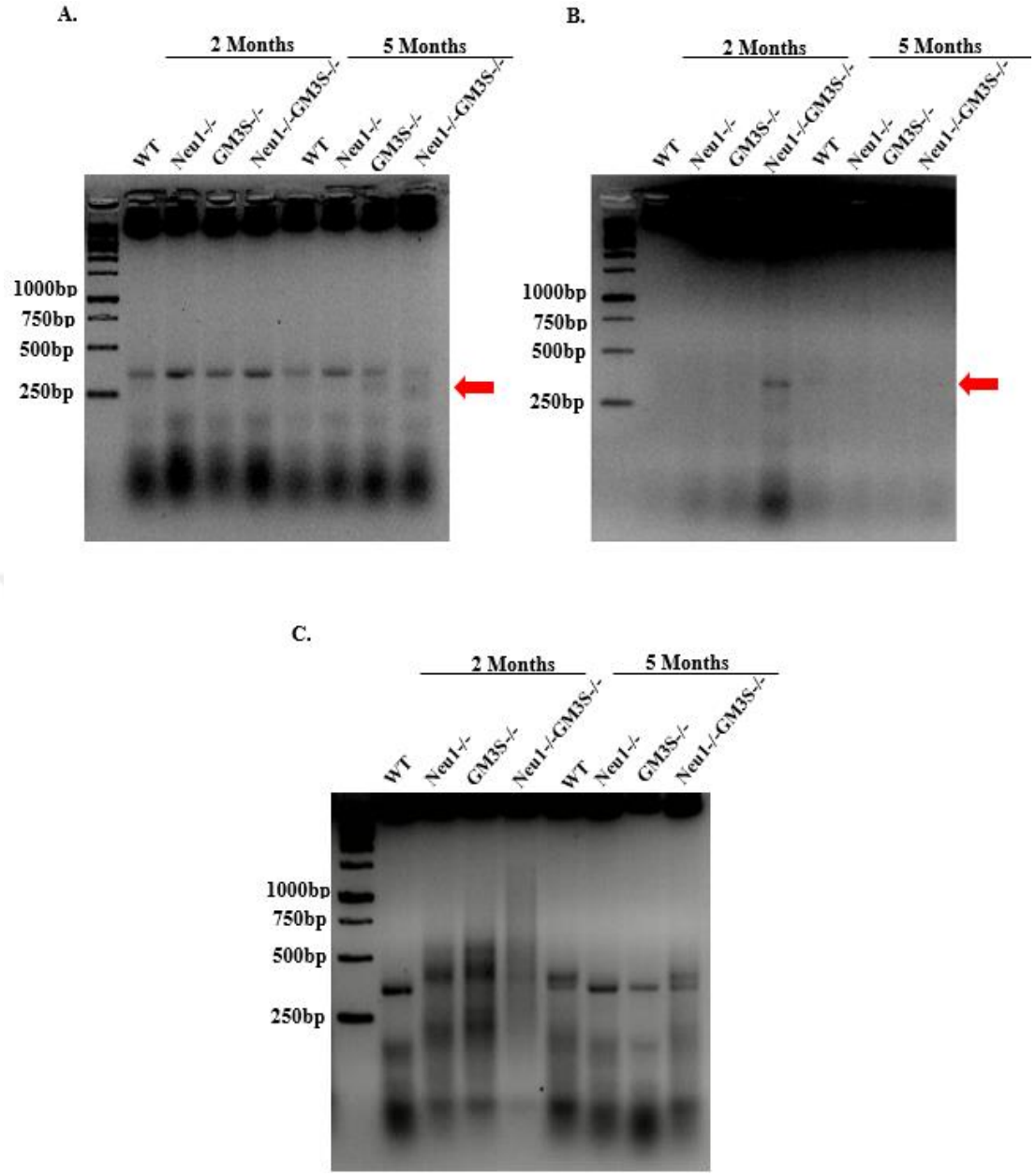

Figure 3.14. DNA isolation and gel electrophoresis for cortex (A), cerebellum (B) and thalamus (C) tissues of 2- and 5-month-old WT, Neu1-/-, GM3S-/- and Neu1-/-GM3S-/- mice (n=3).

3.5. Real Time PCR (RT-PCR)

Real Time PCR was used for analysis of ATF6, Calnexin, XBP-1 as ER stress related genes, SOD2, Catalase, TTase1 as oxidative stress related genes and Bcl-2, Bcl-XL and Bax as apoptosis related genes on mRNA level. Cortex, cerebellum and thalamus brain tissues of 2- and 5-month-old WT, Neu1-/-, GM3S-/- and Neu1-/-GM3S-/- mice

were used for Real Time PCR analysis for a deeper understanding of apoptosis and other cellular stresses which leads to apoptosis depending on changed ganglioside pattern.

In the cortex tissue, expression analysis of ATF6 gene demonstrated the elevated expression level in 2 -month-old Neu1-/- mice compared to age matched GM3S-/- and Neu1-/-GM3S-/- littermates (Figure 3.15 A). Additionally, significantly decreased in the ATF6 expression was determined in the 2 -month-old GM3S-/- and Neu1-/-GM3S-/- mice compared to age matched WT mice (Figure 3.15 A). Therefore, the reduced level of ATF6 in the 2-month-old double gene deficient mice may be due to GM3S gene deficiency. On the other hand, the significant elevated expression level of ATF6 was observed in 5-month-old Neu1-/, GM3S-/- and Neu1-/-GM3S-/- mice compared to age matched WT littermates (Figure 3.15 A). Single and double gene deficiencies may cause the increase in expression level of ATF6 in the 5-month-old mice. The reduction of ATF6 expression in the 5-month-old WT mice compared to 2-month-old WT mice was also shown (Figure 3.15 A). The significant increase of ATF6 marker was observed in 5-month-old GM3S-/- and Neu1-/-GM3S-/- mice compared to its 2-month-old counterparts, showing aging effect on ATF6 expression in the cortex tissue (Figure 3.15 A).

In the cerebellum tissue of 2- and 5-month-old animals, ATF6 expression of 5-month-old WT mice was significantly less than 2-month-old WT mice (Figure 3.15 B). 2-month-old mice groups did not show different expression pattern compared to each other. However, 5-month-old mice had some distinct expression pattern for ATF6 gene (Figure 3.15 B). There was significant increase of ATF6 expression in 5-month-old Neu1-/- mice compared to age matched WT, GM3S-/- and Neu1-/-GM3S-/- littermates (Figure 3.15 B). This result showed the elevated ER stress depending on age in cerebellum tissue of Neu1-/- mice according to gene expression analysis based on mRNA level.

There was no significant difference in the thalamus section of 2-month-old animals for ATF6 gene expression (Figure 3.15 C). However, significant increase was observed in the 5-month-old Neu1-/- mice compared to age matched WT mice, and also 5-month-old Neu1-/-GM3S-/- mice had elevated ATF6 gene expression compared to age matched WT and GM3S-/- littermates (Figure 3.15 C). These results indicated the presence of ER stress in the thalamus tissue of 5-month-old Neu1-/-, Neu1-/-GM3S-/- mice. On the other hand, expression level of ATF6 gene was higher in the 5-month-old

GM3S-/- and Neu1-/-GM3S-/- mice compared to that of young counterparts, implying age effect in the ER stress marker expression (Figure 3.15 C).

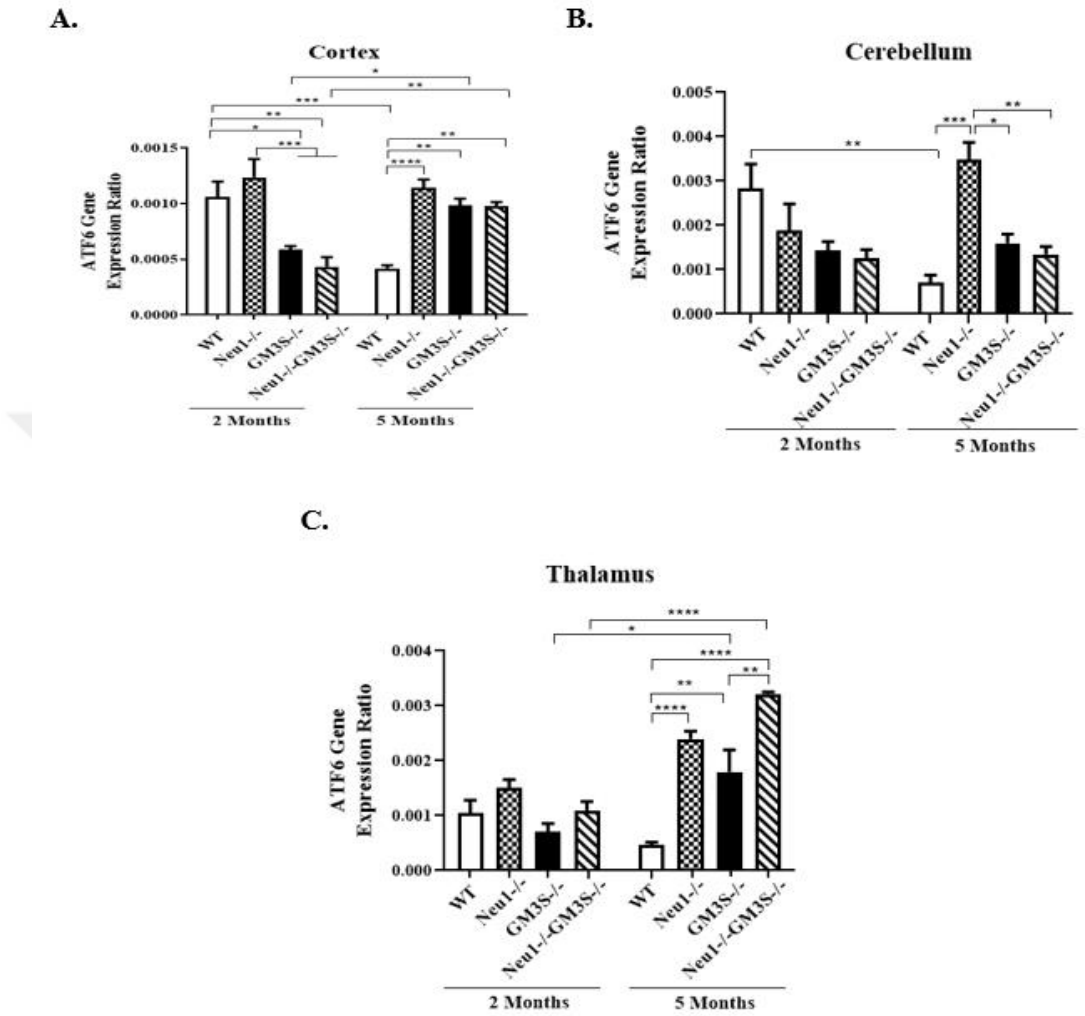

Figure 3.15. ER-stress related ATF6 gene expression levels of cortex (A), cerebellum (B), thalamus (C) tissues of 2- and 5-month-old WT, Neu1-/-, GM3S-/- and Neu1-/-GM3S-/- mice. Expression ratios were calculated with ΔCT method and 2-way-ANOVA analysis was used to determine p-values by using GraphPad. Data were reported as means SEM (n=3, *p<0,05, **p<0,01, ***p<0,001, ****p<0,0001).

Calnexin which is ER stress marker was analyzed by using RT-PCR for cortex, cerebellum and thalamus tissues. In the cortex tissue, there was no significant change in the 2-month-old mice groups for Calnexin gene expression (Figure 3.16 A). The significant increase was found in 5-month-old Neu1-/-, GM3S-/- and Neu1-/-GM3S-/- mice compared to aged matched WT mice (Figure 3.16 A). This result showed the higher ER stress in the 5-month-old single and double gene deficient mice groups.

The calnexin expression analysis results for cerebellum indicated that there was only elevated level of Calnexin in the 5-month-old Neu1-/- mice compared to 5-month-old WT mice (Figure 3.16 B). These results implied that Neu1-/- mice in older groups have higher ER stress in the cerebellum tissue.

In the thalamus tissue, the significant increase in the expression level of Calnexin was determined in the 2-month-old Neu1-/-GM3S-/- mice compared to age matched WT mice, but no significant difference was detected in the other 2-month-old animals (Figure 3.16 C). In 5-month-old animals, the significant elevated expression level of Calnexin was observed in 5-month-old Neu1-/-, GM3S-/- and especially Neu1-/-GM3S-/- mice compared to that of WT littermates. Therefore, it can be said that single and double gene deficiency may cause the increase of ER stress in the aged mice groups.

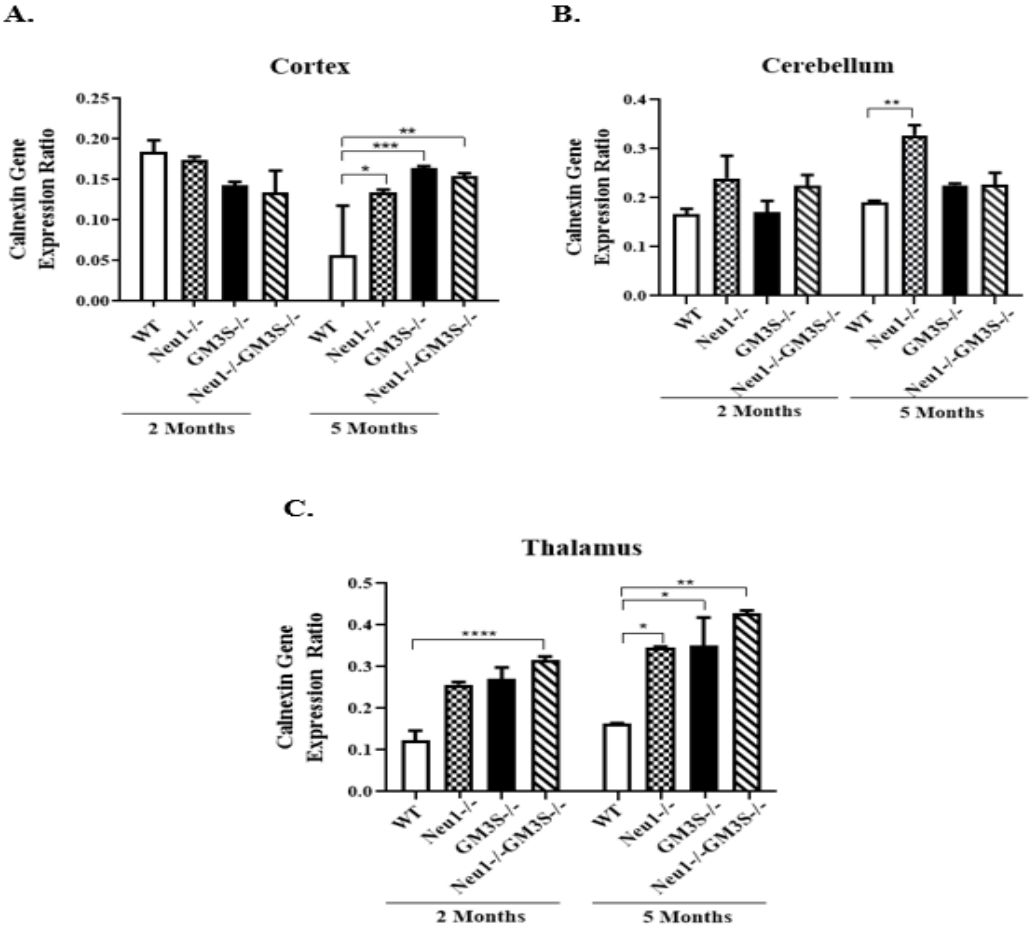

Figure 3.16. ER-stress related Calnexin gene expression levels of cortex (A), cerebellum (B), thalamus (C) tissues of 2- and 5-month-old WT, Neu1-/-, GM3S -/- and Neu1-/-GM3S-/- mice. Expression ratios were calculated with ΔCT method and 2-way-ANOVA analysis was used to determine p-values by using GraphPad. Data were reported as means SEM (n=3, *p<0,05, **p<0,01, ***p<0,001).

In the cortex tissue, the significant increase of XBP-1 gene expression was found in 2-month-old GM3S-/- mice compared to age matched WT and Neu1-/- mice (Figure 3.17 A). Additionally, 5-month-old GM3S-/- mice showed higher XBP-1 expression compared to age matched Neu1-/- and Neu1-/-GM3S-/- mice. On the other hand, the reduction of XBP-1 expression was observed in the 5-month-old WT, Neu1-/-, GM3S-/- and Neu1-/-GM3S-/- mice compared to 2-month-old counterparts (Figure 3.17 A). In the cerebellum and thalamus tissues, no significant change was detected in the expression level of XBP-1 for different age and genotyped mice groups (Figure 3.17 B and C).

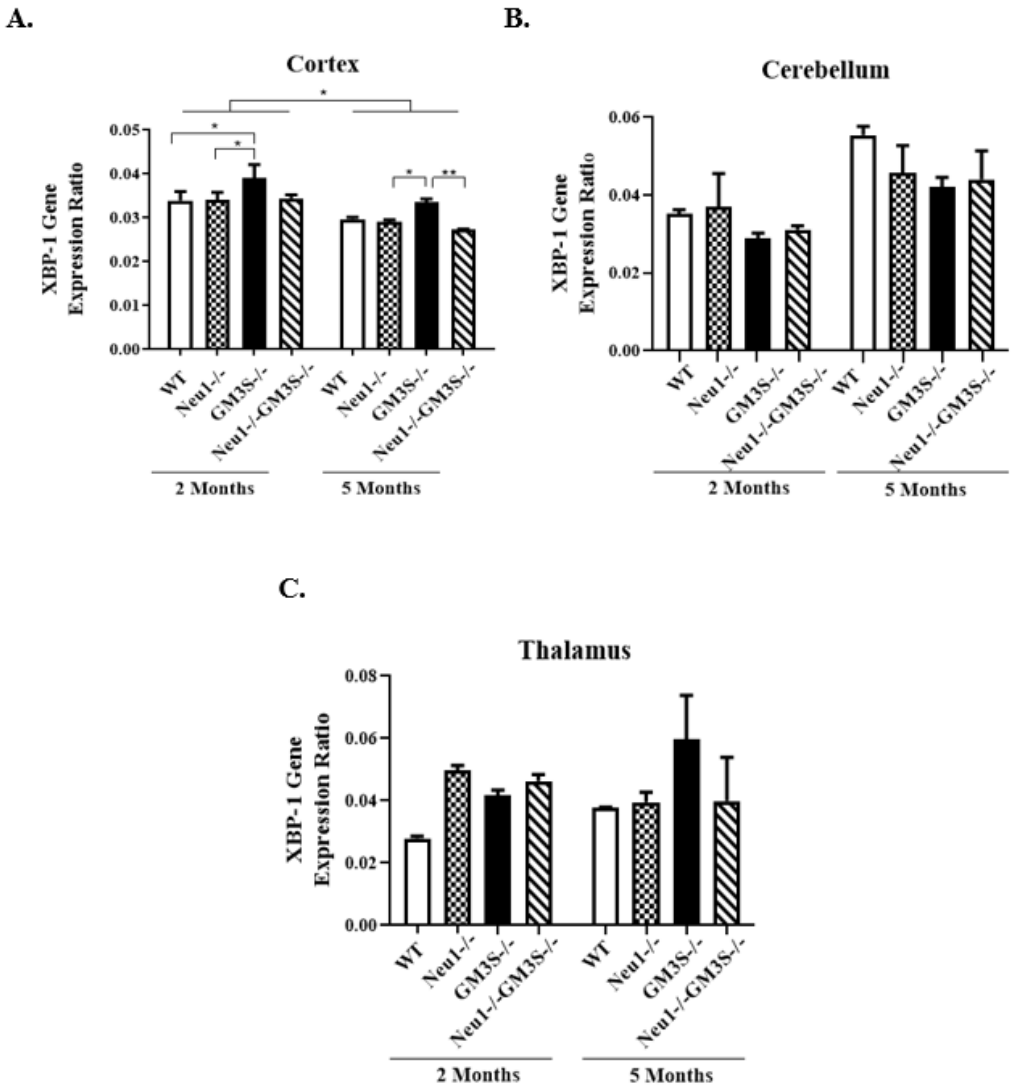

Figure 3.17. ER-stress related XBP-1 gene expression levels of cortex (A), cerebellum (B), thalamus (C) tissues of 2- and 5-month-old WT, Neu1-/-, GM3S-/- and Neu1-/-GM3S-/- mice. Expression ratios were calculated with ΔCT method and 2-way-ANOVA analysis was used to determine p-values by using GraphPad. Data were reported as means SEM (n=3, *p<0,05, **p<0,01).

In the cortex tissue, the expression level of SOD2 was lower in 2-month-old Neu1-/- mice compared to age matched WT and Neu1-/-GM3S-/- mice. Additionally, all 2-month-old mice groups had higher expression level of SOD2 compared to their 5-month-old counterparts. On the other hand, there was increase in the SOD2 expression level in 5-month-old GM3S-/- and Neu1-/-GM3S-/- mice compared to both 5 -month-old WT and Neu1-/- mice (Figure 3.18 A).

The SOD2 expression level in the cerebellum tissue did not indicate significant difference among 2-month-old mice groups. However, several significant changes in the SOD2 expression level were observed in the 5-month-old animals (Figure 3.18 B). Especially, 5-month-old Neu1-/- mice showed significant elevated level in the SOD2 gene compared to age matched WT, GM3S-/- and Neu1-/-GM3S-/- mice. Additionally, 5-month-old Neu1-/- mice demonstrated elevated SOD2 expression level compared to its young counterparts, implying elevated oxidative stress in cerebellum tissue of 5-month-old Neu1-/- mice (Figure 3.18 B).

The significantly elevated SOD2 expression was shown in the 2-month-old Neu1-/-GM3S-/- mice compared to that of WT and GM3S-/- littermates in the thalamus tissue (Figure 3.18 C). In the 5-month-old animals, Neu1-/- mice indicated elevated level in the SOD2 expression when compared to that of WT and GM3S-/- mice, while GM3S-/- and Neu1-/-GM3S-/- mice had higher SOD2 expression level than age matched WT mice in the thalamus tissue (Figure 3.18 C). The significant increase was also shown in 5-month-old Neu1-/- mice compared to 2-month-old Neu1-/- mice. The similar expression pattern was indicated in the 5-month-old GM3S-/- mice compared its young littermates (Figure 3.18 C).

For catalase gene expression of cortex tissue, only significant increase was indicated in 2-month-old Neu1-/- mice compared to that of GM3S-/- mice. In addition to 2-month-old Neu1-/- mice, 5-month-old Neu1-/- mice had increased catalase gene expression compared to WT and Neu1-/-GM3S-/- littermates of the same age groups (Figure 3.19 A). For Neu1-/-, GM3S-/- and Neu1-/-GM3S-/- mice, all older groups had elevated expression level of Catalase than young mice counterparts (Figure 3.19 A).

No significant change of catalase expression was detected in the cerebellum tissue for all distinct age and genotyped mice groups (Figure 3.19 B).

For thalamus section, there was increase in the expression level of Catalase in both young and older Neu1-/-, GM3S-/- and Neu1-/-GM3S-/- compared to age matched WT

littermates. Together, 5-month-old Neu1-/- and Neu1-/-GM3S-/- mice had higher expression level of catalase than 2-month-old counterparts (Figure 3.19 C).

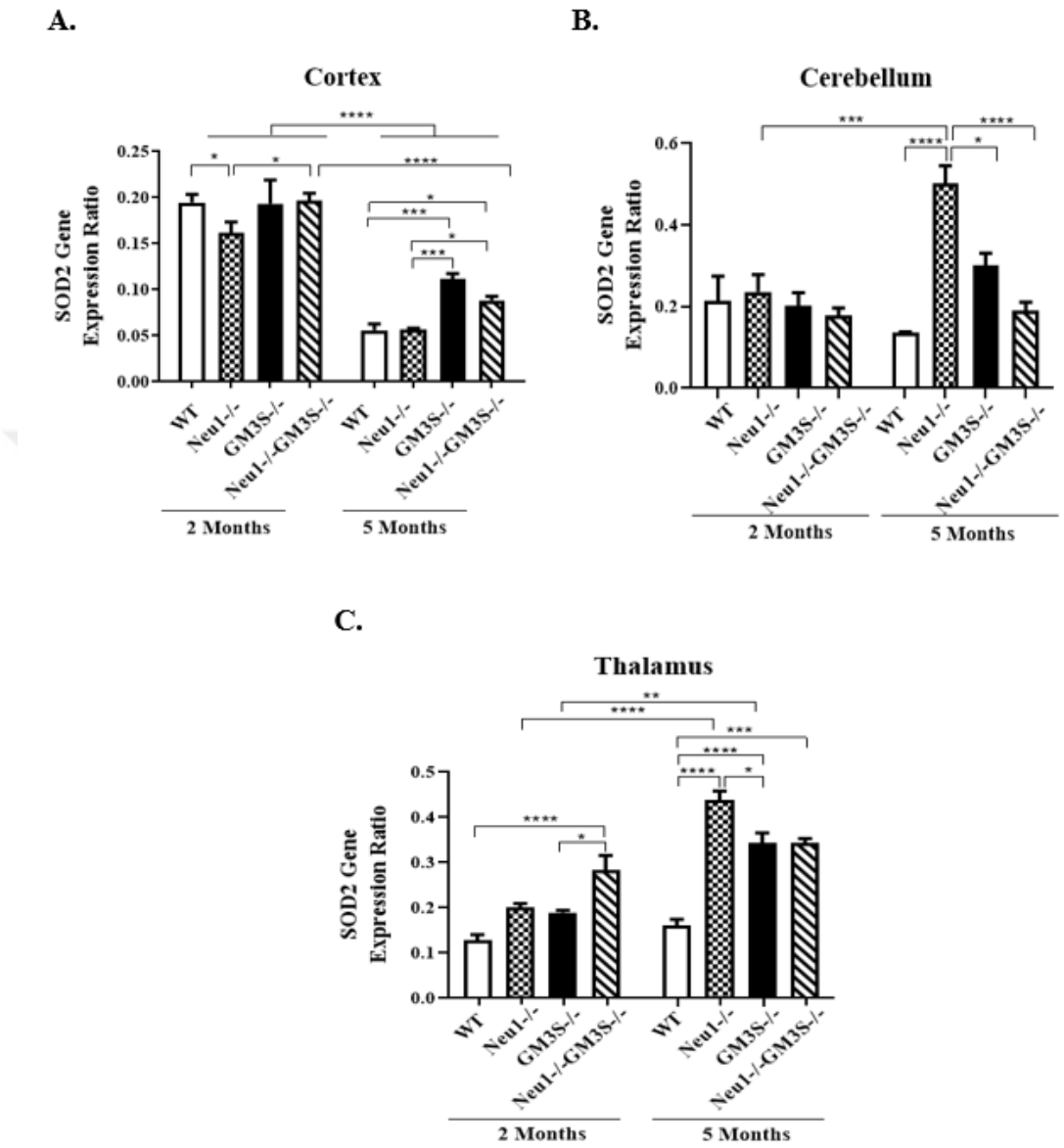

Figure 3.18. Oxidative stress related SOD2 gene expression levels of cortex (A), cerebellum (B), thalamus (C) tissues of 2- and 5-month-old WT, Neu1-/-, GM3S-/- and Neu1-/-GM3S-/- mice. Expression ratios were calculated with ΔCT method and 2-way-ANOVA analysis was used to determine p-values by using GraphPad. Data were reported as means SEM (n=3, *p<0,05, **p<0,01, ***p<0,001, ****p<0,0001).

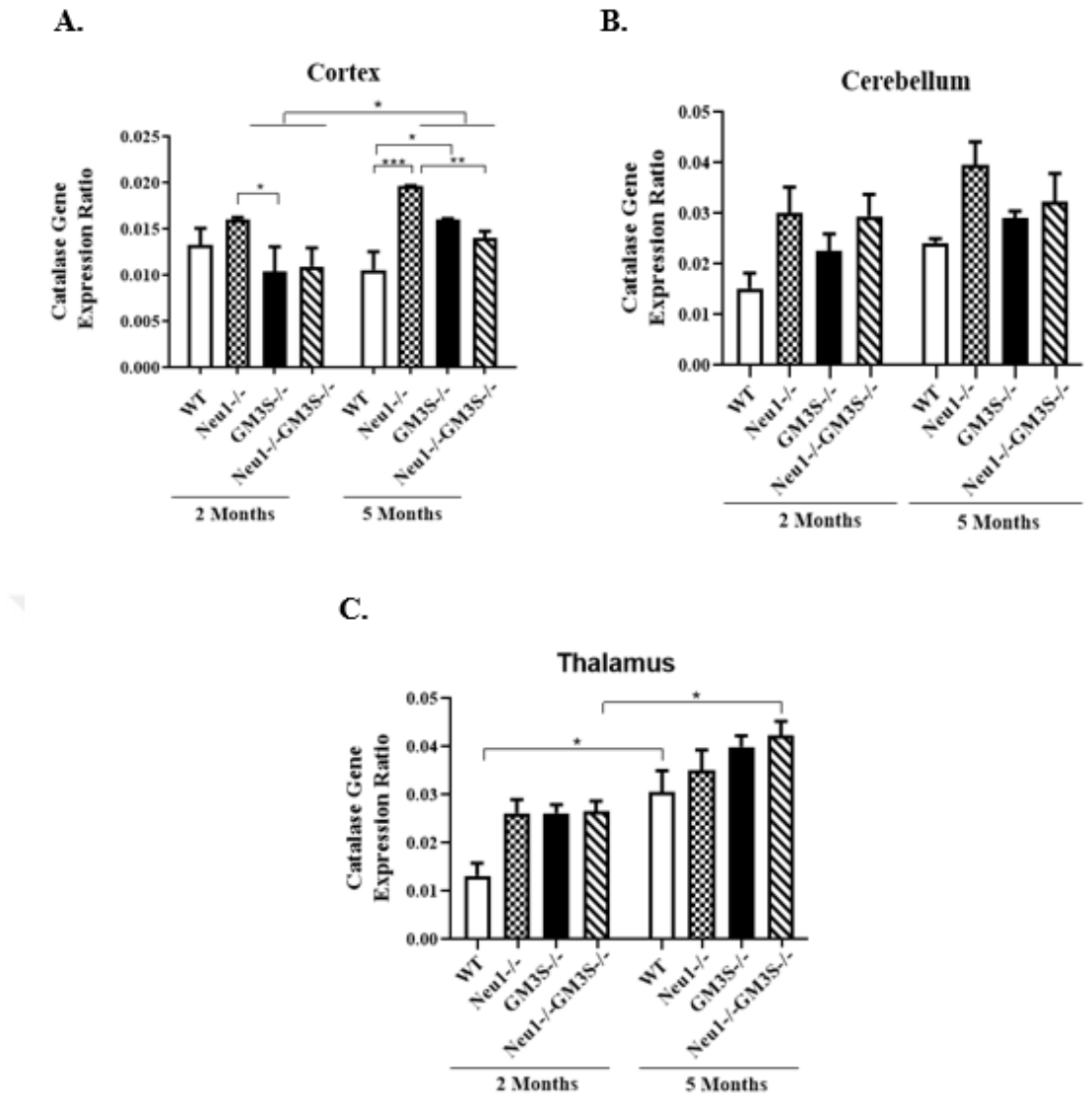

Figure 3.19. Oxidative stress related Catalase gene expression levels of cortex (A), cerebellum (B), thalamus (C) tissues of 2- and 5-month-old WT, Neu1-/-, GM3S-/- and Neu1-/-GM3S-/- mice. Expression ratios were calculated with ΔCT method and 2-way-ANOVA analysis was used to determine p-values by using GraphPad. Data were reported as means SEM (n=3, *p<0,05, **p<0,01, ***p<0,001).

2-month-old Neu1-/-GM3S-/- mice in the cortex indicated elevated expression level of TTase1 than age matched WT, Neu1-/, GM3S-/- littermates. 2-month-old GM3S-/- mice showed increase in the expression level for TTase1 comparing to that of WT and Neu1-/- littermates (Figure 3.20 A). Additionally, 5-month-old GM3S-/- mice had significantly elevated expression level compared to that of WT mice (Figure 3.20A). For WT, GM3S-/- and Neu1-/-GM3S-/- mice, all older groups had lower expression level of TTase1 than young mice counterparts (Figure 3.20 A).

In the cerebellum section, there was no significant difference in the TTase1 expression of 2-month-old mice. However, the significant increase in the TTase1 expression was shown in 5-month-old Neu1-/- mice compared to aged matched WT and GM3S-/-mice, showing increased oxidative stress in the older Neu1-/- mice (Figure 3.20 B). Older Neu1-/- and GM3S-/- mice groups had also higher TTase1 expression level than their younger counterparts (Figure 3.20 B).

For thalamus section, 2-month-old GM3S-/- and Neu1-/-GM3S-/- mice demonstrated elevated TTase1 expression level for oxidative stress marker compared to that of WT littermates (Figure 3.20 C). Although there was slightly increase in the 2-month-old Neu1-/- mice for TTase1 expression compared to age matched WT, it was not found as significant. In the 5-month-old mice groups, the expression level of TTase1 was higher in the Neu1-/-, GM3S-/-, and Neu1-/-GM3S-/- mice compared to age matched WT littermates in the thalamus section (Figure3.20 C). The older group Neu1-/-, GM3S-/-, Neu1-/-GM3S-/- mice indicated excessive expression than their conjugates in the young group (Figure3.20 C).

Bcl-2, anti-apoptotic gene, expression in the cortex showed the reduction in the 2-month-old Neu1-/-GM3S-/-mice compared to that of WT littermates (Figure 3.21 A). On the other hand, 5-month-old GM3S-/- mice had higher antiapoptotic gene expression compared to other 5-month-old WT and Neu1-/-GM3S-/- littermates and 2-month-old GM3S-/- mice (Figure 3.21 A).

Anti-apoptotic gene Bcl-2 did not show any important different expression level in the distinct age and genotype mice groups in the cerebellum tissue of brain (Figure 3.21 B).

In thalamus section, 2-month-old Neu1-/-, GM3S-/- and Neu1-/-GM3S-/- mice indicated higher Bcl-2 expression level than age matched WT mice (Figure 3.21 C). Additionally, the expression level of anti-apoptotic gene was lower in the 5-month-old double gene deficient mice than age-matched WT, GM3S-/- and 2-month-old Neu1-/-GM3S-/- mice (Figure 3.21 C).

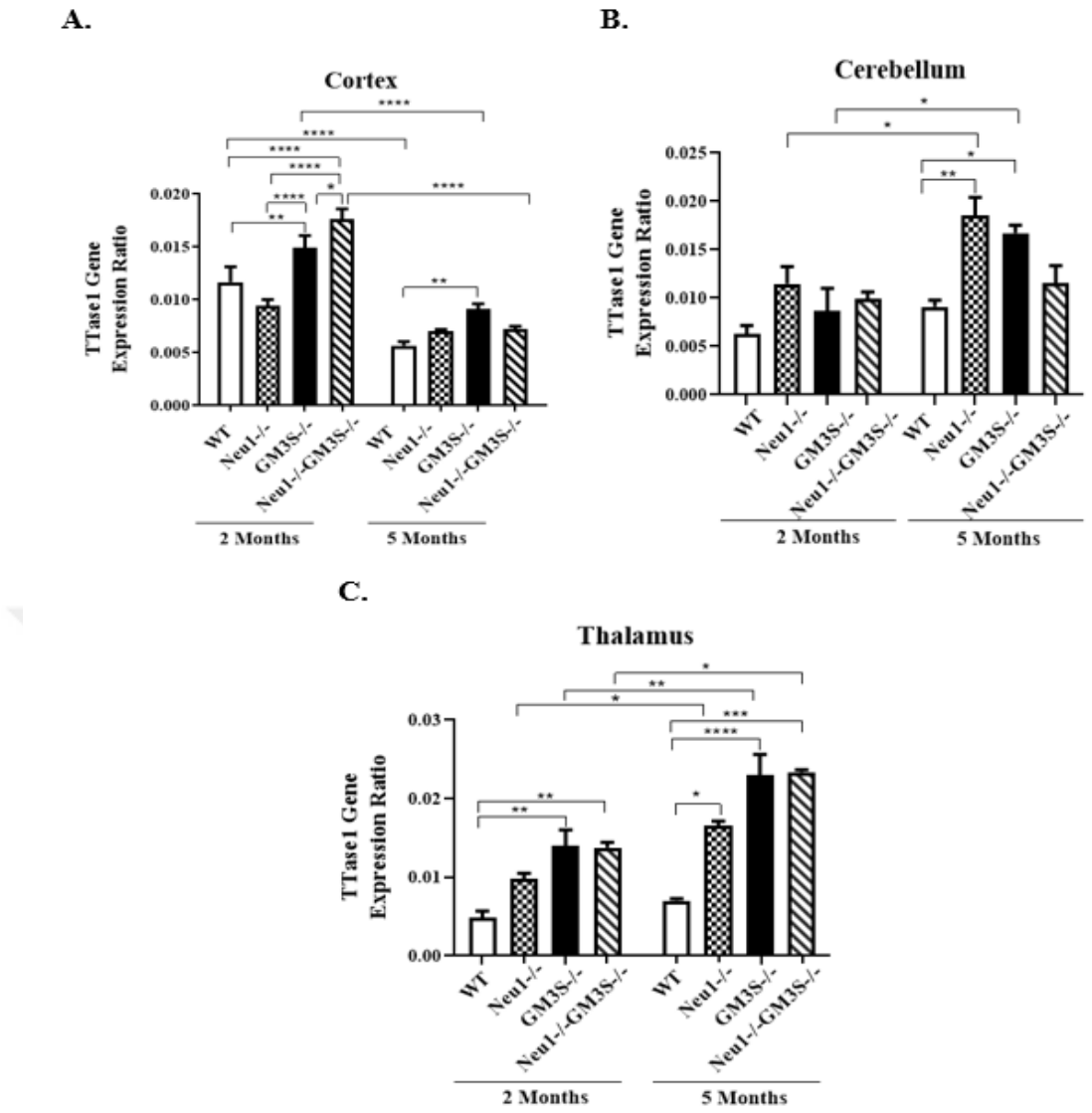

Figure 3.20. Oxidative stress related TTase1 gene expression levels of cortex (A), cerebellum (B), thalamus (C) tissues of 2- and 5-month-old WT, Neu1-/-, GM3S-/- and Neu1-/-GM3S-/- mice. Expression ratios were calculated with ΔCT method and 2-way-ANOVA analysis was used to determine p-values by using GraphPad. Data were reported as means SEM (n=3, *p<0,05, **p<0,01, ***p<0,001, ****p<0,0001).

The expression level of Bcl-XL, known as anti-apoptotic gene, was higher in the cortex of 5-month-old Neu1-/- mice compared to other 5-month-old differently genotyped mice groups (Figure 3.22 A). In cortex, 5-month-old Neu1-/- mice showed elevated anti-apoptotic gene expression compared to young counterparts, while 5-month-old GM3S-/- and Neu1-/-GM3S-/- mice demonstrated significantly and slightly reduced in the expression for anti-apoptotic gene compared to their young counterparts, respectively (Figure 3.22 A).

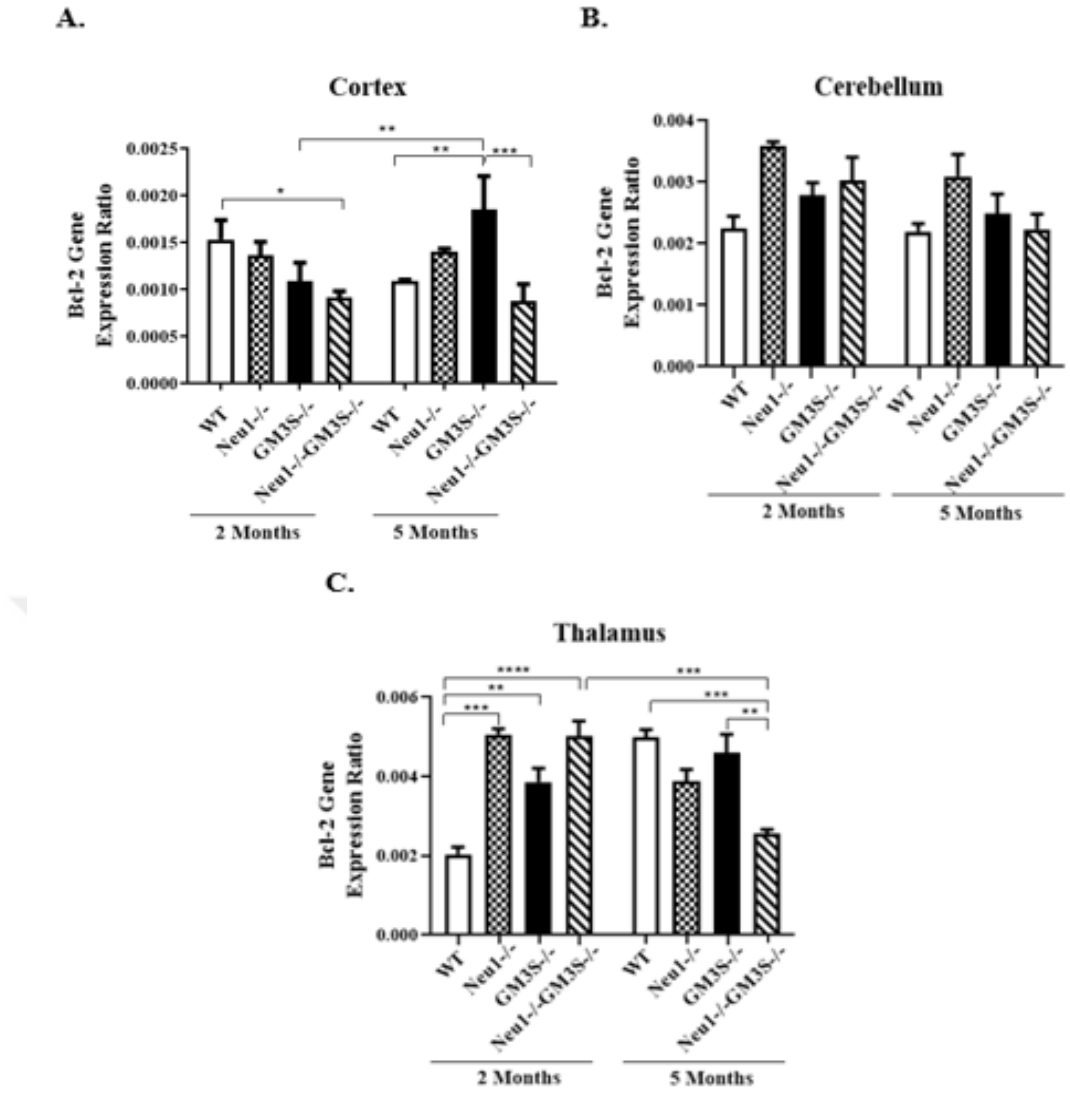

Figure 3.21. Anti-apoptotic Bcl-2 gene expression levels of cortex (A), cerebellum (B), thalamus (C) tissues of 2- and 5-month-old WT, Neu1-/-, GM3S-/- and Neu1-/-GM3S-/- mice. Expression ratios were calculated with ΔCT method and 2-way-ANOVA analysis was used to determine p-values by using GraphPad. Data were reported as means SEM (n=3, *p<0,05, **p<0,01, ***p<0,001, ****p<0,0001).

No significant change was displayed depending on age and genotype in the cerebellum tissue for Bcl-XL gene expression (Figure 3.22 B).

In the thalamus section, 5-month-old double deficient mice showed reduction in the expression level of Bcl-XL compared to age matched Neu1-/- littermates and young counterparts (Figure 3.22 C).

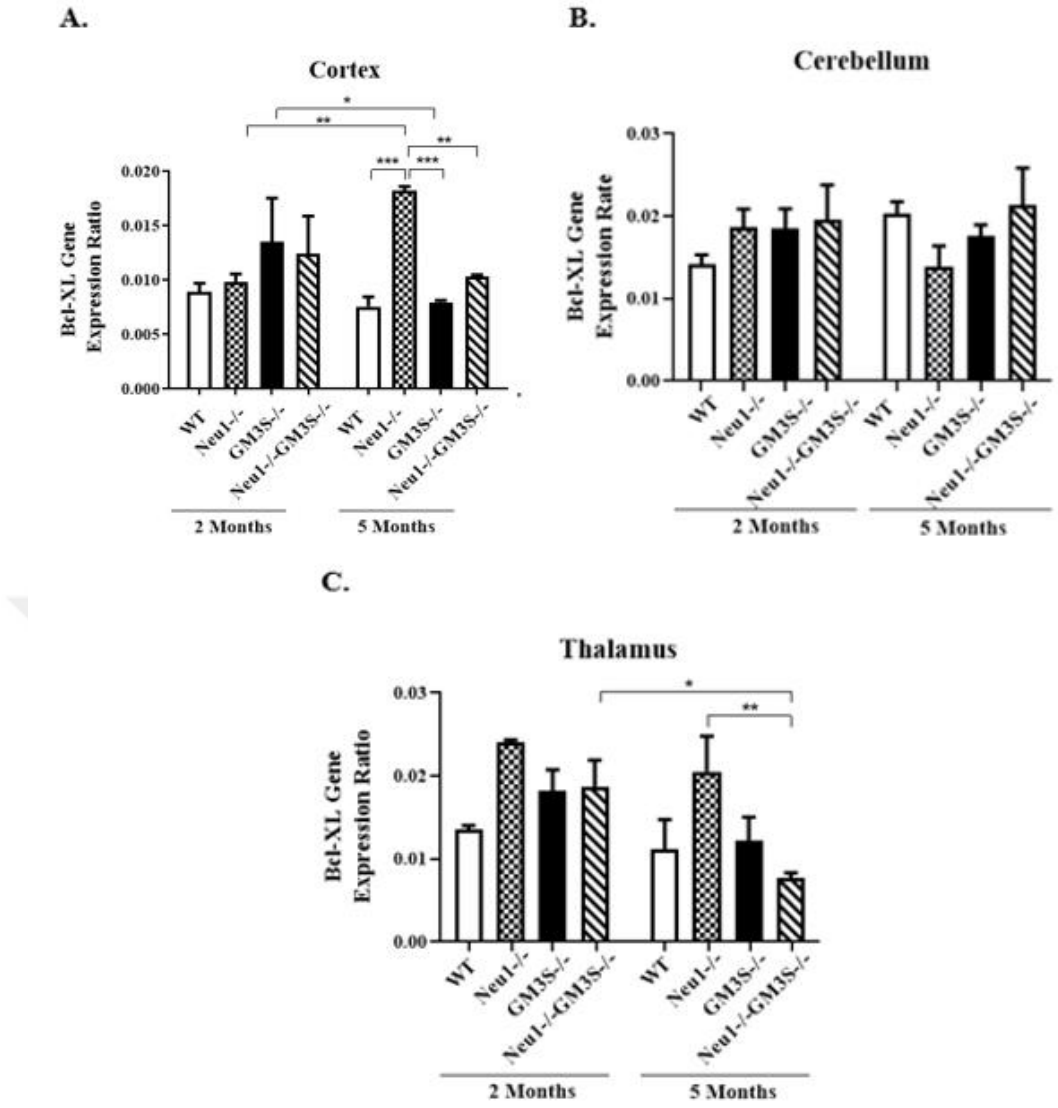

Figure 3.22. Anti-apoptotic Bcl-XL gene expression levels of cortex (A), cerebellum (B), thalamus (C) tissues of 2- and 5-month-old WT, Neu1-/-, GM3S-/- and Neu1-/-GM3S-/- mice. Expression ratios were calculated with ΔCT method and 2-way-ANOVA analysis was used to determine p-values by using GraphPad. Data were reported as means SEM (n=3, *p<0,05, **p<0,01, ***p<0,001, ****p<0,0001).

The expression level of Bax in the cortex section, no significant change was found in the 2- and 5-month-old mice. However, there was significantly increase in the Bax expression level in 5-month-old Neu1-/-GM3S-/- mice compared to 2-month-old Neu1-/-GM3S-/- mice (Figure 3.23 A).

In the cerebellum tissue, 2-month-old Neu1-/-GM3S-/- mice had higher expression level than that of Neu1-/- littermates. Additionally, there was significantly increase in the apoptotic gene (Bax) expression level in the 5-month-old Neu1-/- mice

compared to 5-month-old WT, GM3S-/-, Neu1-/-GM3S-/- and 2-month-old Neu1-/- mice (Figure 3.23 B).

In the thalamus region of brain, 2-month-old Neu1-/-GM3S-/- mice demonstrated elevated Bax, apoptotic gene, expression level than 2-month-old WT mice (Figure 3.23 C). The similar expression pattern was shown in the 5-month-old Neu1-/-GM3S-/- mice compared to that of WT mice (Figure 3.23 C).

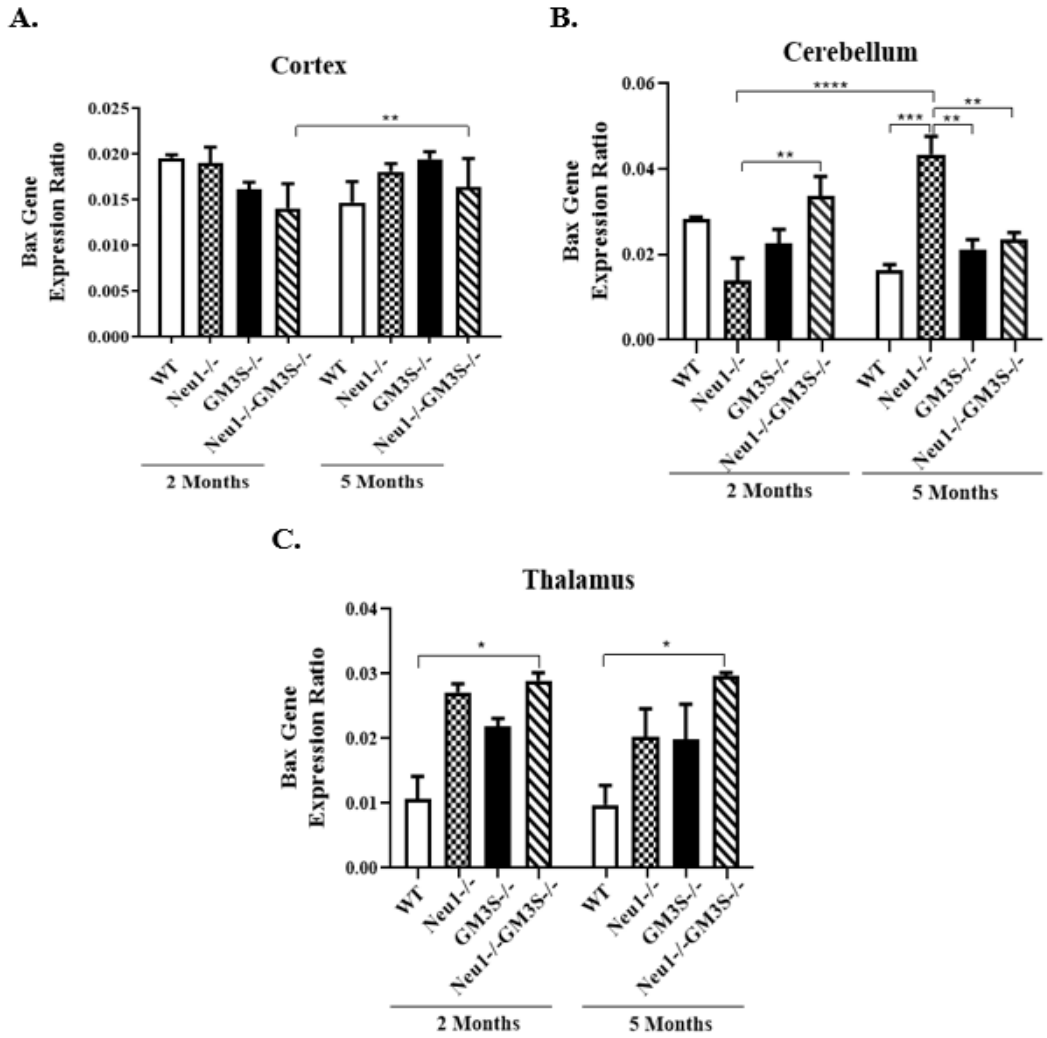

Figure 3.23. Apoptotic Bax gene expression levels of cortex (A), cerebellum (B), thalamus(C) tissues of 2- and 5-month-old WT, Neu1-/-, GM3S-/- and Neu1-/-GM3S-/- mice. Expression ratios were calculated with ΔCT method and 2-way-ANOVA analysis was used to determine p-values by using GraphPad. Data were reported as means SEM (n=3, *p<0,05, **p<0,01, ***p<0,001, ****p<0,0001).

3.6. Western Blot Analysis

It was goaled to show that how possible abnormalities in glycosphingolipid metabolism due to single and double gene deficiency affect the cell death (apoptosis) with Western Blot analysis. Fas-Ligand which plays role in the extrinsic pathway and Caspase 9 and Caspase 3 that responsible in the intrinsic pathway of apoptosis were analyzed on protein level. In addition to apoptosis related genes, endoplasmic reticulum (ER) stress related gene BiP were analyzed by using Western Blot analysis in the 2- and 5-month-old WT, Neu1-/-, GM3S-/- and Neu1-/-GM3S-/- mice. Cortex, cerebellum and thalamus tissues of animals were analyzed.

In cortex tissue, the expression level of Fas Ligand did not exhibit obvious difference in the both 2- and 5-month-old WT, Neu1-/-, GM3S-/- and Neu1-/-GM3S-/- mice (Figure 3.24 A and B).

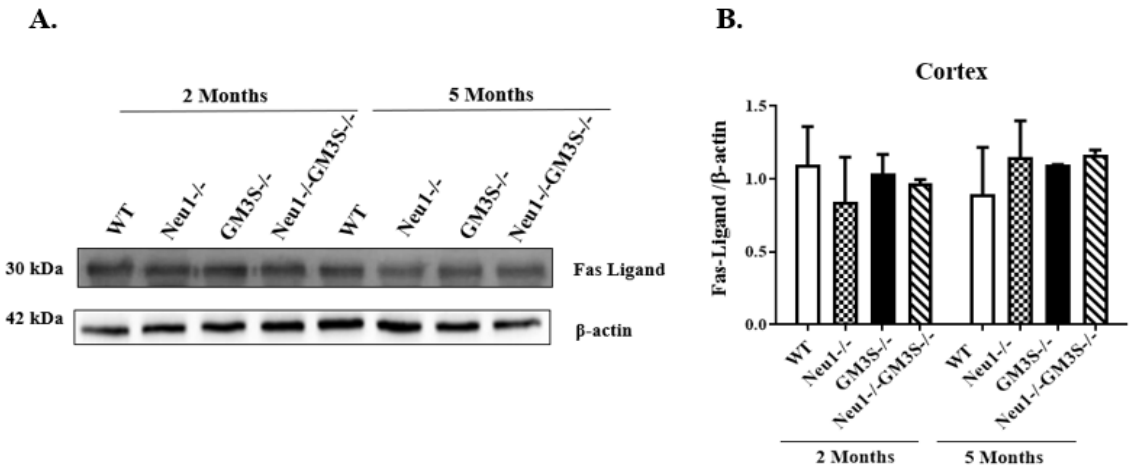

Figure 3.24. Western blot analysis of Fas Ligand in cortex tissue of 2- and 5-month-old WT, Neu1-/-, GM3S-/-, Neu1-/-GM3S-/- mice (A). Intensity analysis of Fas Ligand for 2- and 5-month WT, Neu1-/-, GM3S-/- and Neu1-/-GM3S-/- mice (B). β-actin was used as control. Intensity of each band was detected by using ImageJ and normalized to β-actin intensity. 2-way-Anova analysis was used to determine p-values via GraphPad. Data were reported as means SE (n=3).

The expression level of cleaved caspase 9 in 2 -month-old Neu1-/- mice showed slight increase compared to that of WT littermates. The significant elevated level was observed compared to age matched GM3S-/- mice (Figure 3.25 A and B). Although there

was no significant difference between the 2 -month-old GM3S-/- and Neu1-/-GM3S-/- mice, the slight elevated level of the cleaved caspase 9 in 2 -month-old Neu1-/-GM3S-/- comparing to its GM3S-/- littermates may be associated with the deficiency of Neu1 gene in double gene deficient mice.

The expression level of cleaved caspase 9 did not show noticeable difference between 5-month-old WT and GM3S-/- mice (Figure 3.25 A and B). 5-month-old Neu1-/- mice exhibited detectable change compared to age matched WT, GM3S-/- and Neu1-/-GM3S-/- mice, implying the presence of apoptosis in Neu1-/- mice. The reason of significant increase in 5-month-old Neu1-/-GM3S-/- mice compared to age matched GM3S-/- mice may be related with the deficiency of Neu1 gene in Neu1-/-GM3S-/- mice.

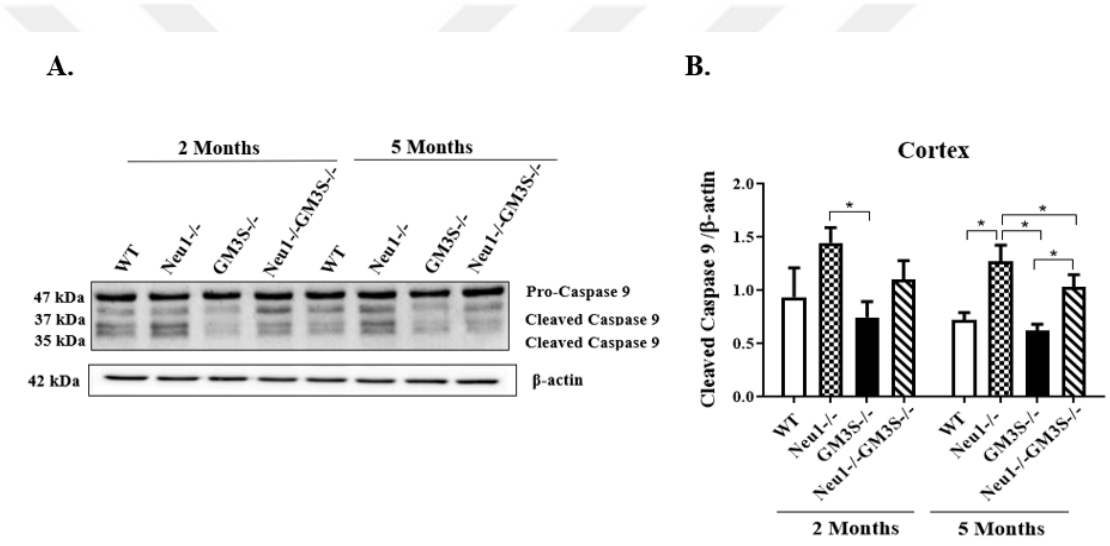

Figure 3.25. Western blot analysis of Caspase 9 in cortex tissue of 2- and 5-month-old WT, Neu1-/-, GM3S-/-, Neu1-/-GM3S-/- mice (A). Intensity analysis of Caspase 9 for 2- and 5-month WT, Neu1-/-, GM3S-/- and Neu1-/-GM3S-/- mice (B). β-actin was used as control. Intensity of each band was detected by using ImageJ and normalized to β-actin intensity. 2-way-Anova analysis was used to determine p-values via GraphPad. Data were reported as means SE (n=3, *p<0,05).

There was no significant change in the expression level of cleaved caspase 3 in 2-month-old WT, Neu1-/-, GM3S-/- and Neu1-/-GM3S-/- mice in cortex tissue. However, significant increase was detected in the 5-month-old Neu1-/- mice compared to its WT, GM3S-/- and Neu1-/-GM3S-/- littermates (Figure 3.26 A and B). Neu1 gene deficiency may have contributes the elevated level of cleaved caspase 3 in the 5-month-old Neu1-/-

GM3S-/- mice since expression of caspase 3 in 5-month-old GM3S-/-mice was like age matched WT.

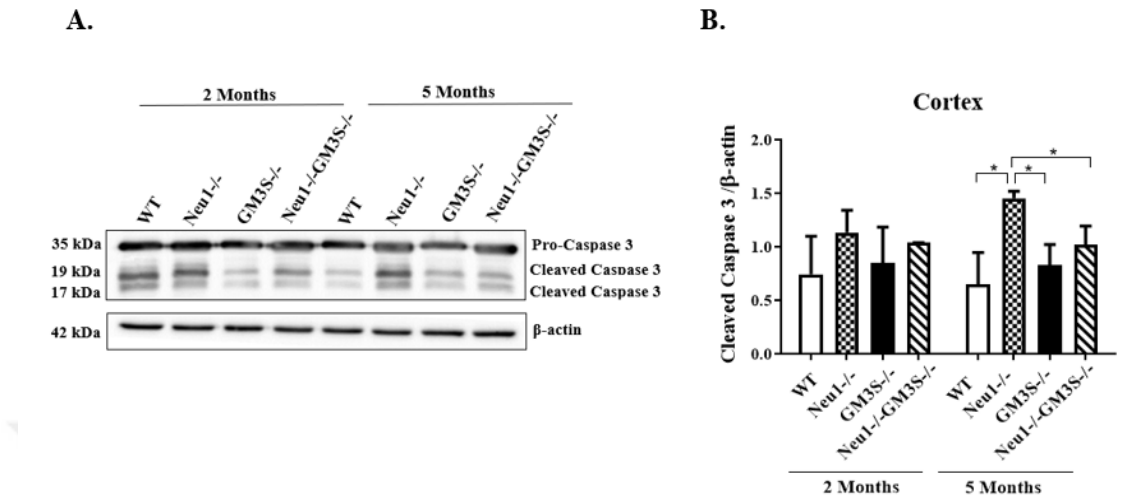

Figure 3.26. Western blot analysis of Caspase 3 in cortex tissue of 2- and 5-month-old WT, Neu1-/-, GM3S-/-, Neu1-/-GM3S-/- mice (A). Intensity analysis of Caspase 3 for 2- and 5-month WT, Neu1-/-, GM3S-/- and Neu1-/-GM3S-/- mice (B). β-actin was used as control. Intensity of each band was detected by using ImageJ and normalized to β-actin intensity. 2-way-Anova analysis was used to determine p-values via GraphPad. Data were reported as means SE (n=3, *p<0,05).

Expression analysis of ER stress related gene, BiP, showed no significant difference in cortex tissue, but there was slight increase in 2-month-old Neu1-/-GM3S-/- mice compared to its WT littermates (Figure 3.27 A and B).

In 5-month-old animals, no significant change for BiP expression was found between the cortex tissue of WT and Neu1-/- mice. However, increasing expression of BiP in 5-month-old Neu1-/- was detected comparing to that of Neu1-/-GM3S-/- littermates. This elevated expression may be indicator of higher level of ER stress in older Neu1-/- mice (Figure 3.27 B). The low expression level of BiP in 5-month-old Neu1-/-GM3S-/- mice may be associated with GM3S gene deficiency since GM3S-/- mice had lower BiP expression level than Neu1-/- littermates (Figure 3.27 B).

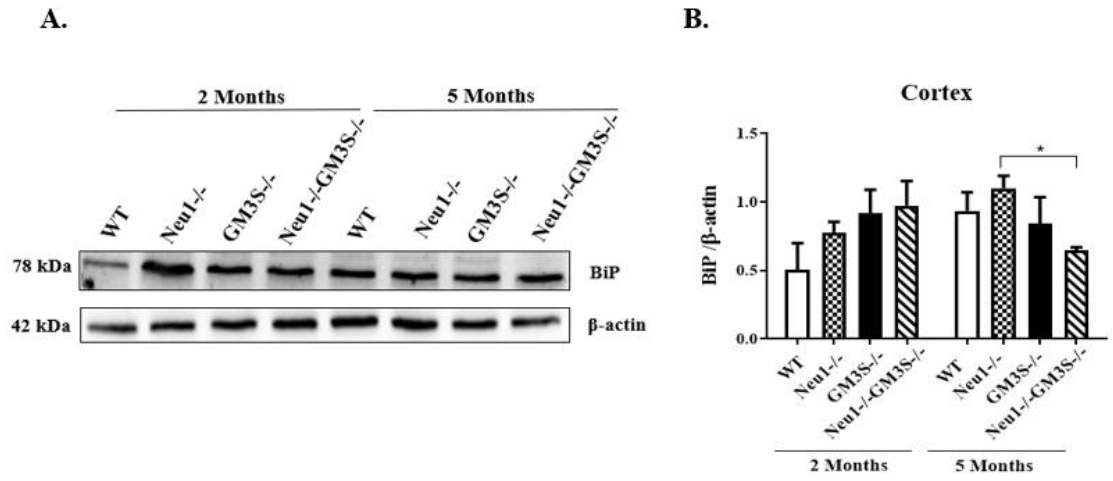

Figure 3.27. Western blot analysis of BiP in cortex tissue of 2- and 5-month-old WT, Neu1-/-, GM3S-/-, Neu1-/-GM3S-/- mice (A). Intensity analysis of BiP for 2- and 5-month-old WT, Neu1-/-, GM3S-/- and Neu1-/-GM3S-/- mice (B). β-actin was used as control. Intensity of each band was detected by using ImageJ and normalized to β-actin intensity. 2-way-Anova analysis was used to determine p-values via GraphPad. Data were reported as means SE (n=3, *p<0,05).

In western blot analysis of cerebellum tissue for Fas-Ligand, any obvious change was not detected depending on distinct age and genotyped mice (Figure 3.28 A and B).

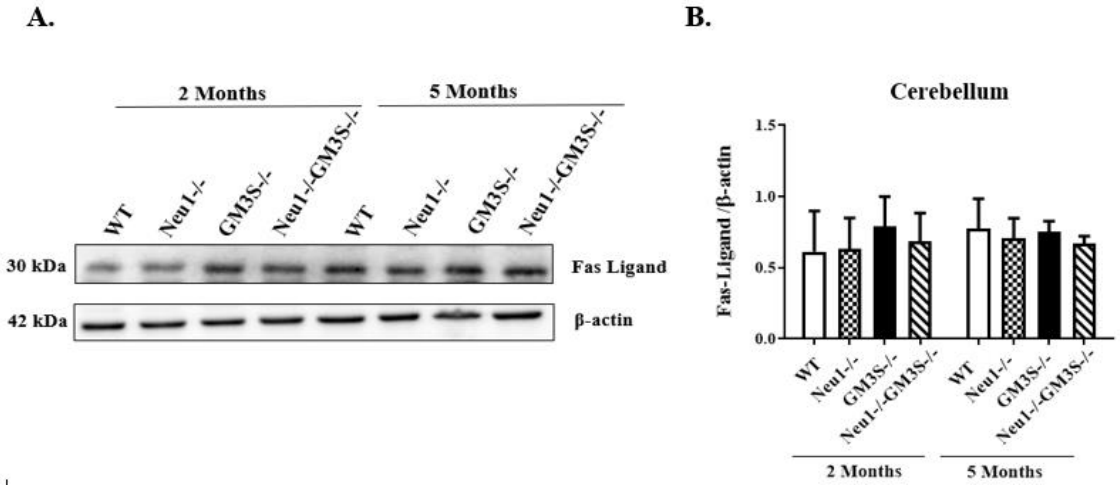

Figure 3.28. Western blot analysis of Fas Ligand in cerebellum tissue of 2- and 5-month-old WT, Neu1-/-, GM3S-/-, Neu1-/-GM3S-/- mice (A). Intensity analysis of Fas Ligand for 2- and 5-month-old WT, Neu1-/-, GM3S-/- and Neu1-/-GM3S-/- mice (B). β-actin was used as control. Intensity of each band was detected by using ImageJ and normalized to β-actin intensity. 2-way-Anova analysis was used to determine p-values via GraphPad. Data were reported as means SE (n=3).

According to results of the experiment for Caspase 9 antibody, which is one of the apoptosis markers, cleaved caspase 9 had the same expression level in the 5-month-old mice groups. Only 2-month-old Neu1-/-GM3S-/- mice demonstrated higher expression level than age matched WT mice in cerebellum tissue (Figure 3.29 A and B).

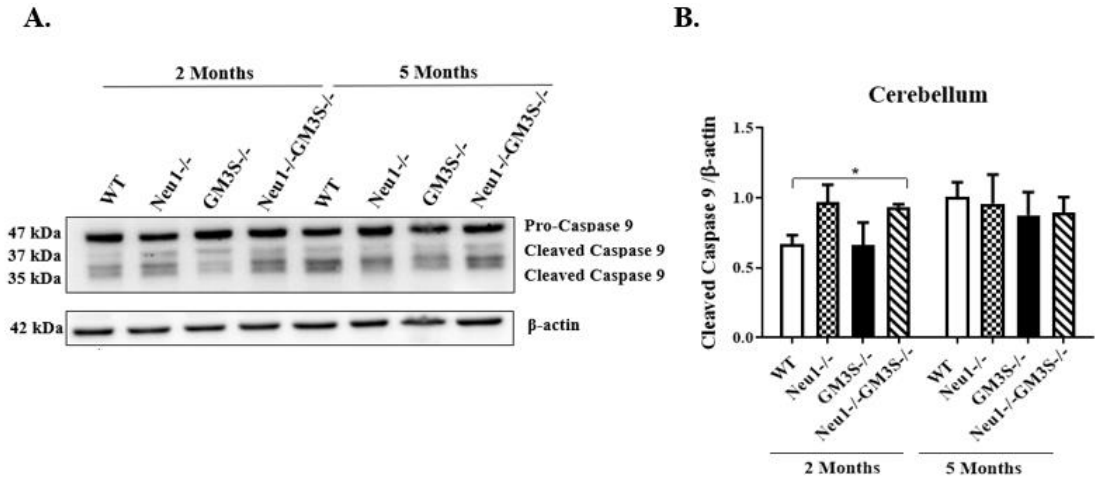

Figure 3.29. Western blot analysis of Caspase 9 in cerebellum tissue of 2- and 5-month old WT, Neu1-/-, GM3S-/-, Neu1-/-GM3S-/- mice (A). Intensity analysis of Caspase 9 for 2- and 5-month-old WT, Neu1-/-, GM3S-/- and Neu1-/-GM3S-/- mice (B). β-actin was used as control. Intensity of each band was detected by using ImageJ and normalized to β-actin intensity. 2-way-Anova analysis was used to determine p-values via GraphPad. Data were reported as means SE (n=3, *p<0,05).

In the cerebellum tissue, the caspase 3 which involved at the final step of apoptosis pathway showed elevated level in 2-month-old Neu1-/- and Neu1-/-GM3S-/- mice compared to its WT littermates. However, no observable change between WT and GM3S-/- mice was detected based on cleaved caspase-3 expression (Figure 3.30 A and B). The higher expression level in the cleaved caspase 3 was also observed in 2-month-old Neu1-/-GM3S-/- mice compared to age matched GM3S-/- mice. The elevated level in double gene deficient mice may be contributed with the absence of Neu1 gene in the Neu1-/-GM3S-/- mice. Elevated expression level of cleaved caspase 3 in 5-month-old Neu1-/-GM3S-/- mice compared to age matched Neu1-/- mice can indicator of apoptosis in the cerebellum tissue (Figure 3.30 A and B).

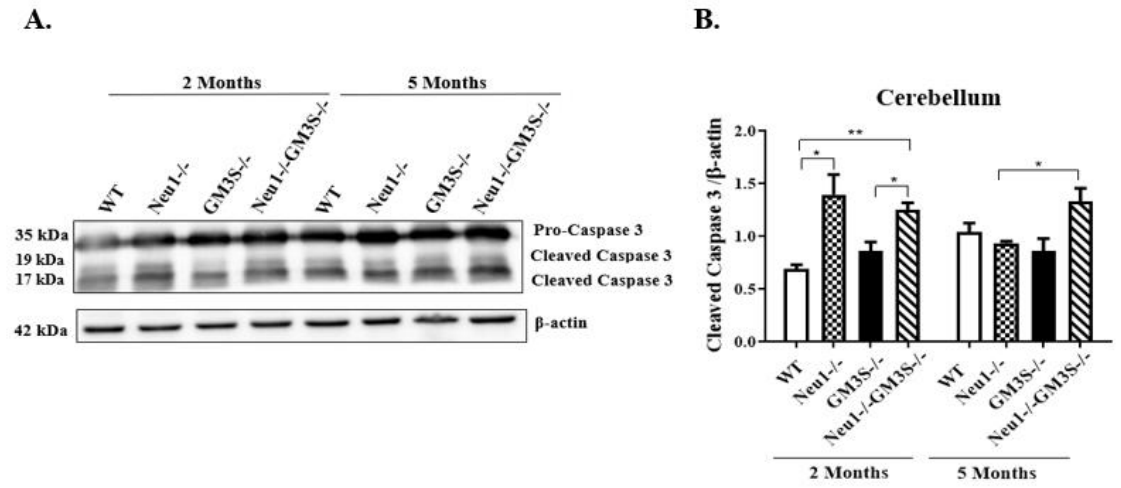

Figure 3.30. Western blot analysis of Caspase 3 in cerebellum tissue of 2- and 5-month-old WT, Neu1-/-, GM3S-/-, Neu1-/-GM3S-/- mice (A). Intensity analysis of Caspase 3 for 2- and 5-month-old WT, Neu1-/-, GM3S-/- and Neu1-/-GM3S-/- mice (B). β-actin was used as control. Intensity of each band was detected by using ImageJ and normalized to β-actin intensity. 2-way-Anova analysis was used to determine p-values via GraphPad. Data were reported as means SE (n=3, *p<0,05, **p<0,01).

BiP expression showed significant increase in 2-month-old GM3S-/- and Neu1-/-GM3S-/- mice compared to its WT mice in cerebellum tissue (Figure 3.31 A and B).

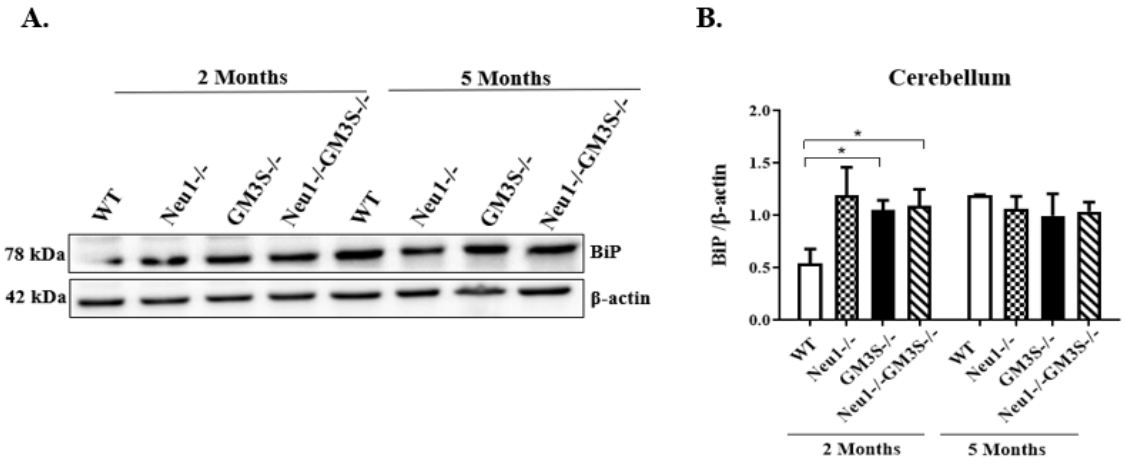

Figure 3.31. Western blot analysis of BiP in cerebellum tissue of 2- and 5-month-old WT, Neu1-/-, GM3S-/-, Neu1-/-GM3S-/- mice (A). Intensity analysis of BiP for 2- and 5-month-old WT, Neu1-/-, GM3S-/- and Neu1-/-GM3S-/- mice (B). β-actin was used as control. Intensity of each band was detected by using ImageJ and normalized to β-actin intensity. 2-way-Anova analysis was used to determine p-values via GraphPad. Data were reported as means SE (n=3, *p<0,05).

In the thalamus tissue, the expression level of Fas-Ligand was also similar in all mice groups as in the cortex and cerebellum tissues (Figure 3.32 A and B). Therefore, Fas-Ligand which is responsible for Fas-Ligand receptor activation in the extrinsic apoptotic pathway had the similar expression in all brain tissues including cortex, cerebellum and thalamus tissues of differently genotyped mice at the any ages.

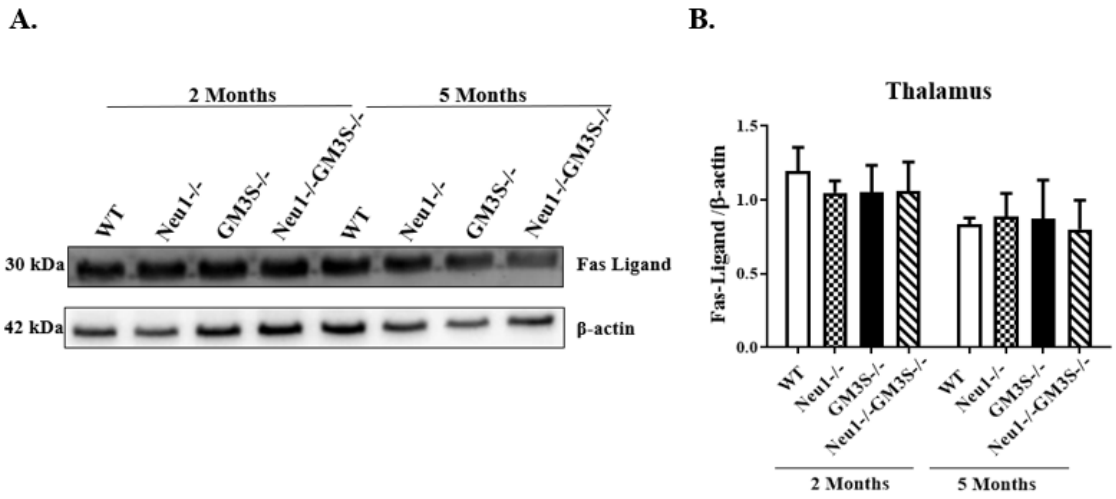

Figure 3.32. Western blot analysis of Fas-Ligand in thalamus tissue of 2- and 5-month-old WT, Neu1-/-, GM3S-/-, Neu1-/-GM3S-/- mice (A). Intensity analysis of Fas Ligand for 2- and 5-month-old WT, Neu1-/-, GM3S-/- and Neu1-/-GM3S-/- mice (B). β-actin was used as control. Intensity of each band was detected with ImageJ and normalized to β-actin intensity. 2-way-Anova analysis was used to determine p-values via GraphPad. Data were reported as means SE (n=3).

Caspase 9 expression did not demonstrate noticeable change in the thalamus tissue of 2- and 5-month-old group (Figure 3.33 A and B). The significant increase was found in only 5-month-old Neu1-/-GM3S-/- mice compared with their age matched GM3S-/- mice. Additionally, older Neu1-/- mice had slightly elevated cleaved caspase-3 level compared to that of control and GM3S-/- mice, however, this difference was not found (Figure 3.33 A and B). Due to no change between 5-month-old WT and GM3S-/- mice, elevated level of cleaved caspase 9 may be affected from the Neu1 gene deficiency in the double gene deficient mice.

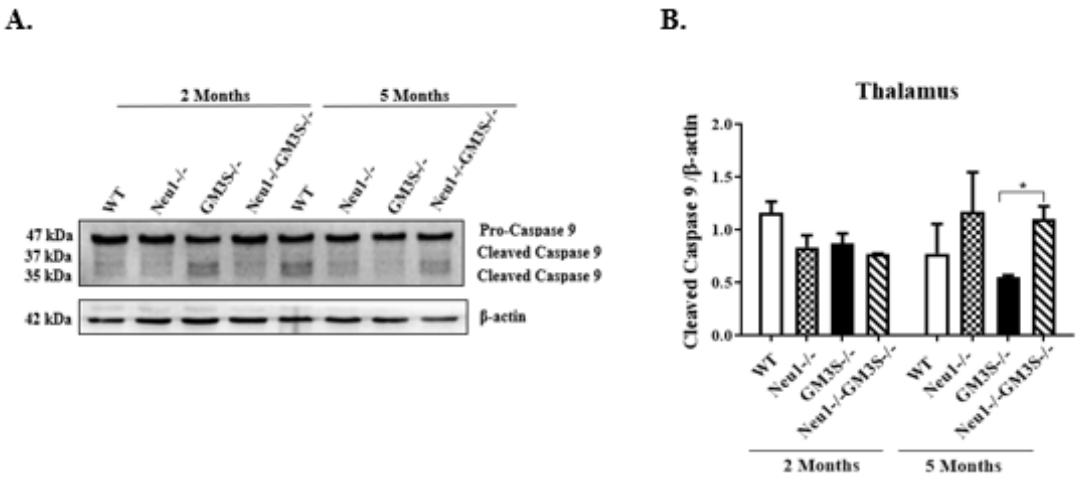

Figure 3.33. Western blot analysis of Caspase 9 in thalamus tissue of 2- and 5-month-old WT, Neu1-/-, GM3S-/-, Neu1-/-GM3S-/- mice (A). Intensity analysis Caspase 9 for 2- and 5-month-old WT, Neu1-/-, GM3S-/- and Neu1-/-GM3S-/- mice (B). β-actin was used as control. Intensity of each band was detected by using ImageJ and normalized to β-actin intensity. 2-way-Anova analysis was used to determine p-values via GraphPad. Data were reported as means SE (n=3, *p<0,05).

There was a reduction in level of the cleaved caspases 3 in 2-month-old Neu1-/-GM3S-/- mice compared to age matched WT, Neu1-/-, GM3S-/- and Neu1-/-GM3S-/- mice (Figure 3.34 A and B).

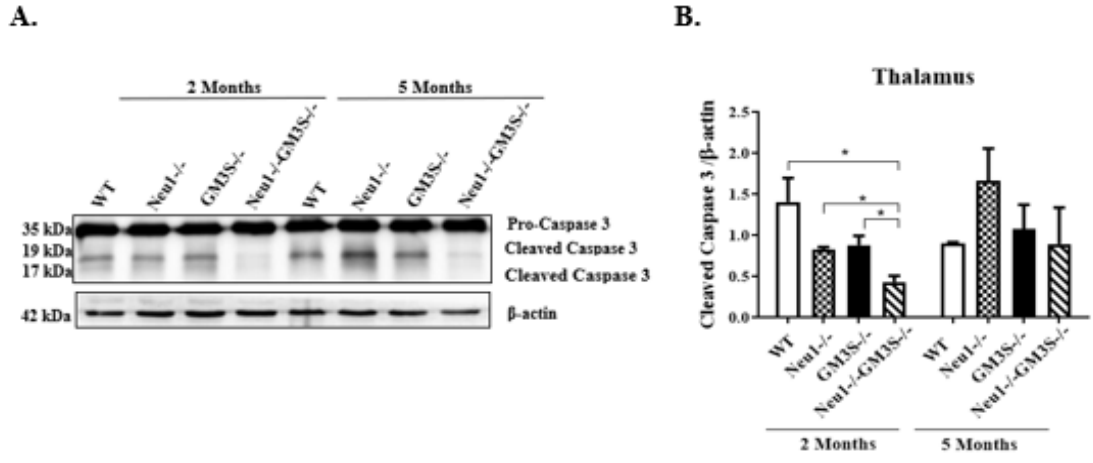

Figure 3.34. Western blot analysis of Caspase 3 in thalamus tissue of 2- and 5-month-old WT, Neu1-/-, GM3S-/-, Neu1-/-GM3S-/- mice (A). Intensity analysis of Caspase 3 for 2- and 5-month-old WT, Neu1-/-, GM3S-/- and Neu1-/-GM3S-/- mice (B). β-actin was used as control. Intensity of each band was detected by using ImageJ and normalized to β-actin intensity. 2-way-Anova analysis was used to determine p-values via GraphPad. Data were reported as means SE (n=3, *p<0,05).

In the thalamus tissue, no significant change was observed for BiP expression in the 2- and 5-month-old WT, Neu1-/-, GM3S-/- and Neu1-/-GM3S-/- mice (Figure 3.35 A and B).

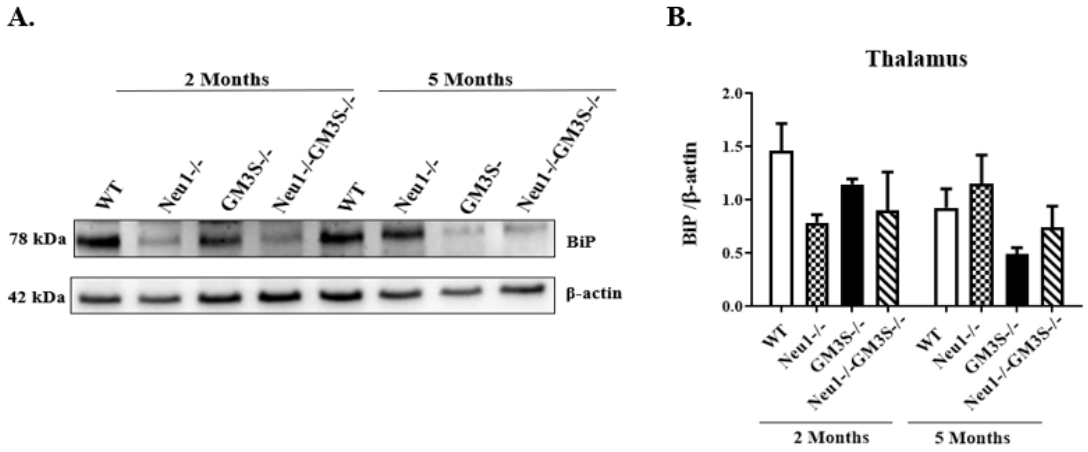

Figure 3.35. Western blot analysis of BiP in thalamus tissue of 2- and 5-month-old WT, Neu1-/-, GM3S-/-, Neu1-/-GM3S-/- mice (A). Intensity analysis of BiP for 2- and 5-month-old WT, Neu1-/-, GM3S-/- and Neu1-/-GM3S-/- mice (B). β-actin was used as control. Intensity of each band was detected by using ImageJ and normalized to β-actin intensity. 2-way-Anova analysis was used to determine p-values via GraphPad. Data were reported as means SE (n=3, *p<0,05).

3.7. Histological Analysis

3.7.1. Hematoxylin – Eosin (H&E) Staining

Abnormalities in tissue morphology depending on alterations in glycosphingolipid metabolism was determined by Hematoxylin – Eosin staining at the 2 and 5 months of age differently-genotyped WT, Neu1-/-, GM3S-/- and Neu1-/-GM3S-/- mice. Morphological alterations were analyzed for cortex, hippocampus, thalamus and cerebellum sections.

The cortex structure consisting of six layers in cortex sections was normal histological view in 2- and 5-month-old WT mice (Figure 3.36 A and 3.37 A). Moderate edema and disorganization in the cortex structure was observed in 2- and 5-month-old Neu1-/- mice. Cells were seen to come together like a plaque. Together, dilatation was

observed in the vessels with edema in Neu1-/- mice at any ages (Figure 3.36 B and 3.37 B). The presence of degenerative signs in cells was detected in some regions of cortex tissue in 2- and 5-month-old Neu1-/- mice. When 2-month-old GM3S-/- mice compared to aged matched Neu1-/- mice, very little edema was observed in 2-month-old GM3S-/- mice, and minimal dilatation in vessels was detected. The six layer of cortex of young GM3S-/- mice was close to aged-matched WT mice (Figure 3.36 C and 3.37 C). However, 5-month-old GM3S-/- showed more dramatic structural changes compared to 2-month-old GM3S-/- mice. The more edema was seen in older GM3S-/- mice compared to 5-month-old Neu1-/- mice. The findings in Neu1-/-GM3S-/- mice was more dramatic compared to other groups. The six layer of cortex was the most affected in 2- and 5-month-old double knock-out mice. The loss in cells, high degree of edema, dilatation of vessels, kariolyzed neurons and vacuolized dense structures were seen dramatically in cortex of 2 and 5-month-old Neu1-/-GM3S-/- mice (Figure 3.36 D and 3.37 D).

The hippocampus section analysis showed that layers in hippocampus were in normal structure in 2- and 5-month-old WT littermates (Figure 3.36 E and 3.37 E). The areas in hippocampus as CA1, CA2, CA3 and CA4 were found to be compatible with the development period in young and older WT mice. The edema, dilatation in the vessels, degeneration of cells in hippocampus of 2- and 5-month-old Neu1-/- and GM3S-/- mice were observed (Figure 3.36 F, G and 3.37 F, G). The loss of cells, high edema, dilatation of vessels and vacuolized structures in the hippocampus of Neu1-/-GM3S-/- mice were quite intense compared to other mice groups (Figure 3.36 H and 3.37 H).

In thalamus section, 2- and 5- month-old WT mice had normal histological appearance based on nucleus structures of thalamus. The presence edema, dilation in the veins, and plaque-like structures were seen in the 2- and 5-month-old Neu1-/- and GM3S-/- mice (Figure 3.36 I, J, K and 3.37 I, J, K). In both young and older Neu1-/-GM3S-/- mice, cell loss, vascular dilation and the presence of dense vacuolized structures were seen as dramatically (Figure 3.36 L and 3.37 L).

The cerebellum section of 2- and 5-month-old mice groups was showed some structural differences depending on genotype. Purkinje cell layer and its organization was normal in both young and older WT mice. The minimal edema, dilation in vessels and disorganization and deletion of Purkinje cells were observed in Neu1-/- mice at any ages. The minimal edema in Purkinje cells and disorganization was also seen in GM3S-/- mice. However, the most loss of Purkinje cells and the presence of highly karyolized neurons were detected in the young and older Neu1-/-GM3S-/- mice (Figure 3.36 P and 3.37 P).

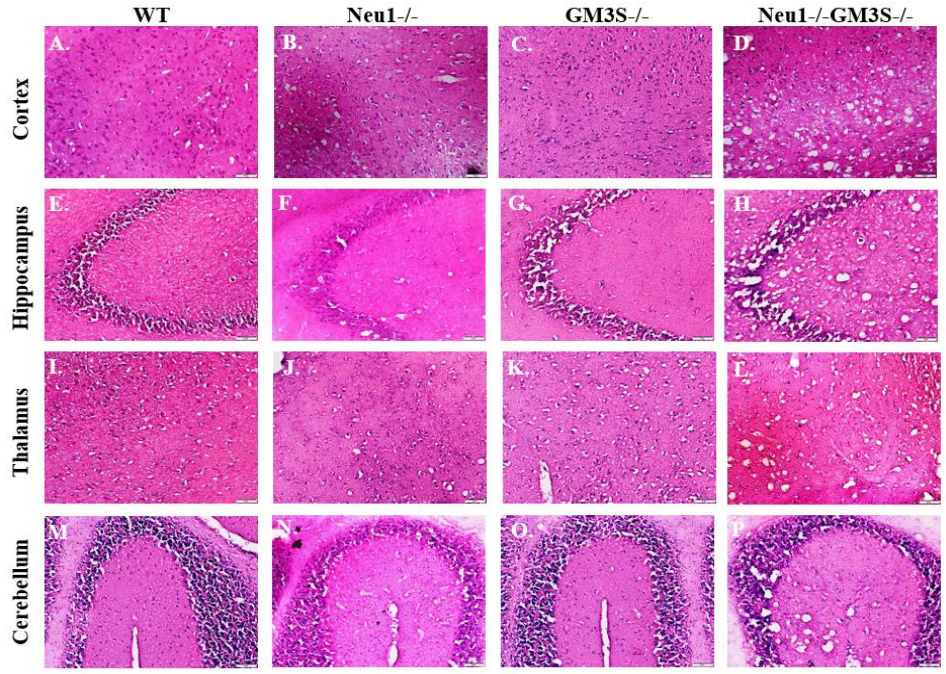

Figure 3.36. Hematoxylin – Eosin staining in 2-month-old WT, Neu1-/-, GM3S-/- and Neu1-/-GM3S-/- mice brain coronal sections, cortex (A, B, C, D), hippocampus (E, F, G, H), thalamus (I, J, K, L) and cerebellum (M, N, O, P). Images were taken at 20X magnification by Olympus light microscope.

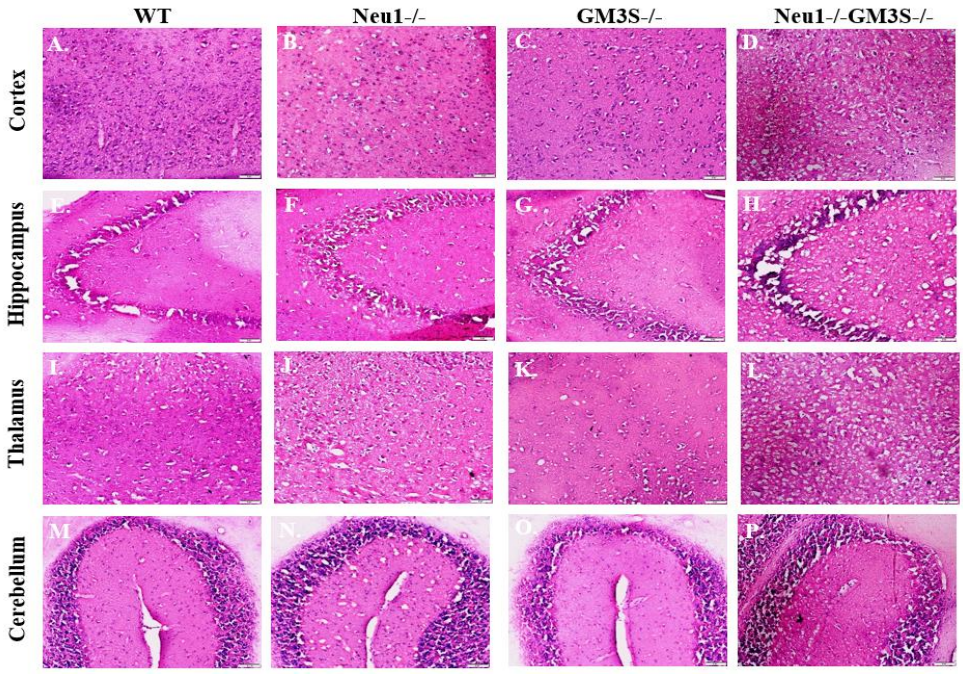

Figure 3.37. Hematoxylin – Eosin staining in 5-month-old WT, Neu1-/-, GM3S-/- and Neu1-/-GM3S-/- mice brain coronal sections, cortex (A, B, C, D), hippocampus (E, F, G, H), thalamus (I, J, K, L) and cerebellum (M, N, O, P). Images were taken at 20X magnification by Olympus light microscope.

3.7.2. Cresyl – Echt Violet Staining

Neuron structure was analyzed by Cresyl – Echt Violet staining in the cortex, hippocampus, thalamus and cerebellum sections of 2- and 5-month-old WT, Neu1-/-, GM3S-/- and Neu1-/-GM3S-/- mice. Abnormalities in the neuron structure were understood depending on age and genotype.

There was no evidence of degeneration in neuronal structure in the cortex, hippocampus, thalamus and cerebellum sections of 2- and 5-month-old WT mice, and the distribution of Nissl granules were normal in WT mice at any ages (Figure 3.38 and 3.39). However, the degeneration of Nissl body distribution was seen in the young and older Neu1-/- mice (Figure 3.38 and 3.39). 2- and 5-month-old GM3S-/- mice was also showed the similar findings seen in Neu1-/- mice, although the degeneration in neuronal structure in this mice group was lower compared to Neu1-/- mice at any ages. In 2 and 5-month-old Neu1-/-GM3S-/- mice, the number of degenerative cells is very dense and the number of degenerative cells in the total volume was also higher compared to other genotyped littermates (Figure 3.38 and 3.39).

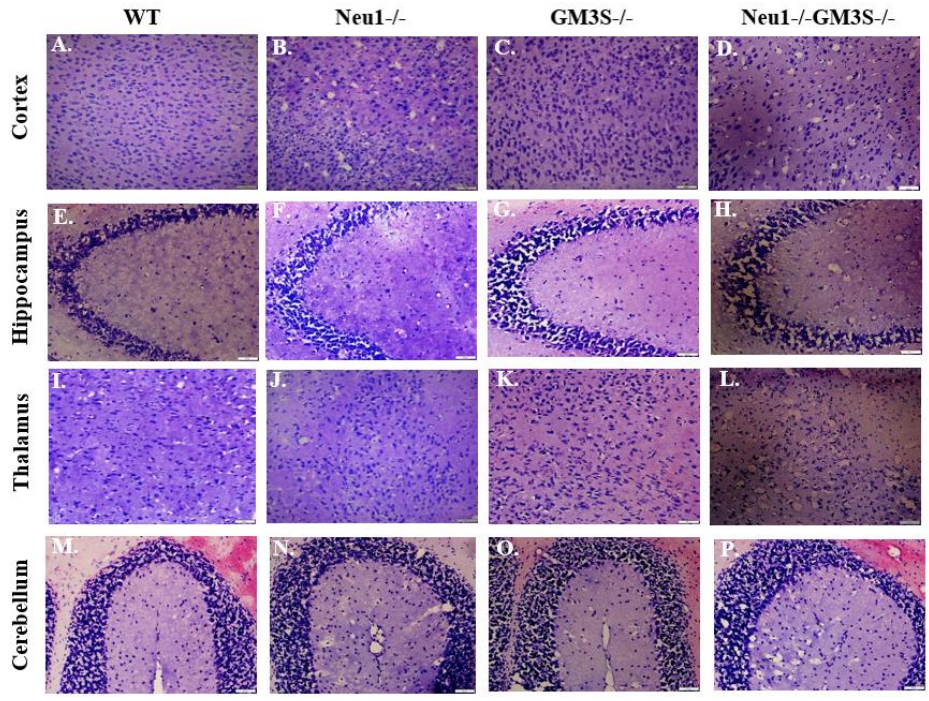

Figure 3.38. Cresyl – Echt Violet staining in 2-month-old WT, Neu1-/-, GM3S-/- and Neu1-/-GM3S-/- mice brain coronal sections, cortex (A, B, C, D), hippocampus (E, F, G, H), thalamus (I, J, K, L) and cerebellum (M, N, O, P). Images were taken at 20X magnification by Olympus light microscope.

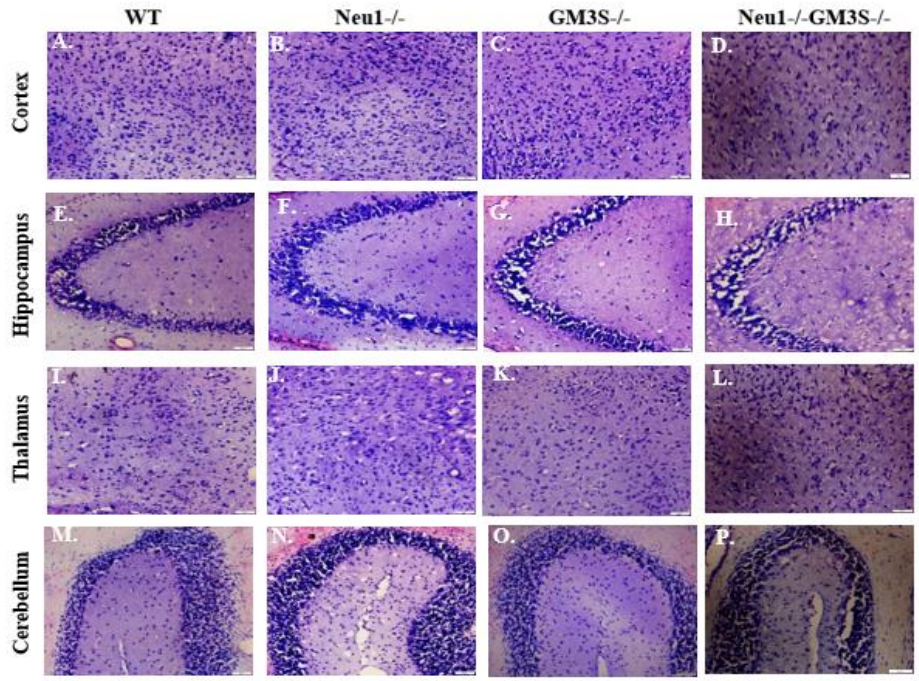

Figure 3.39. Cresyl – Echt Violet staining in 5-month-old WT, Neu1-/-, GM3S-/- and Neu1-/-GM3S-/- mice brain coronal sections, cortex (A, B, C, D), hippocampus (E, F, G, H), thalamus (I, J, K, L) and cerebellum (M, N, O, P). Images were taken at 20X magnification by Olympus light microscope.

3.7.3. Periodic acid – Schiff Stain (PAS) Staining

Glycosphingolipid accumulation was detected with Periodic acid – Schiff Stain (PAS) staining according as altered glycolipid metabolism in 2- and 5-month-old WT, Neu1-/-, GM3S-/- and Neu1-/-GM3S-/- mice sections including cortex, hippocampus, thalamus, and cerebellum.

There was no evidence of glycoconjugates accumulation such as oligosaccharide, glycosphingolipid in cerebral cortex, hippocampus, thalamus and cerebellum sections of 2- and 5-month-old WT mice. In sections of 2- and 5-month-old Neu1-/- mice, glycoconjugate accumulation was observed in some regions of distinct sections (Figure 3.40 and 3.41). However, young and older GM3S-/- mice demonstrated less glycoconjugate accumulation in the different sections compared to Neu1-/- mice. The most intense glycoconjugate accumulation was observed in the all sections of 2- and 5-month-old Neu1-/-GM3S-/- mice, consequently it was the group with the most impaired cellular organization (Figure 3.40 and 3.41).

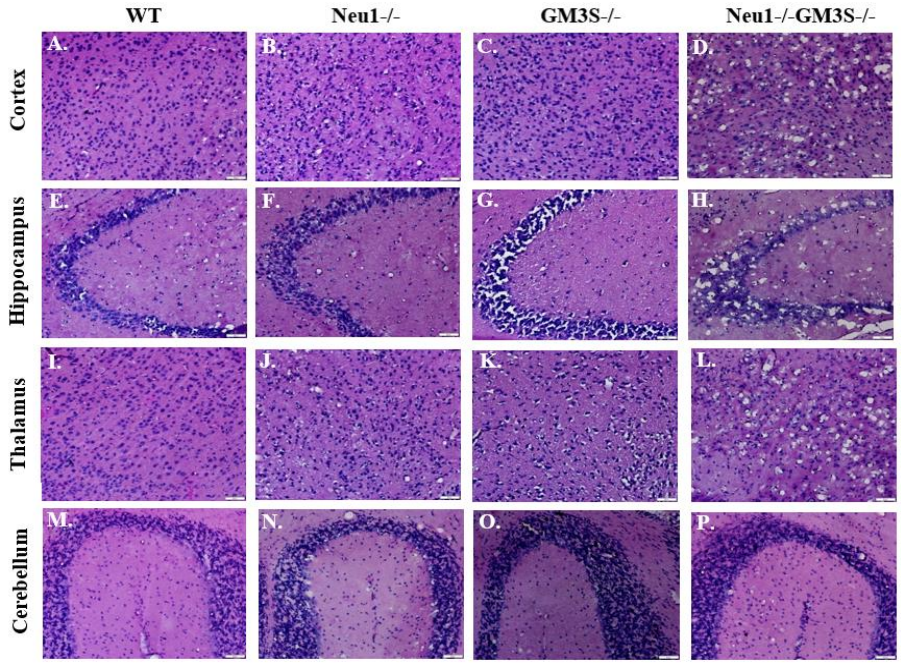

Figure 3.40. Periodic acid - Schiff Stain (PAS) staining in 2-month-old WT, Neu1-/-, GM3S-/- and Neu1-/-GM3S-/- mice brain coronal sections, cortex (A, B, C, D), hippocampus (E, F, G, H), thalamus (I, J, K, L) and cerebellum (M, N, O, P). Images were taken at 20X magnification by Olympus light microscope.

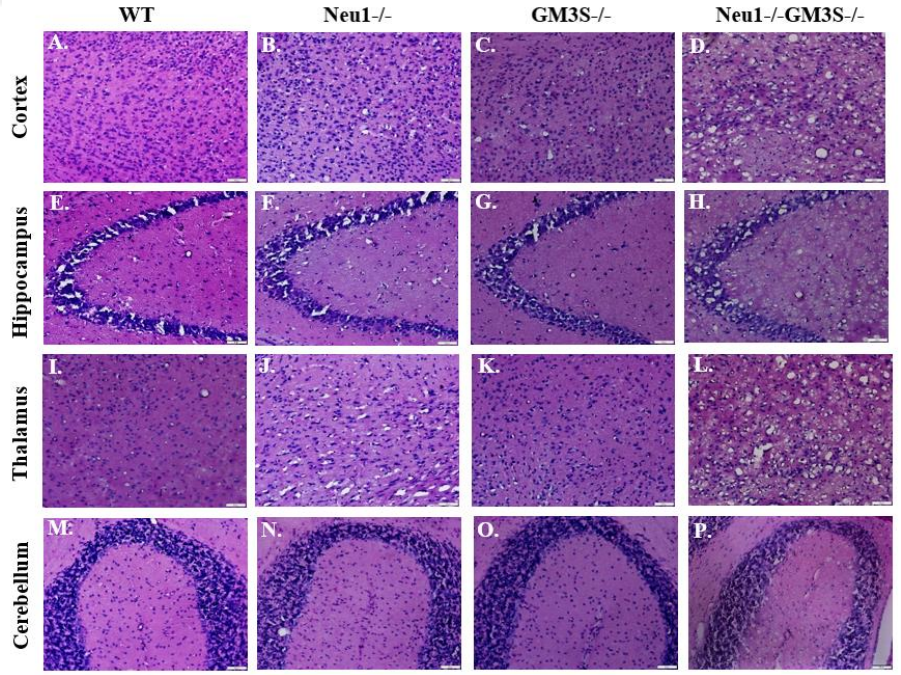

Figure 3.41. Periodic acid - Schiff Stain (PAS) staining in 5-month-old WT, Neu1-/-, GM3S-/- and Neu1-/-GM3S-/- mice brain coronal sections, cortex (A, B, C, D), hippocampus (E, F, G, H), thalamus (I, J, K, L) and cerebellum (M, N, O, P). Images were taken at 20X magnification by Olympus light microscope.

3.7.4. Luxol – Fast Staining

Luxol Fast staining was performed in order to understand the demyelization in distinct tissues of mice depending on aging and genotype due to changes in ganglioside pattern. The cortex, hippocampus, carpus callosum, thalamus and cerebellum sections were analyzed for all differently- genotyped mice.

Demyelination in the cortex, hippocampus, corpus callosum, thalamus and cerebellum sections of 2- and 5-month-old WT mice was not detected according to Luxol – Fast staining (Figure 3.42 and 3.43). The signs of demyelination was observed in the both 2- and 5- month-old Neu1-/- mice, and the partially less demyelination detected in the both ages of GM3S-/- mice compared to Neu1-/- mice. In 2- and 5-month-old Neu1-/-GM3S-/- mice, pronounced demyelination was observed, especially in the corpus callosum section of brain. (Figure 3.42 and 3.43).

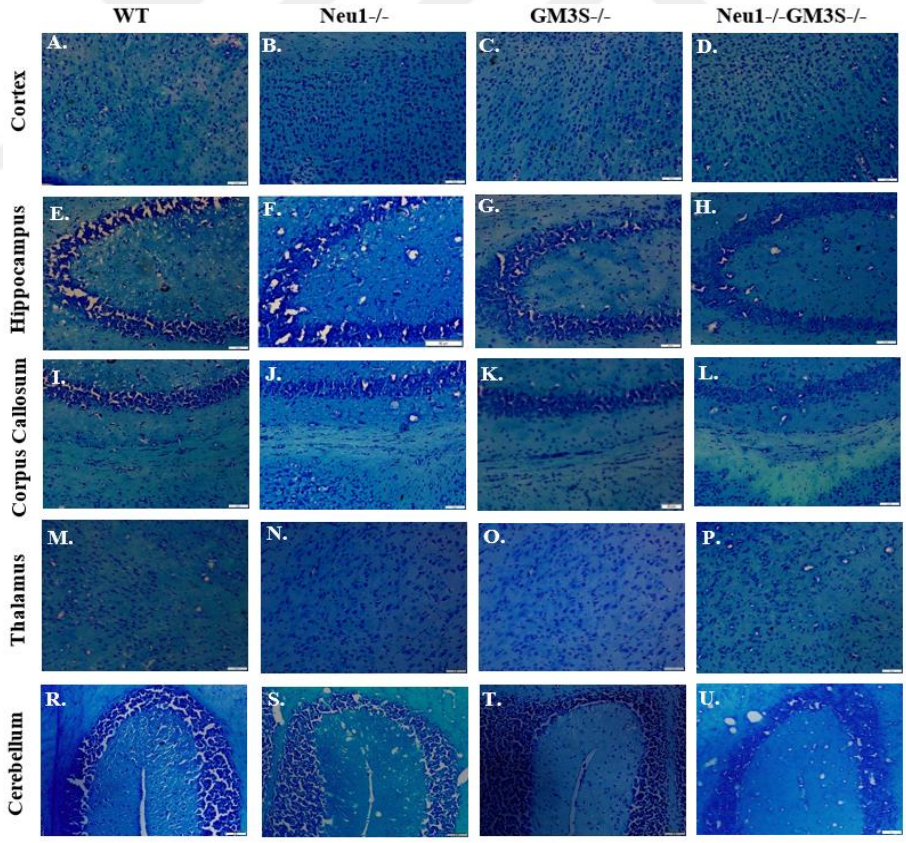

Figure 3.42. Luxol – Fast staining in 2-month-old WT, Neu1-/-, GM3S-/- and Neu1-/-GM3S-/- mice brain coronal sections, cortex (A, B, C, D), hippocampus (E, F, G, H), corpus callosum (I, J, K, L), thalamus (M, N, O, P), and cerebellum (R, S, T, U). Images were taken at 20X magnification by Olympus light microscope.

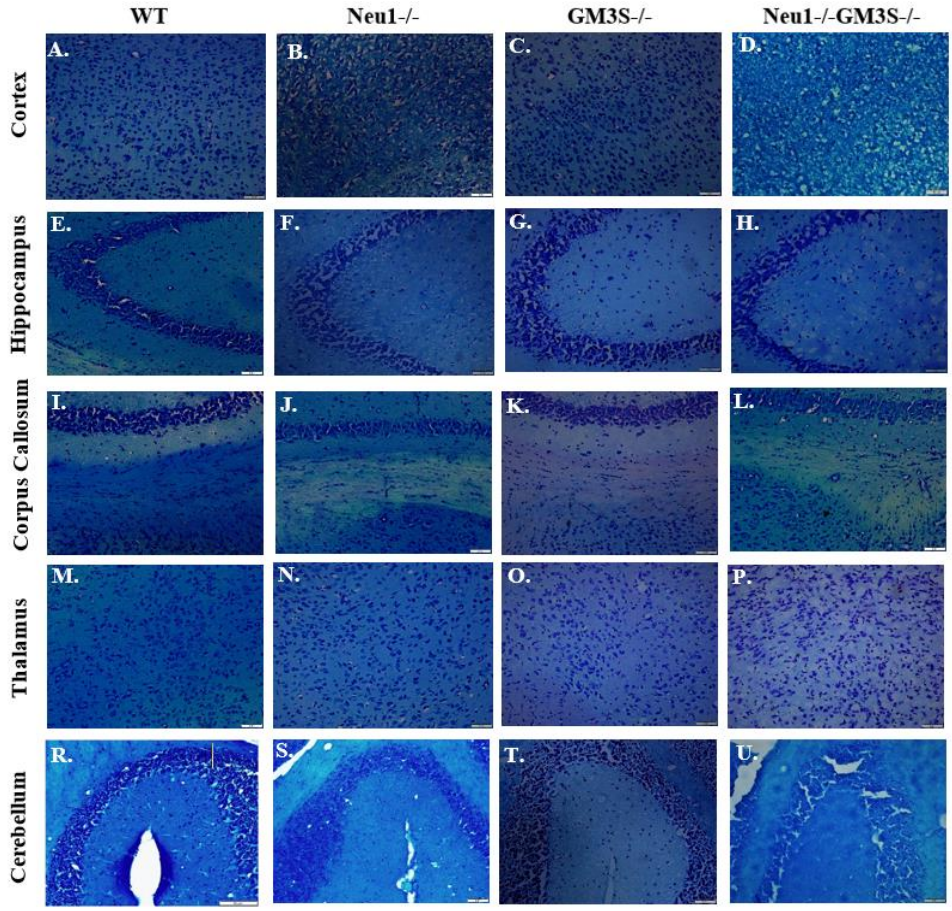

Figure 3.43. Luxol – Fast staining in 5-month-old WT, Neu1-/-, GM3S-/- and Neu1-/-GM3S-/- mice brain coronal sections, cortex (A, B, C, D), hippocampus (E, F, G, H), corpus callosum (I, J, K, L), thalamus (M, N, O, P), and cerebellum (R, S, T, U). Images were taken at 20X magnification by Olympus light microscope.

3.8. Immunohistochemistry Analysis

3.8.1. Oligodendrocyte Analysis

Oligodendrocyte analysis was performed with anti-CNPase antibody in order to understand alteration in the number of oligodendrocytes depending on aging and genotype (Fletcher et al. 2014). Oligodendrocytes are responsible for the production of myelin sheath and myelination (Onyenwoke and Brenman, 2015). Brain sections such as cortex and cerebellum of 5-month-old WT, Neu1-/-, GM3S-/-, and Neu1-/-GM3S-/- mice were immunostained with anti-CNPase antibody and oligodendrocyte number was compared for distinct genotyped mice groups (Figure 3.44).

Immunoreactivity of anti-CNPase antibody showed distinct pattern for the distinct genotyped mice groups. Intensity of CNPase indicating the number of oligodendrocytes was measured by ImageJ and intensity of 5-month-old Neu1-/-, GM3S-/- and Neu1-/-GM3S-/- mice were normalized to 5-month-old WT mice (Figure 3.44 B and D).

In the cortex section, the number of CNPase positive cells decreased in both 5-month-old Neu1-/- and GM3S-/- mice compared to age matched WT mice as approximately 54% and 35% respectively (Figure 3.44 A and B). There was reduction in oligodendrocyte number of Neu1-/- mice compared to that of GM3S-/- mice as approximately 24%.

As shown in Figure 3.44 A and B, CNPase positive cells in the cortex section of 5-month-old Neu1-/-GM3S-/ - mice were decreased approximately 96% relative to WT mice, 91% compared to Neu1-/- mice and 94% compared to GM3S-/- mice.

As can be seen from results of cortex CNPase staining, the most dramatic loss of oligodendrocytes was observed in 5-month-old Neu1-/-GM3S-/- mice and then Neu1-/- mice, whereas the less oligodendrocyte loss was shown in GM3S-/- mice. (Figure 3.44 A and B).

The significant alterations in the oligodendrocyte marker (CNPase) were also shown for the cerebellum section of 5-month-old distinct genotyped mice groups. 5-month-old Neu1-/-, GM3S-/- and Neu1-/-GM3S-/- mice had less CNPase positive cell number than age matched WT mice as approximately 65%, 49% and 70%, respectively. (Figure 3.44 C and D).

5-month-old Neu1-/- and Neu1-/-GM3S-/- mice also showed significant decreasing level of CNPase intensity compared with GM3S-/- mice as approximately 31% and 40% separately in cerebellum tissue (Figure 3.44 C and D). Therefore, Neu1-/- and Neu1-/-GM3S-/- mice had higher oligodendrocyte loss compared to that of control and GM3S-/- littermates in the cerebellum part.

The Luxol-Fast staining, indicator of demyelination, is compatible with the results of oligodendrocyte number analyses because oligodendrocytes are specialized cells that are responsible from myelination process and the loss of oligodendrocytes is hallmark of the demyelination.

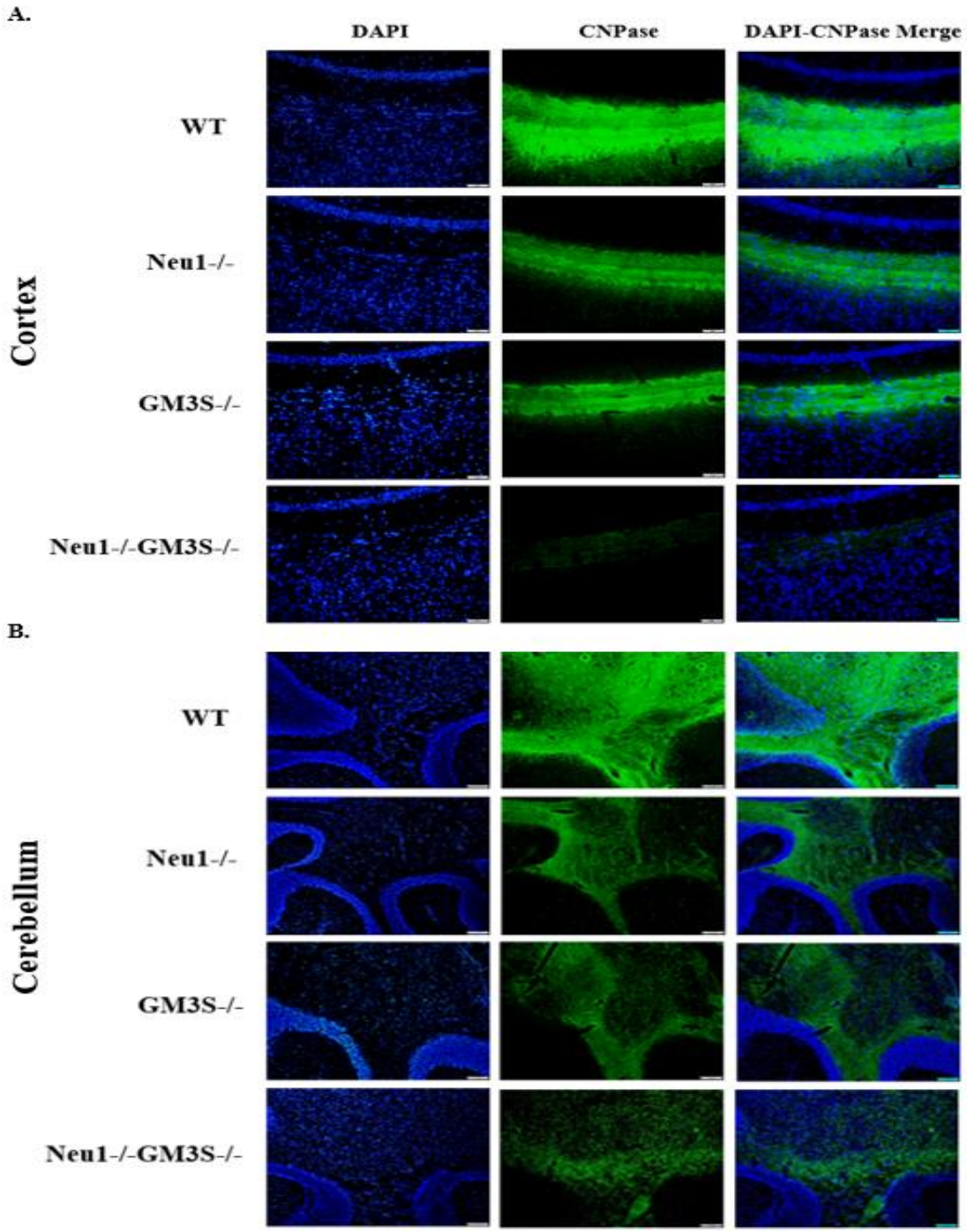

Figure 3.44. Immunostaining of CNPase (oligodendrocyte marker) in 5-month-old WT, Neu1-/-, GM3S-/- and Neu1-/-GM3S-/- mice brain coronal sections, cortex and cerebellum. Images were taken at 20X magnification for cortex (A) and 10X magnification for cerebellum (B) sections. All images were taken under the same light intensity that differs filter types for DAPI and anti-CNPase. Sections were stained with anti-CNPase antibody (green; oligodendrocyte marker) and DAPI (blue; nucleus). Intensity of CNPase for cortex (C) and cerebellum (D) was measured with ImageJ and normalized to WT group. 1-way-Anova analysis was used to determine p values by using GraphPad. Data were reported as means SEM. (n=3, *p<0,05, **p<0,01, ***p<0,001, ****p<0,0001).

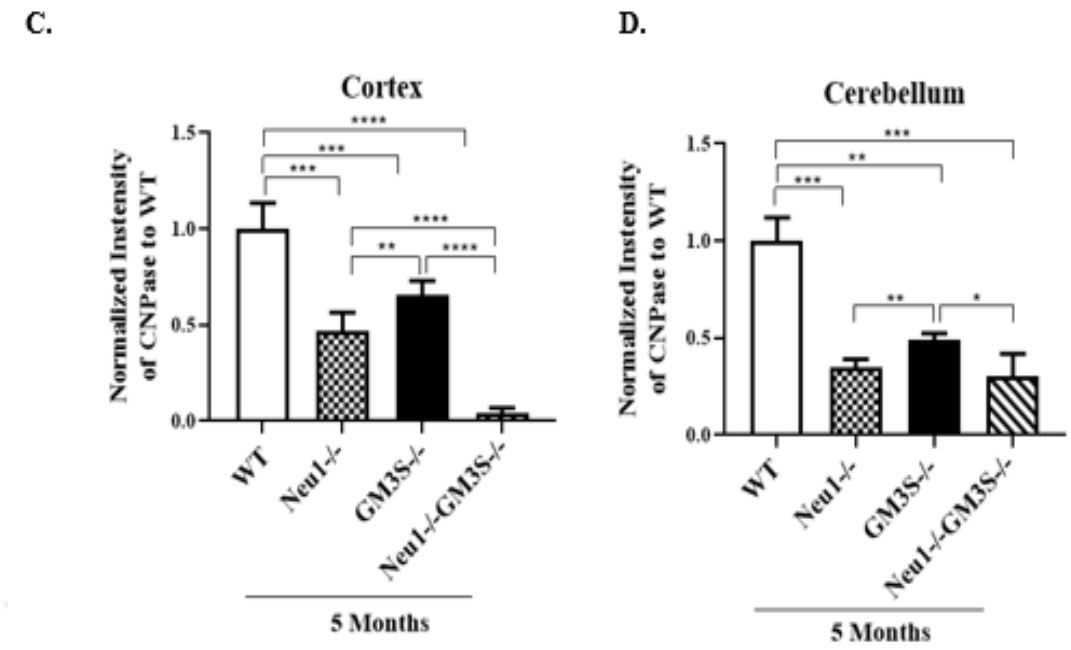

Figure 3.44 (cont.)

3.8.2. Neuron Analysis

Immunostaining of 5 -month-old WT, Neu1-/-, GM3S-/- and Neu1-/-GM3S-/- mice were using by using anti-NeuN antibody to determine the presence of differentiation in the number of neuron cells. Neuronal death can be understood from the NeuN immunoreactivity. The decrease in the immunoreactivity exhibits the neuronal death in the specific section (Gusel'nikova and Korzhevskiy 2015).

In order to understand the immunoreactivity of anti-NeuN antibody for distinct genotyped mice groups, intensity of NeuN for each genotype was measured by using ImageJ and normalized to WT group.

Neu1-/-, GM3S-/- and Neu1-/-GM3S-/- mice displayed distinct patterns compared to age matched WT mice for cortex, hippocampus and thalamus sections (Figure 3.45 R, Figure 3.45 S, Figure 3.45 T).

There was a reduction of the NeuN-positive neurons in the cortex (Figure 3.45 R), hippocampus (Figure 3.45 S) and thalamus as approximately 50% (Figure 3.45 T) in 5-month-old GM3S-/- mice compared to age matched WT mice, implying the reduction in the number of neuron cells in older GM3S-/- mice.

In 5-month-old Neu1-/- mice, the neuronal density decreased in the cortex as approximately 73% (Figure 3.45 R), hippocampus as approximately 80% (Figure 3.45 S) and thalamus as approximately 86% (Figure 3.45 T) compared to age matched WT mice.

The neuronal density reduction was also determined in the cortex of Neu1-/- mice as approximately 47% (Figure 3.45 R), hippocampus as approximately 60% (Figure 3.45 S) and thalamus as approximately 72% (Figure 3.45 T) sections compared to age matched GM3S-/- mice, implying more neuronal death in Neu1-/- mice than that of GM3S-/- littermates.

As depicted in Figure 3.45, the most significant neuronal death was observed in Neu1-/-GM3S-/- mice compared to other mice groups including WT mice as approximately 94%, Neu1-/- mice as approximately 78% and GM3S-/- mice as approximately 88% for the cortex section (Figure 3.45 R).

There was a neuronal density reduction of Neu1-/-GM3S-/- mice in the hippocampus compared with WT mice as approximately 91%, Neu1-/- mice as approximately 55% and GM3S-/- mice as approximately 82% (Figure 3.45 S).

In thalamus section it was observed the decreasing in the neuron number of Neu1-/-GM3S-/- mice compared to WT and GM3S-/- mice as approximately 80% and 60%, respectively (Figure 3.45 T). The decrease in immunoreactivity of anti-NeuN antibody in Neu1-/-GM3S-/- mice displayed dramatically neuronal death compared to all other mice groups.

In the Purkinje layer of cerebellum, no significant difference was found for the distinctly genotyped mice groups according to results of Anti-NeuN staining (Figure 3.45 U).

3.8.3. In Situ Apoptosis Analysis (TUNEL)

Promega-Dead End® Fluorometric Tunel Systems kit was used for the TUNEL analysis in order to detect the apoptosis depending on the genotype. The cortex, hippocampus, thalamus and cerebellum sections of 5-month-old WT, Neu1-/-, GM3S-/- and Neu1-/-GM3S-/- mice were utilized for TUNEL analysis. Green color refers to apoptotic cells while red color is indicator of nucleus of cells. Therefore, the merge of green (apoptotic cells) and red (nuclei of cells) gave the apoptotic (TUNEL) positive cells. TUNEL positive cells were detected with ImageJ program and normalized to WT mice.

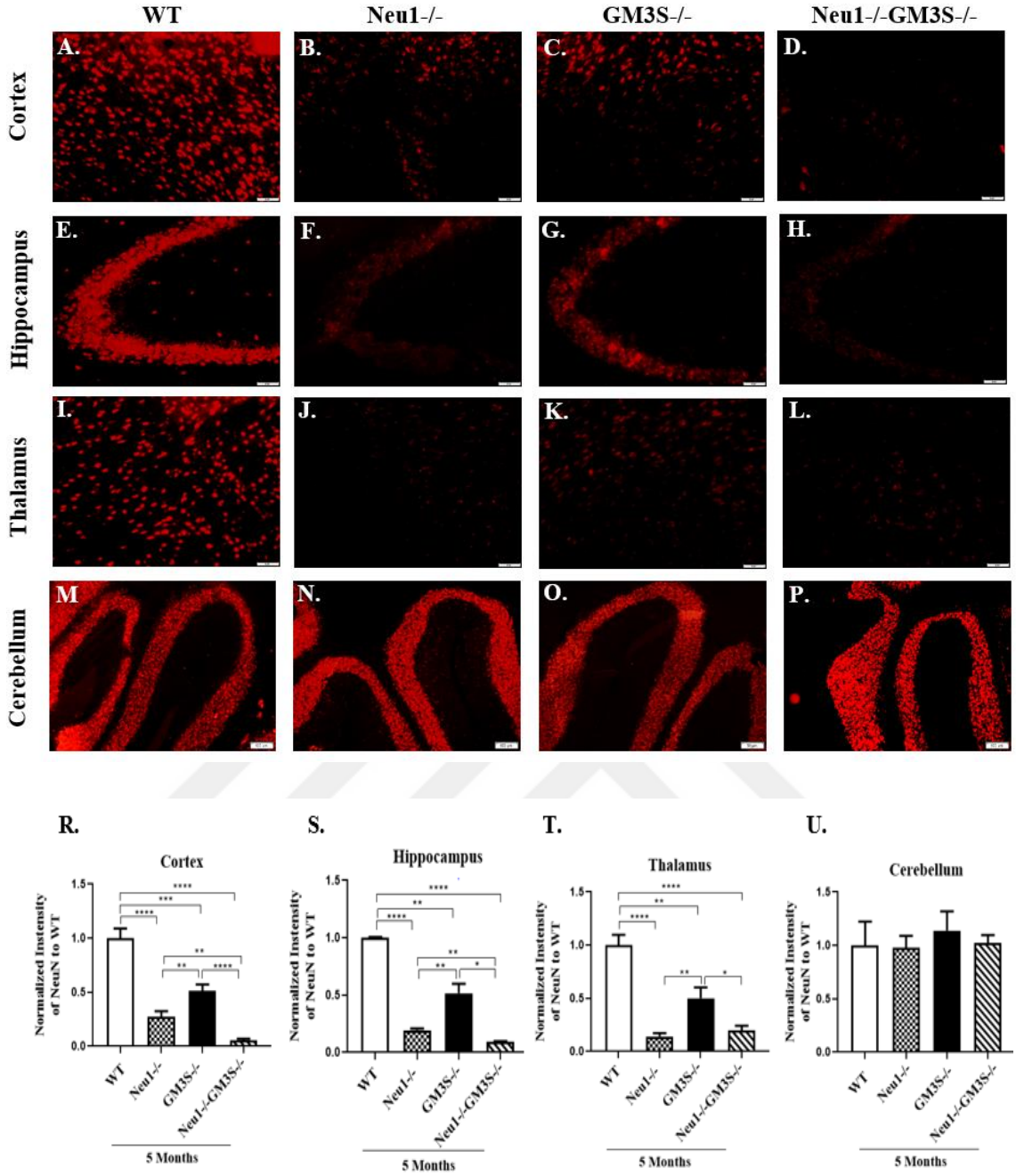

Figure 3.45. Immunostaining of NeuN (neuron marker) in 5-month-old WT, Neu1-/-, GM3S-/- and Neu1-/-GM3S-/- mice brain coronal sections, cortex, hippocampus, thalamus and cerebellum. Images were taken at 20X magnification for cortex (A, B, C, D), hippocampus (E, F, G, H) and thalamus (I, J, K, L) sections; 10X magnification for cerebellum (M, N, O, P) sections. All images were taken under the same light intensity. Intensity of NeuN (R, S, T, U) was measured with ImageJ and normalized to WT group. 1-way-Anova analysis was used to determine p values by using GraphPad. Data were reported as means SEM (n=3, (*p<0,05, **p<0,025, ***p<0,001, ****p<0,0001).

In the cortex of 5-month-old mice groups, although presence of TUNEL positive cell in GM3S-/- mice was detected compared to WT as approximately 3.5-fold, Neu1-/- and Neu1-/-GM3S mice showed dramatically increase TUNEL positive cells compared to WT mice and GM3S-/- mice (Figure 3.46 A and B). 6-fold increase in Neu1-/- mice and 5.3-fold increase of apoptotic cells in Neu1-/-GM3S-/- mice compared with WT was exhibited as in Figure 3.46 A and B. Neu1-/- mice also showed increased apoptosis compared to GM3S-/- mice as approximately 1.8-fold in cortex section. The obvious increase of apoptosis in Neu1-/- and Neu1-/-GM3S-/- mice is compatible with the highly decreasing level of intensity of neuronal marker (NeuN) for the cortex region.

In the cerebellum section of 5-month-old mice groups, WT, Neu1-/-, GM3S-/- and Neu1-/-GM3S-/- mice did not show significant difference in the TUNEL positive cell number (Figure 3.46 C and D). However, there was a slightly increasing in the number of apoptotic cells of Neu1-/- mice compared to age-matched other mice, although it was not found statistically significantly (Figure 3.46 C and D).

The analysis of hippocampus regions based on apoptosis, 2.5-fold, 1.6-fold and 4-fold increased TUNEL positive cell number in Neu1-/-, GM3S-/- and Neu1-/-GM3S-/- mice was found compared to that of control littermates, respectively. Additionally, Neu1 deficient mice indicated significantly increase in the apoptosis compared to GM3S-/- mice as approximately 1.5-fold (Figure 3.47 A and B). The slightly elevated level of apoptotic cell number in the GM3S-/- mice (1-fold) was also determined compared to age matched WT mice, but it was not found as significant based on statistical analysis (Figure 3.47 A and B). The similar neuron loss was also seen in the histochemistry analysis (NeuN) for the hippocampus section.

TUNEL positive cells indicating apoptotic cells was also detected for the thalamus section of 5-month-old mice groups. GM3S-/- mice had slightly higher TUNEL positive cells than age matched WT mice, although it was not significant. It was demonstrated elevated level of apoptotic cells in Neu1-/- and Neu1-/-GM3S-/- mice as approximately 3 and 4-fold compared to age matched WT mice (Figure 3.47 C and D). Neu1-/- and Neu1-/-GM3S-/- mice was also had higher apoptotic cell number as approximately 1.5 and 2-fold than GM3S-/- mice (Figure 3.47 C and D). According to these results, the increased level of apoptosis in Neu1-/-GM3S-/- mice may be derived from GM3S and more importantly Neu1 gene deficiency. The increase of apoptosis in Neu1-/- and Neu1-/-GM3S-/- mice is consistent with the decreasing level of intensity of neuronal marker (anti-NeuN staining) for the thalamus region.

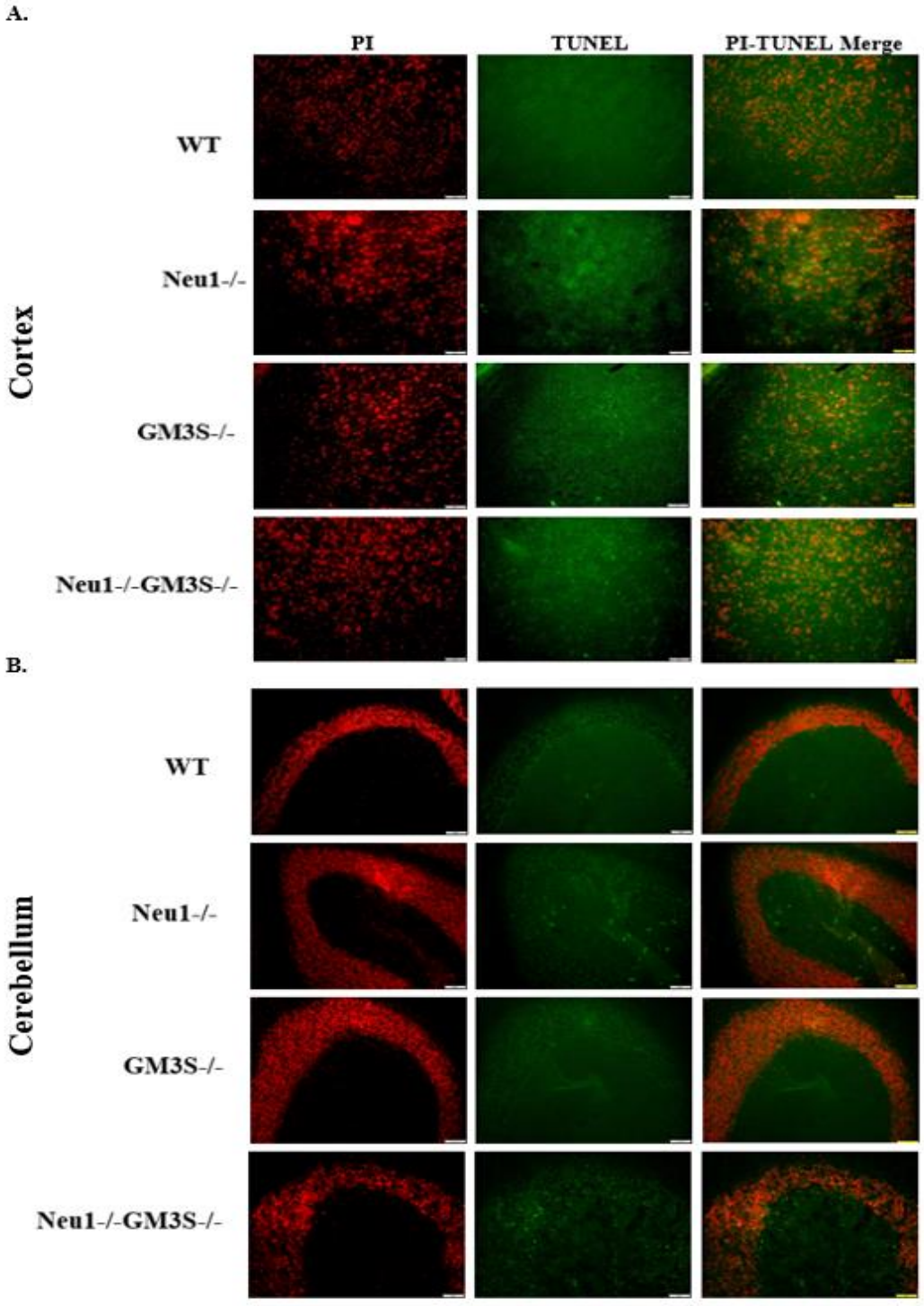

Figure 3.46. Immunostaining of TUNEL in 5-month-old WT, Neu1-/-, GM3S-/- and Neu1-/-GM3S-/- mice brain coronal sections, cortex and cerebellum. Images were taken at 20X magnification for cortex (A) and 10X magnification for cerebellum (B) sections. All images were taken under the same light intensity that differs filter types for PI and TUNEL. Sections were stained with Terminal deoxynucleotidyl Transferase (TdT) as (green) and PI (red; nucleus). Co-localization intensity of PI and TUNEL for cortex (C) and cerebellum (D) was measured with ImageJ and normalized to WT group. 1-way-Anova analysis was used to determine p values by using GraphPad. Data were reported as means SEM. (n=3, *p<0,05, **p<0,025).

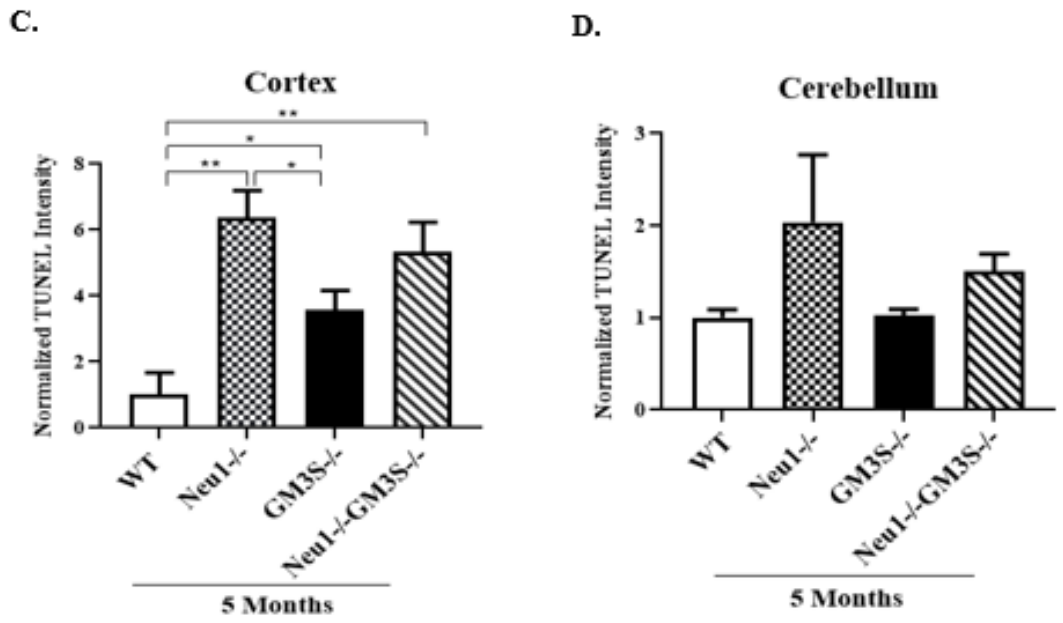

Figure 3.46 (cont.)

3.9. Behavioral Analysis

3.9.1 Rotarod Test

Motor function and activity were evaluated with Rotarod Test in order to understand the effect of changed ganglioside content on activities. 2- and 5-month-old WT, Neu1-/-, GM3S-/- and Neu1-/-GM3S-/- mice were utilized for rotarod test to understand the changes in the motor neuron function and activity depending on age and genotype. Motor function impairments can be associated with the cerebellum tissue of brain since locomotor activities are regulated with cerebellum part (Lee et al. 2018).

There was no significant change in rotarod test of 2-month-old mice. However, it was notified that there was a reduction in the motor coordination and balance of 5-month-old Neu1-/-, GM3S-/- and Neu1-/-GM3S-/- mice compared to 2-month-old Neu1-/-, GM3S-/- and Neu1-/-GM3S-/- mice, respectively (Figure 3.48). As approximately %37, %48 and %76 reduction in the motor function of Neu1-/-, GM3S-/- and Neu1-/-GM3S-/- mice was determined in age related, respectively (Figure 3.48). This motor coordination and balance impairments depending on age can be associated with cerebellum tissue abnormalities seen in single and mostly double gene deficient mice.

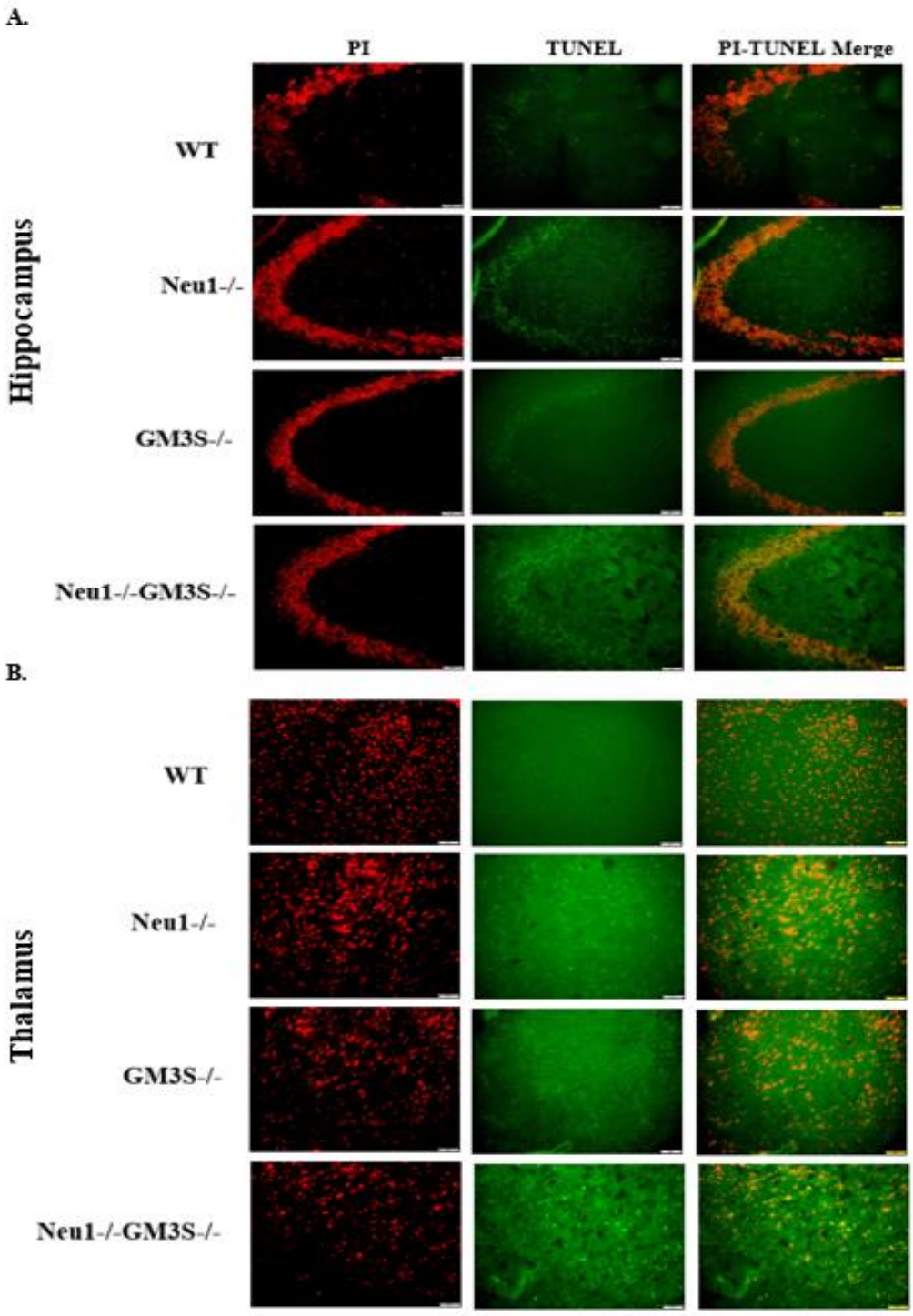

Figure 3.47. Immunostaining of TUNEL in 5-month-old WT, Neu1-/-, GM3S-/- and Neu1-/-GM3S-/- mice brain coronal sections, hippocampus and thalamus. Images were taken at 20X magnification for hippocampus (A) and thalamus (B) sections. All images were taken under the same light intensity that differs filter types for PI and TUNEL. Sections were stained with Terminal deoxynucleotidyl Transferase (TdT) as (green) and PI (red; nucleus). Co-localization intensity of PI and TUNEL for hippocampus (C) and thalamus (D) was measured with ImageJ and normalized to WT group. 1-way-Anova analysis was used to determine p values by using GraphPad. Data were reported as means SEM. (n=3, **p<0,025, ***p<0,001).

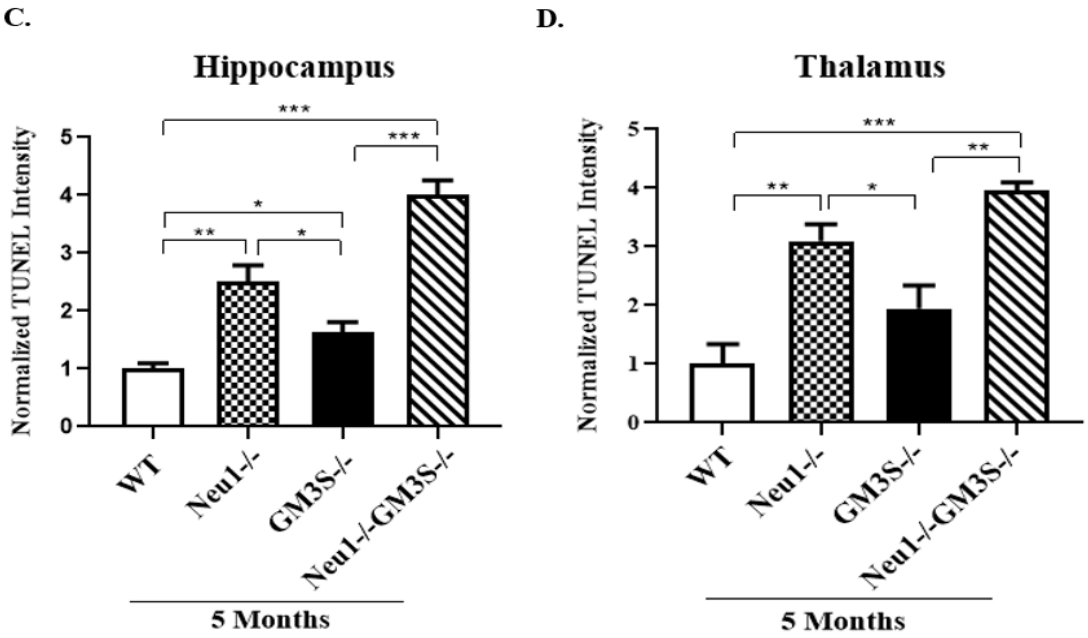

Figure 3.47 (cont.)

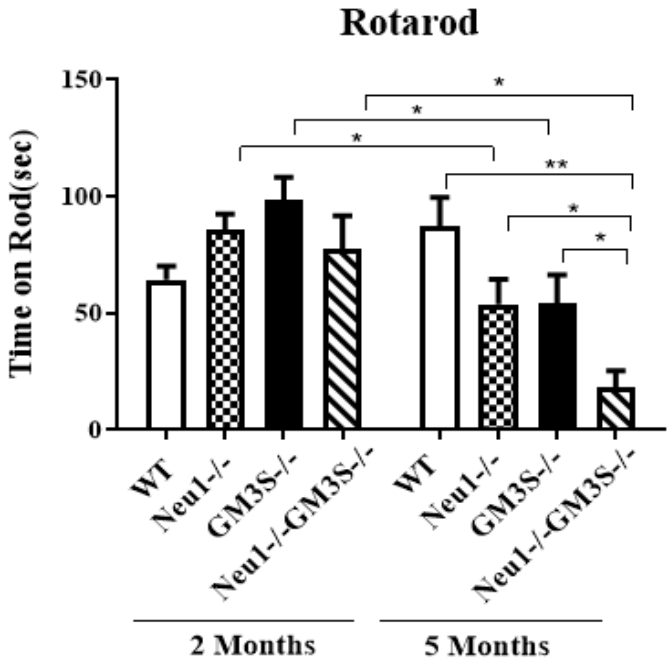

Figure 3.48. Running time on rotarod (sec) of 2- and 5-month-old WT, Neu1-/-, GM3S-/- and Neu1-/-GM3S-/- mice. Each mouse was teached to stay and run on rod and then rotarod test was applied for 3 times for each mouse group. 2-way-Anova was used to determine p-values by using GraphPad and data were reported as means SE (n=6 independent mice for each mice group, *p<0,05).

5-month-old Neu1-/-GM3S-/- mice showed least duration time on the rotating rod compared to other mice according to rotarod test results. Duration time on rotating rod of 5-month-old Neu1-/-GM3S-/- was lower as approximately %76, %66 and %67 compared with age matched WT, Neu1-/- and GM3S-/- mice respectively (Figure 3.48). The intense deterioration in motor function of older Neu1-/-GM3S-/- mice might result from both aging and lack of two genes; Neu1 and GM3S gene and the intense deformation of Purkinje cells in cerebellum of Neu1-/-GM3S-/- mice may be related with this motor function impairment.

3.9.2. Grip Strength Measurement Test

The purpose of the Limb Grip Strength measurement was to show whether ganglioside changes have any effect on nerve-muscle functions and muscle strength in mice depending on age. Fore limb grip strength (grams) were determined for the 2- and 5-month-old WT, Neu1-/-, GM3S-/- and Neu1-/-GM3S-/- mice.

In fore limb grip strength, there was no significant difference in the 2 old WT (75 ± 8), Neu1-/- (70 ± 6) and GM3S-/- (69 ± 10) mice (Figure 3.49). Additionally, 5 -month-old WT (80 ± 15), Neu1-/- (72 ± 5)and GM3S-/- (65 ± 10)mice had similar fore limb grip strength as can be seen in Figure 3.49. Therefore, no age-related changes were observed for WT, Neu1-/- and GM3S-/- mice.

2-month-old Neu1-/-GM3S-/- showed reduction in the fore limb grip strength compared to age matched WT, Neu1-/- and Neu1-/-GM3S-/- mice. The similar reduction was also observed for 5-month-old Neu1-/-GM3S-/- mice. Additionally, there was a significant impairment in the fore limb grip strength of 5 -month-old Neu1-/-GM3S-/- (35 ± 10) mice compared to 2-month-old Neu1-/-GM3S-/- (19 ± 5) mice (Figure 3.49). This indicates the age-related effect of double gene deficiencies in nerve-muscle functions and muscle strength.

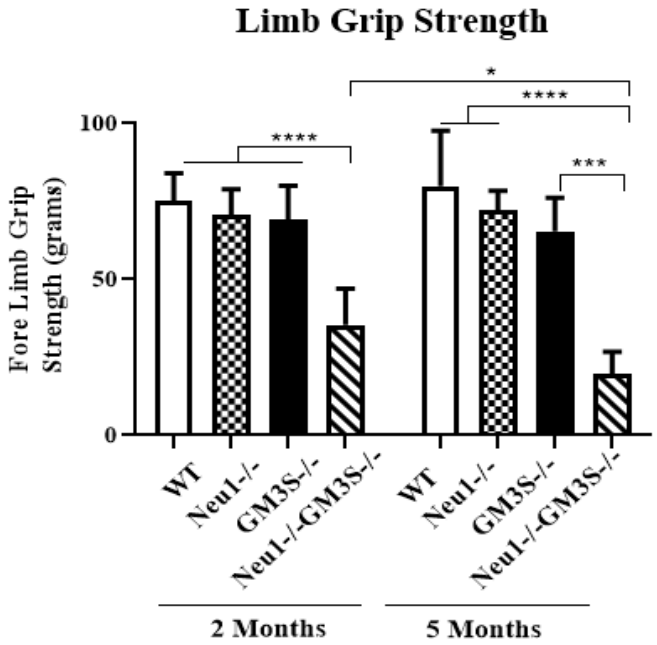

Figure 3.49. The fore limb grip strength of 2- and 5-month-old WT, Neu1-/-, GM3S-/- and Neu1-/-GM3S-/- mice. 2-way-Anova was used to determine p-values by using GraphPad and data were reported as means SE (n=6 for each mice group, *p<0,05, ***p<0,001, ****p<0,0001).

3.9.3. Passive Avoidance Test

Passive Avoidance Test was performed to determine whether the changed ganglioside content causes any age-related damage especially in the hippocampus region of the brain. 2- and 5-month-old WT, Neu1-/-, GM3S-/- and Neu1-/-GM3S-/- mice were used for Passive Avoidance Test. Passive avoidance test apparatus includes two compartments (light and dark) which are separated by sliding door. Passive Avoidance Test was performed for three days. On the first day, mouse was put into light compartment and waited for 1 minutes. On the second day, mouse put into light compartment then sliding door was opened after 1 minute and 0.2 mA electric shock for 2 s was given to mouse when mouse pass to the dark part. On the third day (test day), the same procedure was applied as in the second day and passage time to dark region (Latency Time) was recorded by ShutAvoidv1.8 (Harvard Apparatus) in order to understand whether there is a problem in the learning and memory process depending on age and genotype.

The latency time (sec) of 2- and 5-month-old GM3S-/- mice did not show any difference compared to 2- and 5-month-old WT mice. The average latency time to enter dark compartment is 279 ± 39 s and 296 ± 8 s for 2- and 5-month-old WT while this average time is 275 ± 39 s and 293 ± 16 s for 2 and 5 -month-old GM3S-/- mice (Figure 3.50). As can be seen from these average times, both 2- and 5-month-old WT and GM3S-/- mice had average time which close to 300 seconds representing the end point of experiment. These results showed that GM3S gene deficiency did not have any effect on the learning process for both 2- and 5-month-old animals.

2- and 5-month-old Neu1-/- mice had 66 ± 57 s and 28 ± 7 s average latency times to enter the dark compartment, so these 2 and 5 -month-old Neu1-/- mice showed significant reduction in the latency time (sec) compared to 2- and 5-month-old WT and GM3S-/- mice, implying impairments in the learning process of 2- and 5-month-old Neu1-/- mice (Figure 3.50). The significant change with aging was not detected in Neu1-/- mice (Figure 3.50).

The entrance time to dark compartment on the test day decreased in the 2- and 5-month-old Neu1-/-GM3S-/- (105 ± 104 s, 54 ± 15 s) compared to both 2- and 5-month-old WT and GM3S-/- mice (Figure 3.50). However, there was no change between the 2- and 5-month-old Neu1-/-GM3S-/- mice, implying lack of aging effect in double deficient mice (Figure 3.50). The reduction of latency time in 2- and 5-month-old Neu1-/- GM3S-/- mice could be due to Neu1 gene deficiency because there was no difference observed in 2- and 5-month-old GM3S-/- mice compared to age matched WT mice, significant reduction in latency time was observed in only mice with Neu1 gene deficiency. All in all, learning and memory process was deteriorated in Neu1-/- and Neu1-/-GM3S-/- mice.

3.9.4 Open Field Test

The purpose of this test was to understand whether the change in the content of ganglioside has effect on the anxiety behavior, sedation and locomotor activities of mice depending on the age. In this direction, the movements of the mice along 5 minutes on the square platform were recorded and time in center and total distance of distinct mice groups were determined. Less time spent in the center is associated with anxiety behavior in animals. The difference of the spent time in center in both 2- and 5-month-old animal

groups were observed (Figure 3.51 A). There was reduction of time in center for 2-month-old GM3S-/- mice as %30 compared to WT. However, significant change was not found for 5 -month-old GM3S-/- mice compared to age matched WT mice (Figure 3.51 A).

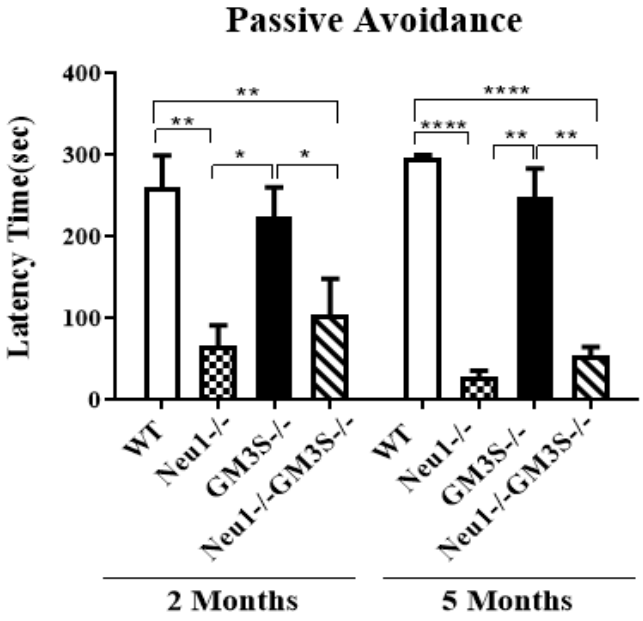

Figure 3.50. The latency time (passage time to dark region on test day) of 2- and 5-month-old WT, Neu1-/-, GM3S-/- and Neu1-/-GM3S-/- mice. 2-way-Anova was used to determine p-values by using GraphPad and data were reported as means SE (n=6 independent mice for each mice group, *p<0,05, **p<0,01, ****p<0,0001).

According to open-field results of 2-month-old animals, the more reduction was observed in Neu1-/- as %57 and Neu1-/-GM3S-/- mice as %90 compared to age matched WT mice, indicating anxiety behaviors in the both 2-month-old Neu1-/- and Neu1-/-GM3S-/- mice (Figure 3.51 A) Especially, 2-month-old Neu1-/-GM3S-/- mice was the least time-consuming animal in center, indicating importantly anxiety like behaviors (Figure 3.51 A). The significant change was not observed between 5-month-old WT and GM3S-/- mice (Figure 3.51 A), although slightly reduction in the time in center was observed in GM3S-/- mice compared to that of WT littermates. On the other hand, the same pattern seen in young mice was observed for 5-month-old Neu1-/- and Neu1-/-GM3S-/-mice. 5-month-old Neu1-/- mice as %67 and Neu1-/-GM3S-/- mice as %88 spent less time in center than age matched WT (Figure 3.51 A). 5-month-old Neu1-/-GM3S-/- mice was the least time-consuming animal in center compared to 5-month-old

animals. Less time spent in the center is related with anxiety behaviors in the 5 -month-old Neu1-/- and Neu1-/-GM3S-/- mice. Results indicated Neu1 gene deficiency may have a more potential effect on the anxiety behaviors seen in 2- and 5-month-old Neu1-/-GM3S-/- mice.

The total distance covered by 2- and 5- month old Neu1-/-GMS3-/- mice is less than their age matched WT mice, which indicates that these mice may have problems in their locomotor activities and there may be a damage in cerebellum part (Figure 3.51 B)

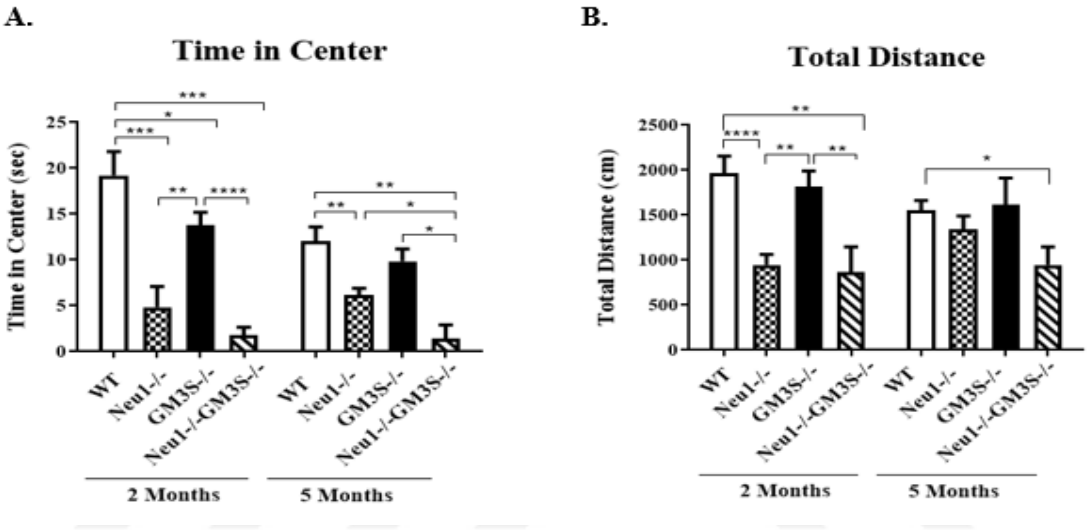

Figure 3.51. Open Field test of 2- and 5-month-old WT, Neu1-/-, GM3S-/- and Neu1-/-GM3S-/- mice. Mice movements; Time in Center (A) and Total distance (B) was recorded. 2-way-Anova was used to determine p-values by using GraphPad and data were reported as means SE (n=6 independent mice for each mice group, *p<0,05, **p<0,01, ***p<0,001, ****p<0,0001).

3.10. TLC Analysis of Urinary Oligosaccharides

Oligosaccharide analysis from urines of 2- and 5-month-old WT, Neu1-/-, GM3S-/- and Neu1-/-GM3S-/- mice were performed with thin layer chromatography the accumulation of sialylated oligosaccharides in urines is mostly common indicator of the sialidosis disease (Pelt et al. 1988). Therefore, it was goaled to demonstrate whether there is oligosaccharide accumulation in urines of Neu1-/- and Neu1-/-GM3S-/- mice due to deficiency of Neu1 gene in these mice. Previously, it was reported the markers for the sialidosis diagnosis by thin layer chromatography (Mutze et al. 2017). As depicted in Figure 3.52, bands which marked with red arrows refer to accumulated oligosaccharides

in sialidosis patient. The intensities of band 1 and band 2 were determined by using ImageJ. There was no band intensities in 2- and 5-month-old WT and GM3S-/- mice. This result clearly showed the lack of complex oligosaccharide accumulation in WT and GM3S-/- mice at any ages.

Oligosaccharide accumulation were seen in 2- and 5 -month-old Neu1-/- and Neu1-/-GM3S-/- mice (Figure 3.52). There was no significant change in the oligosaccharide accumulation for 2- and 5-month-old Neu1-/- mice. Therefore, it can be specified that the oligosaccharide accumulation did not show any difference depending on age for Neu1-/- mice (Figure 3.53 A and B). However, accumulation of oligosaccharides exhibited elevated level in 5-month-old Neu1-/-GM3S-/- mice compared to its young counterparts as approximately 1.5-fold, indicating age related oligosaccharide accumulation in Neu1-/-GM3S-/- mice (Figure 3.53 A and B).

On the other hand, it was noticed that there was approximately 2-fold and 5-fold elevated oligosaccharide accumulation in 2- and 5-months Neu1-/-GM3S-/- mice compared with same aged Neu1-/- littermates, respectively (Figure 3.53 A and B). This result showed that oligosaccharide accumulation increases in the case of double gene deficiency. The absence of complex gangliosides may cause the elevated oligosaccharide accumulation.

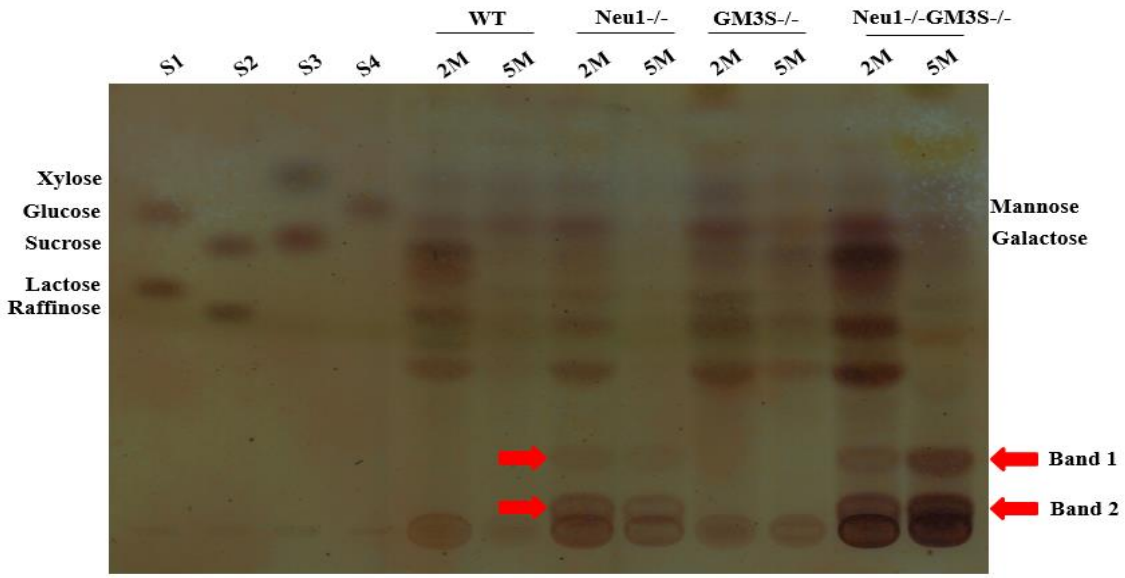

Figure 3.52. Thin layer chromatography and orcinol staining of urinary oligosaccharides of 2- and 5-month-old age WT, Neu1-/-, GM3S-/- and Neu1-/-GM3S-/- mice. S1; Glucose and Lactose, S2; Sucrose and Raffinose, S3; Xylose and Galactose and S4; Mannose.

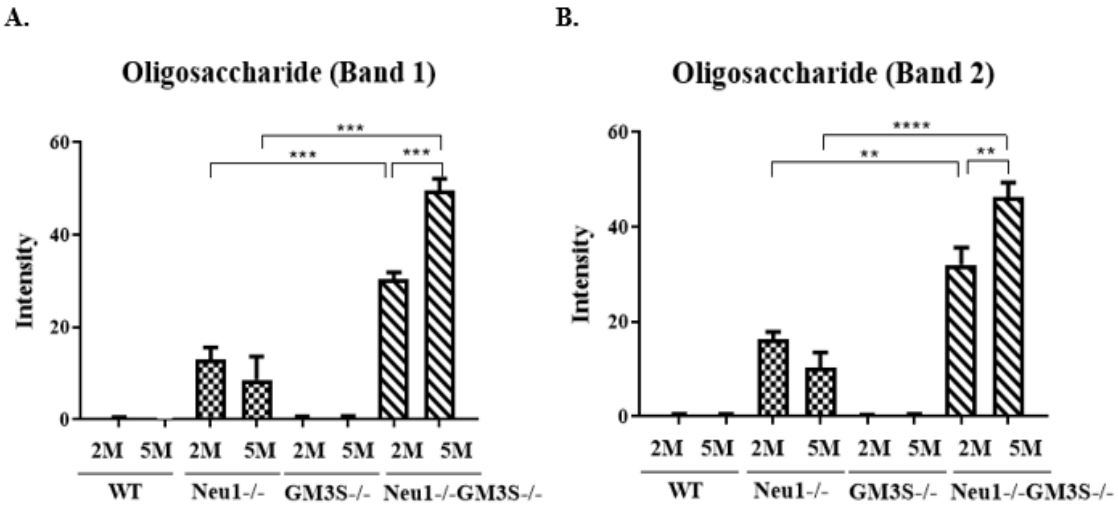

Figure 3.53. Intensity analysis of Band 1 (A) and Band 2 (B) for sialidosis diagnosis from the urines of 2- and 5-month old WT, Neu1-/-, GM3S-/- and Neu1-/-GM3S-/- mice. 2M represents the 2 -month-old mice groups; 5M represents 5 -month-old mice groups. Intensity of each band was detected by using ImageJ and 2-way-Anova analysis was used to determine p-values via GraphPad. Data were reported as means SE (n=3, **p<0,01, ***p<0,001, ****p<0,0001).

CHAPTER 4

DISCUSSION

Sialidases are enzymes and removes sialic acid residues from sialoglycoconjugates. Lysosomal Neu1 sialidase is responsible for the degradation and catabolism of sialoglycoconjugates in lysosomes (Frisch and Neufeld 1979). Substrates for Neu1 sialidase are commonly oligosaccharides and glycopeptides, and it also plays role in the catabolism of glycolipids (Schneider et al. 1991). βgalactosidase (β-Gal) and lysosomal protective protein Cathepsin A (PPCA) form a complex with the Neu1 sialidase (Horst et al. 1989). Protective protein Cathepsin A supplies glycosidase stabilization, and the lack of protective protein Cathepsin A leads to lysosomal storage disorder known as galactosialidosis (D'Azzo et al. 1996). Lysosomal storage diseases (LSDs) are rare hereditary metabolic disorders due to several gene mutations (Neufeld 1991). Deficiency of activator proteins, transporter proteins or lysosomal enzymes such as hydrolases results in accumulation of specific substrates including glycoproteins, glycosaminoglycans, gangliosides, sphingolipids, glycosphingolipids and other lipids in lysosomes (Ferreira and Gahl 2017). On the other hand, the deficiency of Neu1 sialidase causes other lysosomal storage disorder known as sialidosis. Sialidosis is a systematic disorder including two clinical variants (Type I and Type II) depending of severity and age of onset (Seyrantepe et al. 2003), and any therapy has not been developed for sialidosis patients. The common indicator of sialidosis is the accumulation of sialylated oligosaccharides in tissues and extraction of accumulated substances in urines or body fluids (Pelt et al. 1988). Neu1 gene deficient mice was firstly created by d'Azzzo et al. 2002 to supply the understanding of Neu1 role in cellular and physiological pathways. Mice nullizygous at Neu1 locus showed the similar symptoms seen in patients suffering from early onset of sialidosis (Type II) consisting of nephropathy, neurological impairment, edema, spleen enlargement, urinary extraction of oligosaccharides, deformity of spine and hematopoiesis (d'Azzo et al. 2002). It was previously demonstrated the symptoms seen in single Neu1 deficient mice, and roles of lysosomal Neu1 sialidase in the catabolism sialoglycoconjugates was implied. Together, accumulation of glycolipids such as GM3, GD3, GM4 and LM1 gangliosides in visceral organs of sialidosis patients, and investigation of GM3 ganglioside as lysosomal sialidase

substrate was also reported *in vitro*. However, role of lysosomal Neu1 sialidase enzyme alone and combined with GM3S on glycolipid metabolism in brain has not been elucidated previously *in vivo*. Within the frame of this thesis study, biological role of lysosomal Neu1 sialidase in glycosphingolipid metabolism in the case of lack of -a and -b series gangliosides was investigated. In accordance with this purpose, double gene deficient mice was created with the crossing of existing Neu1 deficient mice with GM3S deficient mice, and thereby combined biological roles of Neu1 and GM3S genes were understood *in vivo*. GM3S deficient mice, GM3S-/-, were used for goals of thesis because mutant mice could not produce GM3 ganglioside, and thereby -a and -b series gangliosides which are composed of central nervous system for several cell processes (Yamashita et al. 2003). In this research, two age groups such as 2- and 5-month-old single gene and double gene deficient mice were analyzed to understand whether there was an age-related change in ganglioside metabolism and cellular processes.

Smaller size of 1-month-old Neu1-/- mice compared to that of WT littermates was shown previously by d'Azzo et al. 2002. Weight measurement process carried out within thesis showed that Neu1-/- mice were smaller than WT and GM3S-/- mice throughout their life span, and body weight of 20-week-old Neu1 deficient mice was also lesser than age matched WT and GM3S-/- mice as approximately 1.3 and 1.2- fold, respectively (Figure 3.3 B and D). Gross appearances of 20 week-old mice were also exposed the smaller size of Neu1-/- mice compared to that of control littermates. On the other hand, Yamashita et al. 2003 was demonstrated that mutant mice, GM3S-/-, viable without major problems and mutant mice did not show significant difference in body weights compared to wild type mice. Body weight measurement results indicated that body weight of 20-week-old GM3S mutant mice did not difference from the age-matched WT mice. In addition to weight measurement, gross appearance of male 5-months-old WT and GM3S-/- mice based on size did not show major difference (Figure 3.3 E). The most weight loss was demonstrated in newly created double gene deficient mice, Neu1-/-GM3S-/-. Almost 1.7, 1.3, and 1,5-fold weight losses were determined in 20-week-oldNeu1-/-GM3S-/- mice compared to that of WT, Neu1-/- and GM3S-/- littermates, respectively (Figure 3.3 B and D). Gross appearance revealed that 5-month-old male Neu1-/-GM3S-/- mouse had the smallest length compared to other that of littermates. Additionally, the sudden death was observed in Neu1-/-GM3S-/- mice at the age of 20 weeks, although GM3S mutant mice shows normal life span (Yamashita et al. 2003), and Neu1 mutant mice can live until

the ages of 6 to 7 months (d'Azzo et al. 2002). Therefore, the older mice groups for experiments were planned as 5 months of age.

Thin layer chromatography analysis was performed to investigate whether the presence of lysosomal sialidase, Neu1, in the ganglioside synthesis and degradation pathway. Accumulation of glycolipids like GM3, GD3, GM4 and LM1 in visceral organs of sialidosis patients except brain was reported (Breiden and Sandhoff 2020), and it was also notified the GM3 ganglioside as substrate of lysosomal sialidase *in vitro* (Fingerhut et al. 1992). Although the presence of several studies about Neu1 sialidase, effect of Neu1 sialidase on complex ganglioside pathway in brain remain unclear. Our results demonstrated that -a series gangliosides including GM1 and GD1a, and -b series gangliosides such as GD1b and GT1b did not show different band intensities for both ages of WT and Neu1-/- mice in the cortex and cerebellum tissues (Figure 3.5 and 3.10). Together, for WT and Neu1-/- mice, there was no expression difference for -a and -b series gangliosides between young and older mice groups, implying no age-related accumulation. In brain, the effect of Neu1 sialidase on GM3 ganglioside was not observed *in vivo* in the case of Neu1 deficiency, although GM3 ganglioside was remarked as substrate of Neu1 sialidase *in vitro* (Fingerhut et al. 1992). In this respect, it can be said that the there are some alterations between *in vitro* and *in vivo* conditions. On the other hand, in a recent study it was shown that GM3 ganglioside accumulation does not occur in all cell types in the case of Neu1 deficiency and GM3 ganglioside is a target of Neu3 and Neu4 sialidase in brain (Aerts et al. 2019). In our results, the accumulated GM3, GD3 gangliosides were not determined in brain tissues of Neu1 deficient mice like in sialidosis patients. The accumulation of these gangliosides seen in organs of sialidosis patients might be observed in the visceral organs of Neu1 deficient mice, if the TLC analysis was applied for other organs of Neu1-/- mice in addition to brain. In previous studies, it was already reported the absence of a- and b- series gangliosides such as GM1a, GD1a, GD1a, GD1b and GT1b in brain (Yamashita et al. 2003), inner ear (Yoshikawa et al. 2009) and retinas (Hiraoka et al. 2019) of GM3S-/- mice because GM3S mutant mice cannot produce GM3 ganglioside known as precursor of -a and -b series gangliosides. Consistently with that, thin layer chromatography results for cortex and cerebellum brain tissues indicated that -a and -b series gangliosides were absent in 2- and 5-month old GM3S-/- mice (Figure 3.5 and 3.10). In addition to GM3S-/- mice, no expression of -a and -b series gangliosides were observed at 2 and 5 months of age Neu1-/-GM3S-/- mice. GM3S deficiency could cause the lack of these gangliosides in double gene deficient

mice. On the other hand, expression of -o series gangliosides in GM3S-/- mice in order to compensate the absence of -a and -b series gangliosides were shown in several studies (Yamashita et al. 2003 and Yoshikawa et al. 2009). Cortex ganglioside profile revealed the expression of -o series acidic gangliosides such as GM1b, GD1α in 2 and 5 months of age GM3S-/- and Neu1-/-GM3S-/- mice (Figure 3.6). The decreased expression of GM1b and GD1α gangliosides in young Neu1-/-GM3S-/- mice compared to GM3S-/- mice may reflect the activity of other sialidases in order to compensate the Neu1 sialidase deficiency. Unlike the cortex tissue, GalNAc-GM1b (extended GM1b), -o series acidic ganglioside, expression was observed in addition to GM1b and GD1α gangliosides in the cerebellum tissue of 2- and 5-month-old GM3S-/- and Neu1-/-GM3S-/- mice (Figure 3.11). These results clearly showed the presence of different ganglioside pattern in distinct parts of brain. For the expression of -o series gangliosides in GM3S-/- and Neu1-/-GM3S-/- mice, no difference between 2 and 5-months old animals indicated that there was no age-related accumulation. These results clearly showed that compensatory expression of -o series acidic gangliosides in GM3S-/- and Neu1-/-GM3S-/- mice owing to GM3S gene deficiency. -o series ganglioside expression was absent in the any ages of WT and Neu1-/- mice for both cortex and cerebellum tissue, indicating that no compensatory mechanism was available in these genotyped mice due to presence of -a and b- series gangliosides.

In several lysosomal storage disorders such as Tay-Sachs disease, Lactosylceramide (LacCer) accumulation was indicated previously (Seyrantepe et al. 2017). Lactosylceramide is pioneer for the o- series of gangliosides that refers to GA2, GA1, GM1b and GD1c in the ganglioside pathway (Schengrund 2015). While there was no accumulation of LacCer in the cortex and cerebellum tissue of WT and Neu1-/- mice at any ages (Figure 3.8 A and 3.13 A), the significant elevated level of this lipid at 2 and 5 months of age GM3S-/- and Neu1-/- GM3S-/- mice was indicated in both cortex and cerebellum tissues (Figure 3.8 A and 3.13 A). Accumulation of LacCer in 2- and 5-month-old GM3S-/- mice reflected blockage in the conversion of LacCer intermediate to GM3 ganglioside due to deficiency of GM3S gene as seen in previous studies (Yoshikawa et al.2015). The accumulation of LacCer in the 2- and 5-month-old Neu1-/-GM3S-/- mice resulted from deficiency of GM3S gene.

Neutral ganglioside profile was compared for differently-genotyped mice by TLC. GA2 and GA1 gangliosides are neutral gangliosides produced from Lactosylceramide (LacCer) and GA2 gangliosides separately (Schengrund 2015). Glycosphingolipids

harvested from the zebrafish embryos with knockdown of GM3S showed the elevated level of LacCer and GA2 gangliosides (Boccuto et al. 2014). Additionally, the elevated level of alternative series (o-, globo, neolacto- series) in the GM3S deficient patients was shown by mass spectrometric analysis (Fragaki et al. 2013). In neutral ganglioside analysis of cortex and cerebellum tissues, higher level of GA2 and GA1 (-o series) neutral gangliosides was observable in GM3S-/- and Neu1-/-GM3S-/- mice at any ages, although there was no expression of these neutral gangliosides in WT and Neu1-/- mice at any ages (Figure 3.8 B, C and 3.13 B, C). The higher band intensity for GA2 and GA1 gangliosides in double gene deficient mice at any ages caused by the absence of GM3S gene. Age related accumulation of these neutral gangliosides was not detected in the cortex section, but slightly increasing level of GA2 and significant elevated level of GA1 were determined in the cerebellum tissue of 5-month-old GM3S-/- and Neu1-/-GM3S-/- mice compared to their young counterparts (Figure 3.13 B and C). This result indicator of age dependent accumulation for GA2 and GA1 gangliosides in the cerebellum tissue. As a result of these findings, alternative enzymatic modification of LacCer due to GM3S deficiency causes the highly production of other derivatives such as -o series acidic and neutral gangliosides. Lipid profile for gangliosides are different from each other for distinct brain sections such as cortex and cerebellum therefore, other brain sections such as thalamus may be used for deeper understanding of role of these enzymes on glycosphingolipid metabolism. No difference in Neu1-/- mice was notified compared to WT littermates for -o, -a and -b series gangliosides with Thin Layer Chromatography (TLC), although TLC is a wide-spread method for identification of complex structures in a solution (Ando et al. 1978). However, mass spectrophotometry (MS), one of the powerful techniques, can be required for the further identification of unknown compounds. Therefore, MS can be performed in order to determine the presence of Neu1 sialidase role in glycolipid pathway as further investigations. In addition to brain, glycolipid content can be explored by TLC in other tissues including kidney, liver, spleen in Neu1 deficient and double gene deficient mice due to effect on Neu1 sialidase in other tissues besides brain.

In several lysosomal storage disorders, it was speculated that apoptosis seen in lysosomal storage disorders is related with the accumulated complex lipids consisting of glycolipids and gangliosides, and secondary metabolites such as oligosaccharides (Huang et al. 1997). The relation between the gangliosides and apoptosis was notified for several gangliosides. It was claimed that GM3, GD3 and GD1b gangliosides lead to apoptosis

activation depending on elevated expressions on membrane in various cell types (Giussani et al. 2014). Apoptosis with higher expression of GM3 synthase and elevated GM3 ganglioside in several cancer cells was also shown previously (Giussani et al. 2014). On the other hand, patients due to homozygous nonsense mutation in the GM3 synthase displayed the reduction in mitochondrial membrane potential that triggers the apoptosis (Fragaki et al. 2012). Cartilage explants of GM3S knock-out mice had also higher TUNEL positive cell ratio compared to same aged control group due to elevated inflammation, thereby indicating the regulatory role of GM3 ganglioside in the apoptosis (Sasazawa et al. 2014). All these information actually notified the presence of controversial role of GM3 ganglioside in apoptosis, although GD3 and GD1b gangliosides have apoptotic roles in several cell types. On the other hand, role of sialidases for apoptosis were demonstrated in several studies, especially in cancer cells. Sialidase Neu2 role in the desialylation of Fas ligand and activation of extrinsic apoptotic pathway by Neu2 expression in human cancer cells were determined (Nath et al. 2018). Fluctuations of Neu3 (Kakugawa et al. 2002) and Neu4 (Yamaguchi et al. 2005) expression in distinct cancer cells were also determined by regulating apoptotic pathway. Additionally, role of Neu1 sialidase and its effects on apoptotic pathway was shown in colon (Uemure et al. 2009), ovarian (Ren et al. 2016), and carcinoma (Thulasiraman et al. 2019) cells. Especially, it was claimed that Neu1 expression reduced in several cancer types (Uemure et al. 2009). Although no fact about the apoptosis in brain of Neu1 deficient mice, neuronal apoptosis in spinal cord neurons has been shown in mouse model of GM1-gangliosidosis that occurs in the absence of βgalactosidase (β-Gal) complexing with Neu1 sialidase (Tessitore et al. 2004). DNA isolation and agarose gel electrophoresis analysis, one of the apoptosis determination method, was applied for the investigation of apoptosis according as genotype and age in this research. The presence of fragmented DNAs and apoptosis were shown previously in several lysosomal storage disorders. Huang et al. 1997 was clarified the availability of fragmented DNAs after the ethidium bromide staining of agarose gel in the cortex, cerebellum and brain stem of Sandhoff mice (Hexb-/-,) and cerebellum of Hexa-/- mice. The small and fragmented DNAs except genomic DNA on agarose gel are indicator of apoptosis (Stewart 1994). In our research, results indicated different pattern for distinct brain sections. There was no extra band in the 2-month-old single and double deficient mice compared to same aged control littermates, whereas an extra band in 5-month-old GM3S-/- and Neu1-/-GM3S-/- mice was observed on agarose gel for cortex tissue (Figure 3.14 A). Extra bands were only

seen in young Neu1-/-GM3S-/- mice for cerebellum tissue (Figure 3.14 B). In the thalamus tissue, it was demonstrated that there were extra bands in both 2 and 5-month-old mice which had single gene deficient (Neu1-/- and GM3S-/- mice) and double gene deficient (Neu1-/-GM3S-/-) mice (Figure 3.14 C). The fragmented DNAs were more clearly observed in the thalamus tissue compared to other cortex and cerebellum tissues and these fragmented DNAs can be associated with apoptosis (Figure 3.14 C). Though differences among brain tissues were observed, apoptotic analysis were performed with other methods such as Western Blot, Real-Time PCR, Immunostaining and Immunohistochemistry for a deeper understanding of apoptosis in differently-genotyped mice depending on changed glycolipid metabolism and accumulated oversialylated conjugates.

It was goaled to investigate that how possible abnormalities in glycosphingolipid metabolism and accumulated oversialylated conjugates caused by single and double gene deficiency leads to apoptosis. Western Blot and Real-Time PCR analysis were used as biochemical methods. In addition to apoptotic markers, ER stress and oxidative stress related genes which induce the programmed cell death were studied. In our study, three brain sections were analyzed by Real-Time PCR for the investigation of ER stress, oxidative stress and apoptosis due to possible abnormalities in glycosphingolipid metabolism. In previous reports, the apoptosis associated with ER stress and oxidative stress has been reported in several lysosomal storage disorders such as infantile neuronal ceroid lipofuscinosis (Zhang et al. 2006) and GM1-gangliosidosis that occurs in the absence of βgalactosidase (β-Gal) complexing with Neu1 sialidase (Futerman and Van Meer 2004). For that reason consequently, impact of glycosphingolipid and glycoprotein metabolism for cellular events was clearly presented. Wei et al. 2008 analyzed the ER stress and oxidative stress markers in fibroblasts from patients with following several lysosomal storage disorders: neuronal ceroid lipofuscinosis, GM1 gangliosidosis, Tay-Sachs disease, Gaucher disease type II (GD II), Niemann–Pick C type 2 (NPC2). mRNA levels of ER stress markers such as ATF6, calnexin, spliced XBP-1 and Grp78 highly expressed in these patient' fibroblasts compared to control groups, indicating presence of ER stress in these cells (Zhang et al. 2006, Wei et al. 2008). Protein and mRNA levels of oxidative stress markers such as SOD2, Catalase and TTase1 were also elevated in fibroblasts of patients when expression levels of patients were compared to control groups (Wei et al. 2008). In the same study, in order to understand the relation between ER – oxidative stress and apoptosis, Annexin V-FITC staining was applied and the higher

apoptotic cells were determined in patient cells, representing the relation between cellular stress and apoptosis in lysosomal storage disorders due to changes in glycolipid-glycoprotein metabolism and accumulated secondary metabolites (Wei et al. 2008). In our thesis study, ATF6, Calnexin and XBP-1 markers were used as ER stress markers for all mice. In cortex tissue, 2-month-old Neu1-/- mice had elevated expression for ATF6 compared to age matched GM3S-/- and Neu1-/-GM3S-/- mice, implying higher ER stress in young Neu1-/- mice (Figure 3.15 A). ATF6 expression level was also higher in the cortex of older single and double gene deficient mice compared to same aged WT littermates (Figure 3.15 A). Additionally, there was increase in the level of ATF6 expression in age dependent manner for single and double gene deficient mice (Figure 3.15 A). Calnexin, ER stress marker, is responsible for protein folding (Kleizen and Braakman 2004). Calnexin expression was also higher in cortex of older Neu1-/-, GM3S-/- and Neu1-/-GM3S/- mice compared to age matched WT littermates (Figure 3.16 A). The expression level of X-box binding protein was also analyzed for the ER stress analysis. X-box binding protein, transcriptional factor, is spliced in the case of ER stress depending on the IRE1 activation (Walter and Ron 2011). Spliced form of XBP leads to activation of unfolded protein response (UPR) in cells, and the expression level of spliced XBP-1 is proportional with the ER stress (Walter and Ron 2011). By mRNA analysis, unspliced form of XBP-1 was studied in this research, and reduction in the expression of unspliced XBP-1 was shown due to aging in cortex of older Neu1-/-, GM3S-/- and Neu1-/-GM3S-/- littermates compared to control mice (Figure 3.17 A). Together, expression of unspliced XBP-1 was lower in the young and older Neu1-/- mice compared to age matched GM3S-/- littermates (Figure 3.17 A). The reduction in the unspliced form of XBP1 may be related with the increase in spliced XBP-1, which is an ER stress indicator, but for a better understanding of this, the expression of spliced XBP-1 can be determined as a further investigation. For cortex tissue, ER stress analysis on mRNA level showed that single and double gene deficiencies lead to ER stress in especially older mice compared to control groups. The importance of glycolipid and glycoprotein metabolism for cellular stress have been indicated in previous studies (Wei et al. 2008), and it has been notified that sphingolipid composition regulates lipid hemostasis and block ER stress (Ho et al. 2018). Therefore, it can be said that the ER stress alterations seen in GM3S-/- mice may be related with the abnormalities of glycosphingolipid metabolism, and highly expression of alternative series (-neolacto, -globo, -o series) besides absence of complex gangliosides in GM3S-/- mice. On the other hand, the accumulation of

oversialylated oligosaccharides in brain of sialidosis patients, and highly oversialylated substrates of Neu1 sialidase in brain of Neu1-/- mice were identified in previous studies. Additionally, the intense glycoconjugate accumulation was shown in Neu1-/- mice in our results of PAS staining. According to these findings, the accumulation of oversialylated substances and glycoconjugates in brain may lead to ER stress seen in Neu1-/- mice.

In ER stress analysis for cerebellum tissue, ATF6 mRNA expression was significantly higher in 5-month-old Neu1-/- mice compared to other same aged but differently-genotyped mice (Figure 3.15 B). Similar to ATF6 expression, older Neu1 knock-out mice showed elevated expression level for Calnexin compared to age-matched WT mice (Figure 3.16 B), while no significant difference was detected for unspliced XBP-1 gene expression in differently-genotyped mice (Figure 3.17 B). As a results of these findings, Neu1 gene deficiency causes ER stress, may be driven from the highly accumulation of glycoconjugates in brain of Neu1-/- mice seen by PAS staining in the cerebellum tissue of older mice.

ER stress analysis for thalamus tissue also showed the significantly increased mRNA level of ATF6 in Neu1-/-, GM3S-/- and Neu1-/-GM3S-/- mice when mice were aging (Figure 3.15 C). Additionally, older single and double gene deficient mice showed elevated level in ATF6 and Calnexin expression compared to the same aged WT mice (Figure 3. 15 C and 3.16 C), but significant difference was not found for XBP-1 expression (Figure 3. 17 C). These results indicated the presence of ER stress in thalamus tissue of older mice in the case of defects in Neu1 and GM3S genes. The reason of ER stress can be due to alterations in the glycosphingolipid metabolism due to GM3S deficiency and highly accumulation of oversialylated glycoconjugates in the case of Neu1 deficiency. In a previous study, the absence of UPR activation and ER stress in spinal cord of 5-month-old Neu1-/- mice was indicated (Tessitore et al. 2004). However, the observed alterations and presence of ER stress in 5-month-old Neu1-/- mice may be due to usage of cortex, cerebellum and thalamus tissues instead of spinal cord in our study.

In addition to ER stress markers, oxidative stress markers (SOD2, catalase and TTase1) were analyzed by Real-Time PCR for three tissues. Superoxide Dismutase 2 (SOD2) is an antioxidant enzyme and it supplies the detoxification of superoxide radicals by converting superoxide to hydrogen peroxide and oxygen. Therefore, SOD2 activity is very important for maintenance of healthy state of a cell (Bostwick et al. 2000). Impairments in antioxidant defense system were reported previously in lysosomal storage disorders (Plotegher and Duchen, 2017), but antioxidant defense mechanism has been

determined to vary significantly among distinct lysosomal storage disorders. For instance, the SOD2 expression level reduced in yeast model of Niemann-Pick type C1 (Vileça et al. 2014), while its expression showed elevated level in MPS IV patient erythrocytes (Donida et al. 2015). It was suggested that mitochondrial dysfunction prevents the activation of defense system, thereby the SOD2 expression decreases (Vileça et al. 2014). On the other hand, it was also reported that SOD2 activity increases due to response of cells to reactive oxygen species (Donida et al. 2015). Our results for SOD2 expression in cortex showed that 5-month-old mice had lower SOD2 expression compared to young mice groups (Figure 3.18 A). This finding may be indicator of problems in defense mechanism of older mice for the cortex tissue. Catalase expression analysis was also done for oxidative stress analysis. Catalase plays role in the elimination of hydrogen peroxide, and it is also player of antioxidant defense mechanism (Vileça et al. 2014). Fluctuations in its expression was already reported. The decreased level of catalase was determined in mice model of NPC1, in the meanwhile increased level of catalase expression was reported in GD patients' blood samples (Vidal-Donet et al. 2013). In the cortex tissue of our study, 5-month-old single and double gene deficient mice had higher catalase expression compared to young littermates, these results may be indicator of the presence of reactive oxygen species in older gene deficient mice (Figure 3.19 A). The last oxidative stress marker was TTase1 which is also an antioxidant defense mechanism player. The elevated level depending on oxidative stress was established in the past researches (Wie et al. 2008). In cortex tissue, the elevated expression level was shown in 2-month-old GM3S-/- and Neu1-/-GM3S-/- mice compared to age matched Neu1-/- and WT littermates, while decreased expression level was detected in 5-month-old single and double gene deficient mice compared to young littermates (Figure 3.20 A). In cortex tissue, the reduction level of defense mechanism markers (SOD2 and TTase1) may be sign of the impairments in the defense mechanism depending on aging in single and double deficient mice. However, the reduction of SOD2 and TTase1 expression levels in the cortex of older WT mice compared to young WT littermates showed the inconclusive results for these oxidative stress markers in the cortex tissue. On the other hand, the elevated level of catalase in older single and double gene deficient mice may be due to response of cells to reactive oxygen species. Overall, there were some altered expression of distinct oxidative stress markers in cortex tissue. The more investigations may be done for understanding of oxidative stress in cortex tissue by measurement of ROS levels by flow cytometry. Alterations seen in oxidative stress markers of single and double gene

deficient mice in cortex may be due to changed glycosphingolipid metabolism and accumulated of glycoconjugates in cortex because previously it was determined the elevated level of oxidant products in the case of fluctuations in sphingolipid expression (Nokolova – Karalashian and Reid, 2011).

In cerebellum tissue, the oxidative stress marker, SOD2, showed increased level in older Neu1-/- mice compared to other same aged mice groups, while no significant difference was detected for the catalase gene expression (Figure 3.18 B and 3.19 B). The TTase1 gene expression was higher in 5-month-old Neu1-/- and GM3S-/- mice, implying oxidative problems in 5-month-old gene deficient mice in the cerebellum (Figure 3.20 B). The presence of response to reactive oxygen species in the case of gene deficiencies was shown in cerebellum tissue.

In thalamus tissue, 5-month-old Neu1-/- mice showed elevated level of SOD2 expression compared to age matched control group and GM3S deficient mice (Figure 3.18 C). The higher expression level was also indicated in older GM3S-/- and Neu1-/-GM3S-/- mice compared to younger littermates. There was increase in the expression level of Catalase and TTase1 in both young and older Neu1-/-, GM3S-/- and Neu1-/-GM3S-/- compared to age matched WT littermates. Together, 5-month-old Neu1-/- and Neu1-/-GM3S-/- mice had higher expression level of catalase than 2-month-old counterparts (Figure 3.19 C and 3.20 C). As a result of these findings related with oxidative stress, there was elevated level of oxidative stress markers in cortex, cerebellum and thalamus tissues of 5-month-old single and double deficient mice except expression of SOD2 and TTase1 in cortex tissue. As dedicated in previous studies, the accumulated glycoconjugates and alterations in glycosphingolipid metabolism can be responsible for oxidative stress. Additionally, mitochondrial dysfunction and apoptosis were shown in GM3S deficient patients previously, therefore the altered oxidative stress seen in GM3S-/- mice may be due to mitochondrial dysfunction seen in patients. However, the mitochondrial membrane potential may be measured in GM3S-/- mice to claim the presence of mitochondrial dysfunction in GM3S-/- mice for deeper understanding.

For understanding of apoptosis, expression levels of Bcl-2, Bcl-XL and Bax genes were compared according as age and genotype. Bcl-2 and Bcl-XL which are known as anti-apoptotic genes prevent the expression of apoptotic genes such as Bax and Bak (Yoo and Kim 2015). In the cortex tissue analysis, 2-month-old Neu1-/-GM3S-/- mice had lower Bcl-2, antiapoptotic gene, expression compared to young control group (Figure 3.21 A). 5-month-old Neu1-/- and GM3S-/- mice showed elevated anti-apoptotic Bcl-XL

and Bcl-2 gene expression compared to young counterparts, respectively (Figure 3.22 A and 21 A). Within these results, it is difficult to claim supporting idea for antiapoptotic gene expression young and older mice groups. On the other hand, older Neu1-/-GM3S-/- mice indicated reduced expression level of Bcl-2 and Bcl-XL antiapoptotic genes compared to age-matched GM3S-/- and Neu1-/- mice, respectively. For Bax expression, apoptotic gene expression was higher in older double deficient mice group compared to young counterparts (Figure 3.23 A), indicating elevated apoptosis and reduced antiapoptotic gene expression in cortex of older Neu1-/-GM3S-/- mice.

In the cerebellum tissue, Bcl-2 and Bcl-XL expression did not show any significant difference in distinctly-genotyped mice (Figure 3.21 B and Figure 3.22 B). However, the Bax expression was significantly higher in 5-month-old Neu1-/- mice compared to same aged littermates (Figure 3.23 B). These results showed the effect of Neu1 deficiency on apoptosis in older age groups for cerebellum tissue.

Thalamus tissue analysis for apoptotic markers demonstrated that both Bcl-2 and Bcl-XL had lower expression level in 5-month-old Neu1-/-GM3S-/- mice than both age matched single deficient mice groups and young counterparts (Figure 3.21 C and Figure 3.22 C). Consistently with that, Bax expression was elevated in young and older double deficient mice compared to age matched control groups in thalamus (Figure 3.23 C), indicating presence of apoptosis. According to comparisons obtained by real time PCR analysis, alterations in ER stress, oxidative stress and apoptosis in gene deficient mice compared to control groups for all tissues may be caused by accumulated oversialylated compounds due to Neu1 deficiency and alternative glycosphingolipid accumulation in the case of GM3S deficiency.

The more genes related with apoptosis were analyzed by Western Blot for a more detailed understanding. Apoptosis have two pathways known as intrinsic (mitochondrial) and extrinsic pathway. Radiation, toxins, ER stress, oxidative stress, metabolic stress, hypoxia or DNA damages lead to mitochondrial changes such as formation of pores on membrane of mitochondria. Released cytochrome c from the mitochondria depending on pore formation causes the apoptosome formation. With the apoptosome formation, Caspase 9 and Caspase 3 are activated in order, and events end with the apoptosis in the intrinsic pathway (Elmore, 2007). On the other hand, apoptotic death receptors such as Fas receptor, TRAILR provokes the extrinsic pathway activation by binding of ligands such as Fas Ligand, TNF-alpha. Dimerization of receptors after ligand binding supplies the Caspase 8 and 10 activation which lead to activation of apoptotic markers such as Bax

and Bak, and executioner caspase known as caspase 3 (Elmore 2007). The brain tissues, cortex, cerebellum and thalamus, were studied by Western Blot analysis. Caspase 9, Caspase 3, Fas Ligand and BiP antibodies were analyzed for two age groups and differently-genotyped mice. For expression of Fas- Ligand which is related with extrinsic apoptosis pathway, distinct brain sections did not show any different expression level depending on age and genotype (Figure 3.24, 3.28 and 3.32). However, some variations were observed in the intrinsic pathway markers; Caspase 9 and Caspase 3. The 2-month-old Neu1-/- mice had significantly and slightly higher expression level of Cleaved Caspase 9 and Caspase 3 respectively when young Neu1 deficient mice was compared with age matched GM3S-/- mice (Figure 3.25 and 3.26). These findings implied the significant effect of Neu1 deficiency compared to GM3S deficiency for apoptosis in cortex tissue. Cleaved Caspase 9 and Caspase 3 level were also significantly higher in cortex of 5-month-old Neu1-/- mice compared to other age-matched littermates, indicating programmed cell death in 5-month-old Neu1-/- mice for cortex tissue (Figure 3.25 and 3.26). Together, the reason of significantly and slightly increase of Cleaved Caspase 9 and Caspase 3 in 5-month-old Neu1-/-GM3S-/- mice compared to age-matched GM3S-/- mice may be related with the deficiency of Neu1 gene in Neu1-/-GM3S-/- mice. Expression of BiP, ER stress marker, was also higher in 5-month-old Neu1-/- mice compared to same aged Neu1-/-GM3S-/- mice in cortex tissue. The low level of BiP in the 5-month-old Neu1-/-GM3S-/- mice may associated with GM3S gene deficiency since GM3S-/- mice had lower BiP expression level than Neu1-/- littermates (Figure 3.27).

In the cerebellum tissue, the elevated expression of Cleaved Caspase 9 and Caspase 3 in 2-month-old Neu1-/-GM3S-/- mice compared to same aged WT and GM3S-/- mice was clearly notified the impression of Neu1 gene deficiency in the cerebellum tissue since young Neu1-/- mice had further expression of Cleaved Caspase 9 and Caspase 3 compared to that of WT littermates (Figure 3.29 and 3.30). BiP expression which is related with ER stress showed significant increase in 2-month-old GM3S-/- and Neu1-/-GM3S-/- mice compared to its WT littermates in cerebellum tissue (Figure 3.31). Additionally, there was higher expression of BiP in 2-month-old Neu1-/- mice than age matched WT although it was not significant.

Western blot analysis of thalamus tissue was indicated the significant increase in Cleaved Caspase 9 of 5-month-old Neu1-/-GM3S-/- mice compared with their age matched GM3S-/- mice (Figure 3.33). Due to no change between 5-month-old WT and GM3S-/- mice, elevated level of Cleaved caspase 9 may be affected from the Neu1 gene

deficiency in the double gene deficient mice. However, different expression pattern for Cleaved Caspase 3 was showed in thalamus of young littermates compared to cortex and cerebellum tissues (Figure 3.34). In thalamus tissue of older group, although it was not significant, the elevated level Cleaved Caspase 3 was demonstrated in Neu1-/- mice compared to that of control littermates (Figure 3.34). ER stress marker, BiP, did not show any difference in thalamus tissue according as genotype and age (Figure 3.35). Western blot results suggested more potential effect of Neu1 deficiency on intrinsic apoptotic pathway activation compared to GM3S gene deficiency, especially in the cortex and cerebellum tissues. As a general, Cleaved Caspase 3 and Caspase 9 expression in GM3S-/- mice did not show significant differences compared to WT mice for almost all brain sections. Previously, it has been shown the controversial role of GM3 ganglioside in apoptosis and potential apoptotic role of GD3 and GD1b gangliosides. Actually, the brain analysis of GM3S-/- mice for apoptosis has not been shown before this thesis study. The less expression of apoptotic markers in GM3S-/- mice compared to Neu1-/- and Neu1-/-GM3S-/- mice may be due to absence of GM3, GD3 and GD1b gangliosides, known as apoptotic gangliosides, in brain of GM3S-/- mice. Although ER and oxidative stress was observed in GM3S-/- mice compared to control littermates, the higher level of apoptosis according to protein and RNA analysis was not observed. The reason of this situation may be due to supplying the cellular hemostasis after the activation of anti-oxidant defense mechanisms and UPR, and absence of apoptotic gangliosides in GM3S-/- mice. On the other hand, the reason of higher apoptotic marker expression observed in Neu1-/- mice may be driven from accumulation of (non)-identified oversialylated Neu1 sialidase substrates in lysosomes and releasing of them by exacerbated lysosomal exocytosis shown in previous researches (Annunziata et al. 2013). Together, the elevated ER stress and oxidative stress according to RT-PCR results, and highly glycoconjugate accumulation obtained by PAS staining in our research may cause the apoptotic pathway activation in Neu1-/- mice. Double knock-out mice had also higher apoptotic marker expression compared to control littermates depending on GM3S and mostly Neu1 deficiency.

Central nervous system (CNS) is affected in many lysosomal storage disorders leading to neuronal vulnerability. In a previous study, it has been reported the degeneration of neurons in mice model of sialidosis (Neu1-/-) and galactosialidosis (PPCA-/-) disorders. By H&E staining, neuron loss in Purkinje cells and vacuolization in the epithelial cells throughout brain of sialidosis mice model were already reported (de

Geest et al. 2002). Our H&E results clearly showed the presence of edema, dilation in the veins and plaque-like structures in distinct sections of Neu1-/- and GM3S-/- mice at any ages, but it was concluded the quite intense structural alterations including cell loss, vascular dilation and vacuolized structures in Neu1-/-GM3S-/- mice (Figure 3.36 and 3.37).

Cresyl – Echt violet staining exposed the dramatically neuron degeneration in double knock-out mice and Neu1-/- mice, whereas less neuronal degeneration was seen in GM3S-/- mice (Figure 3.38 and 3.39). This morphological changes may be driven from the accumulated oversialylated substrates of Neu1 sialidase (Annunziata et al. 2013). Additionally, the partial morphological changes and neuronal degeneration in GM3S-/- mice can be related with precursors and alternative glycosphingolipid accumulation owing to GM3S deficiency besides the absence of complex gangliosides.

PAS staining was used to determine the accumulated glycoconjugates such as polysaccharides, glycoproteins, glycolipids. Previous studies showed the accumulation of glycosphingolipids, glycolipids and secondary metabolites such as oligosaccharides in several lysosomal storage disorders. The accumulated glycosphingolipids, glycolipids, oligosaccharides affect the central nervous system which cause the neurodegeneration in lysosomal storage diseases. The accumulation of glycogen in Pompe disease (Kamphoven et al. 2004), glycosphingolipids in cerebral cortex of GM1 gangliosidosis (Wakley 1998) and hippocampus of Sandhoff mice model (Richardson et al. 2016) by the PAS staining was already investigated. Additionally, neurons of sialidosis (Sekijima et al. 2013), GM1-gangliosidosis, GM2-gangliosidosis (Sandhoff disease) patients (Tsay and Dawson 1976) in the CNS had highly accumulated sialyloligosaccharides. In this research, PAS staining was used for the investigation of accumulated glycoconjugates in brain in order to understand the potential effect of glycoconjugate accumulation on structural changes in brain and neuron survival. Our results indicated the presence of glycoconjugate accumulation in Neu1-/- mice and mostly Neu1-/-GM3S-/- mice at any ages, whereas the amount of accumulated glycoconjugates was less in the GM3S-/- mice at any ages (Figure 3.40 and 3.41). The highly accumulated glycoconjugates observed in Neu1-/- and Neu1-/-GM3S-/- mice can be indicator of accumulated complex oligosaccharide and oversialylated substrates of Neu1 sialidase. The partial accumulation of glycoconjugates in GM3S-/- mice can be precursors and alternative glycosphingolipids due to deficiency of GM3S enzyme.

The myelination is important for neuron survival and function, and the delayed or abnormal myelination process, known as demyelination, is the hallmark of the lysosomal storage disorders due to accumulated substances (Rama Rao and Kielian 2016). Mice models of several lysosomal storage diseases such as Krabbe, Multiple Sulfitase, GM2-gangliosidosis showed the demyelination (Saher and Stumpf 2015). The brain of mice model and patients of GM1-gangliosidosis had also higher demyelination (Kaye et al. 1992; Folkerth et al. 2000). Additionally, demyelination in these lysosomal storage disorders caused the neurological impairments (Onyenwoke and Brenman 2015). In this research, demyelination in distinct mice groups was shown with Luxol Fast staining. Although moderate and less demyelination was seen in young and older Neu1-/- and GM3S-/- mice littermates separately, the most demyelination was observed in the double knock- out mice especially in the corpus callosum part of brain (Figure 3.42 and 3.43). Less demyelination in GM3S-/- mice at any ages compared to Neu1-/- and Neu1-/-GM3S-/- mice can be derived from the expression of GM1b and GD1α gangliosides which contributes to myelination and axon-myelin interactions (Schnaar 2010). On the other hand, the significant demyelination seen in Neu1-/- mice can be due to highly accumulated glycoconjugates observed by PAS staining, since it was previously demonstrated that accumulated glycoconjugates is the main reason of neuron loss and demyelination (Futerman and Van Meer 2004). All in all, immunostaining results indicated the presence of structural deformations, neuronal degeneration, glycoconjugate accumulation and demyelination in brain of GM3S-/-, Neu1-/- and mostly in Neu1-/-GM3S-/- mice. It can be supposed that glycoconjugate accumulation seen by PAS staining in Neu1-/- mice and especially Neu1-/-GM3S-/- mice may leads to intense structural changes, neuronal degeneration and demyelination in brain. Together, these results can be related with the impairments seen in behavioral analysis.

Immunohistochemistry analysis was applied for 5-month-old mice in order to understand presence of oligodendrocyte and neuron loss due to altered glycolipid metabolism and accumulated oversialylated compounds. Oligodendrocytes are specialized cells that are responsible for the coating of axon by production of myelin and myelin sheath (Onyenwoke and Brenman 2015). The effect of altered glycolipid metabolism on oligodendrocytes were understood by anti-CNPase staining which is oligodendrocyte marker (Pefeoren et al. 2014). Impairments in myelin sheath results in demyelization was also understood from the alterations in oligodendrocyte number due to role of oligodendrocyte for the myelin production (Fletcher et al. 2014). Cortex and

cerebellum tissues of 5-month-old Neu1-/- and Neu1-/-GM3S-/- mice showed loss in oligodendrocytes compared to control groups, indicating reduction in oligodendrocyte number due to fluctuations in the glycolipid metabolism and secondary metabolites (Figure 3.44), whereas loss in the oligodendrocyte number of GM3S-/- mice was partially less. These results were compatible with the Luxol – Fast staining.

The elevated apoptosis in the cartilage explants due to elevated inflammation have been also demonstrated in 4-month-old GM3S deficient mice by previous studies (Sasazawa et al. 2014). However, there was no evidence for apoptosis in the brain of GM3S-/- mice. Together, apoptosis has not been shown in brain of Neu1-/- mice previously, but the effect of glycoconjugate accumulation on neuron death was implied previously (Futerman and Van Meer 2004). In this thesis concept, neuronal loss was indicated by anti-NeuN staining in 5-month-old differently genotyped mice. Results clearly indicated neuronal loss in 5-month-old GM3S-/-, Neu1-/- and Neu1-/-GM3S-/- mice in the cortex (Figure 3.45 R), hippocampus (Figure 3.45 S) and thalamus tissues (Figure 3.45 T), while no significant difference was detected in the cerebellum tissue (Figure 3.45 U) of 5-month-old mice. NeuN antibody detects the granular layer of cerebellum instead of Purkinje layer, therefore the neuron loss might not be detected in the Purkinje layer of cerebellum in distinctly genotyped mice. However, Cresyl - Echt violet staining clearly showed the degeneration in neuronal structure of cerebellum section of 5-month-old Neu1-/- mice, and especially Neu1-/-GM3S-/- mice (Figure 3.38 and 3.39). Although neuron loss was seen in the GM3S-/- mice compared to same aged WT mice in all sections of brain, the most dramatic neuronal loss was indicated in the all sections of Neu1-/- and Neu1-/-GM3S-/- mice. The less neuron loss in GM3S-/- may be related with the absence of GD3 and GD1b ganglioside which causes the activation of apoptosis in various types of cells in the case of higher abundancy. Neuronal loss in 5-month-old distinctly-genotyped mice was confirmed by TUNEL staining. The apoptotic neurons (TUNEL positive cells) in 5-month-old Neu1-/- and Neu1-/-GM3S-/- mice was elevated in the cortex (Figure 3.46 A), hippocampus (Figure 3.47 A) and thalamus (Figure 3.47 B) tissues compared to that of control littermates, but the slightly elevated level of TUNEL positive cells was only indicated in Neu1-/- mice for cerebellum tissue (Figure 3.46 B) compared to age-matched other mice. Additionally, there was also increasing level of the apoptotic cells in GM3S-/- mice for cortex, thalamus and hippocampus sections, however the increase seen in GM3S-/- mice was not as much as Neu1-/- and Neu1-/-GM3S-/- mice. Overall, the immunohistochemistry analysis revealed presence of

oligodendrocyte and neuron loss due to Neu1 and GM3S genes deficiencies, however the higher deleterious effect of Neu1 deficiency was concluded compared to GM3S deficiency according to statistical analysis. Therefore, double gene deficient mice also demonstrated dramatically oligodendrocyte and neuron loss depending on GM3S deficiency and more importantly Neu1 deficiency.

Behavioral analysis was performed to understand whether changed ganglioside content and accumulated oversialylated compounds lead to any-age related behavioral differences. Motor function and activity depending on age and genotype was elucidated with Rotarod Test. Motor function impairments can be associated with the cerebellum tissue of brain since cerebellum regulates locomotor activities (Lee et al. 2018). The significant difference among the motor activities of young mice was not detected. Previously, no detectable difference was found in motor coordination between 1.5- to 2-month-old GM3S knock-out mice and same aged control mice in the rotarod test (Yoshikawa et al. 2009). Supporting this data, there was no change in the motor activities of 2-months-old GM3S-/- compared to that of control littermates (Figure 3.48). Impairment in motor coordination due to aging in Neu1-/-, GM3S-/- and Neu1-/-GM3S-/- mice has been demonstrated by a reduction in time on rod (Figure 3.48). The motor coordination problem in 5-month-old Neu1-/- and GM3S-/- mice could be caused by deformation of Purkinje cells located in the cerebellum tissue based on Hematoxylin-Eosin staining. Additionally, muscle degeneration causing muscle problems previously determined in Neu1-/- mice at the 4 months of age compared to same aged wild type by Zanoteli et al. 2010. Therefore, motor function problems in the 5-month-old Neu1-/- mice might be due to previously shown muscle degeneration. In older mice groups, the most deterioration in motor function observed in Neu1-/-GM3S-/- mice could result from both aging and absence of two genes (Figure 3.48). Together, the most dramatic morphological deformation and neuronal degeneration in the Purkinje layer of older Neu1-/-GM3S-/- mice can be related with this motor function impairment.

Fore-limb grip strength was used to understand the problems in the nerve-muscle functions and muscle strength in mice. The most effected mice was Neu1-/-GM3S-/- mice, meanwhile no difference among control, and single gene deficient mice groups (Figure 3.49). Together, results clearly notified the presence of age-related impairments in fore limb grip strength of double gene deficient mice, indicating more deleterious impact of double gene knock-out conditions.

The disruption in hippocampus part was understood by behavioral test known as passive avoidance. Passive avoidance supplied that whether there is a problem in the learning and memory process of differently-genotyped mice in age dependent manner. In brain, distinct parts are responsible for the learning and memory. Hippocampus have specifically contribution to meaning and memory process together with cerebellum, amygdala (Lee et al. 2018). According to passive avoidance results, the most affected mice were Neu1-/- and Neu1-/-GM3S-/- mice for both ages, while no impairment in the learning of GM3S deficient mice was detected (Figure 3.50). These results clearly showed that deficiency of Neu1 gene have deleterious contributions for learning processes. The reason of GM3S-/- mice not having any problem in the learning process might be partial neuron loss in hippocampus part of GM3S-/- compared to Neu1-/- and Neu1-/-GM3S-/- littermates according to NeuN and TUNEL immunohistochemistry analysis. The dramatic neuron loss in hippocampus was seen in older Neu1-/- and Neu1-/-GM3S-/- mice based on NeuN and TUNEL staining, therefore the dramatic neuronal death in hippocampus of Neu1-/- and Neu1-/-GM3S-/- mice might cause the obvious learning and memory defects in these mice.

Impairments in neuropsychological behaviors were also determined by Open-Field test depending on age and genotype. In a previous research, anxiety behavior in elevated plus maze was determined in GM3S-/- mice at 6-weeks of age due to changes in ganglioside pattern (Niimi et al. 2011), and it was noticed that changed ganglioside expression pattern associates with impairments of neuropsychological behaviors. The production and processing of anxiety is controlled by the amygdala and hippocampus parts of brain (Mah et al. 2016). Previously it was reported that signals send from the hippocampus to amygdala and hypothalamus regulate the anxiety like behaviors (Hill et al. 2015). Therefore, not only amygdala is important for these anxiety related behaviors, but also hippocampus have a regulatory role for these behaviors. Less spent time in open filed represents anxiety-related behaviors. 2-month-old Neu1-/-, GM3S-/- and Neu1-/-GM3S-/- mice spent less time center than age-matched WT as approximately %57, %30 and %90 respectively, showing anxiety-behaviors in all single and double gene deficient mice (Figure 3.51 A). In older mice group, Neu1-/- mice as %67 and Neu1-/-GM3S-/- mice as %88 spent less time in center than age matched WT (Figure 3.51 A). Results indicated the Neu1 gene deficiency have a more potential effect on the anxiety behaviors seen in both young and older Neu1-/-GM3S-/- mice. In young and older mice, the most anxiety-related behaviors were shown in older Neu1-/-GM3S-/- mice, implying influence

of both aging and lack of two genes (Figure 3.51 A). Additionally, anxiety like behaviors may be related with the oligodendrocyte, neuron loss and neuronal degeneration in the hippocampus of these mice models analyzed by the molecular, histological and IHC analysis.

Until today, the accumulation of secondary metabolites such as oligosaccharides, glycoaminoacids has been reported in several lysosomal storage disorders resulting from the deficiency of lysosomal enzymes, hydrolases, sialidases (Wraith 2009). For instance, accumulation and of oligosaccharides, glycosaminoglycans and glycoproteins in urine extracts was elucidated in sialidosis, mucoplysaccharidosis and mannosidosis diseases, respectively (Xia et al. 2013). Oligosaccharide analysis from the urines of differently-genotyped mice was carried out in order to show the oligosaccharide pattern in urines depending on defects in Neu1 sialidase and GM3S enzyme. It was already clarified accumulation of sialylated oligosaccharides in urines of sialidosis patients (Pelt et al. 1988), and prominent oligosaccharidurıa in the young Neu1 knock-out mice at the 1 and 2 months of age (d'Azzo et al. 2002). Additionally, markers for the sialidosis diagnosis in thin layer chromatography was clearly identified by Mutze et al. 2017. Consistently with that; bands for sialidosis diagnosis was labeled as depicted in Figure 3.52. However, these bands (oligosaccharides) were only seen in 2- and 5-month-old Neu1-/- and Neu1-/-GM3S-/- mice. These bands used in sialidosis diagnosis were lack in the other genotypes at any ages. Although no significant difference between young and older Neu1-/- mice was detected for oligosaccharides, there was higher oligosaccharide accumulation in 5-month-old Neu1-/-GM3S-/- mice compared to its young counterparts as approximately 1.5-fold (Figure 3.53 A and 3.53 B.). These findings demonstrated age dependent manner for accumulation of oligosaccharides in double gene deficient mice. At the same time, higher oligosaccharide accumulation in both young and older Neu1-/-GM3S-/- mice was notified when mice compared to age matched Neu1-/- littermates as approximately 2-fold in young and 5-fold in older mice (Figure 3.53 A and 3.53 B), implying more impact of double gene deficiency in the oligosaccharide accumulation compared to Neu1 gene deficiency. Previously, the accumulation of oligosaccharides in urines of Sandhoff (Hexb-/-) mice was known in addition to glycosphingolipid accumulation (Liu et al. 1999). The complex gangliosides were eliminated by creating double knock-out (Hexb-/-Galgt-/-) mice model for therapy (Liu et al. 1999). However, double knock-out mice had higher level of accumulated oligosaccharides in urines compared to Hexb-/- mice. Together, Hexb-/- mice had better phenotype than double-

knock-out mice. These findings suggest that absence of complex gangliosides in double knock-out mice makes them more sensitive to accumulated oligosaccharides, and it was claimed that the presence of complex gangliosides protects the CNS (Liu et al. 1999). In the light of this previous research, it may be said that higher accumulation of oligosaccharides observed in Neu1-/-GM3S-/- mice compared to Neu1-/- mice can be due to elimination of complex gangliosides (-a and -b series) in double knock-out mice. It was already notified that severity of diseases are associated with the extracted oligosaccharides (Liu et al. 1999). Therefore, worse symptoms in Neu1-/-GM3S-/- mice can be derived from the lack of complex gangliosides which causes elevated sensitivity of oligosaccharide accumulation, and highly extracted oligosaccharides in urines.

CHAPTER 5

CONCLUSION

Sialidosis is a lysosomal storage disorder due to deficiency of lysosomal Neu1 sialidase that involved in the removal of sialic acid residues found in sialoglycoconjugates. The accumulation of oligosaccharides in the urines of patients is the main diagnosis way of disease, and the accumulation of gangliosides in the visceral organs including GM3, GD3, GM4, LM1 were hallmark of the sialidosis patients. The role of Neu1 sialidase in the glycopeptides was also clarified. However, Neu1 impact on the glycolipid metabolism was not clear, *in vivo*. It was hypothesized that there might be role of Neu1 sialidase in the glycolipid metabolism. In this thesis study, newly generated double knockout mouse model (Neu1-/-GM3S-/-) was compared with single knockout mice (Neu1-/- and GM3S-/-) and control group in order to clarify the potential role of lysosomal Neu1 sialidase alone and together with GM3S enzyme in glycolipid metabolism. The most severe phenotype was observed in the newly created double knockout mice, and lived maximum at the age of 5 months.

Thin-layer chromatography results for brain tissue revealed the highly production of -o series acidic and neutral gangliosides caused by enzymatic modification of LacCer due to GM3S deficiency at the both ages of GM3S-/- and Neu1-/-GM3S-/- mice, while no significant difference was notified in the young and older Neu1 deficient mice compared to that of control littermates. Mass spectrophotometry can be required for the deeper understanding of unknown compounds that cannot be identified by TLC analysis. In addition to brain, the other tissues such as kidney, liver, spleen can be analyzed in terms of glycosphingolipid content in Neu1 deficient and double gene deficient mice because Neu1 deficiency causes a systematic disorder which affect the several tissues in addition to brain.

Western blot and RT-PCT analysis of apoptotic markers and, other oxidative stress and ER stress markers which leads to apoptosis showed altered expression level among distinct brain tissues. Although analysis of these markers have been shown in several lysosomal storage disorders, this research is the first study that supplies the understanding of specific gene expressions that cause the apoptosis in brain of Neu1-/-, GM3S-/- and Neu1-/-GM3S-/- mice. ER stress and oxidative stress analysis by RT-PCR

showed that single and double gene deficiency leads to ER stress and oxidative stress in distinct tissues of older mice groups compared to control groups. Presence of cellular stress in 5-month-old GM3S-/- mice besides Neu1-/- mice indicated importance of alterations in ganglioside pattern for cellular processes. Higher expression of apoptotic markers in the cortex and thalamus tissues of older Neu1-/-GM3S-/- mice group was also showed effect of both Neu1 and GM3S deficiencies for apoptotic pathway activation. In addition western blot results suggested more potential effect of Neu1 deficiency on intrinsic apoptotic pathway activation compared to GM3S gene deficiency especially in the cortex and cerebellum tissues.

The effect of abnormal lipid metabolism on neuron cells was investigated by immunostaining, immunohistochemistry analysis and behavioral analysis. H&E staining clearly indicated the presence of vacuolization and edema in cortex, hippocampus, thalamus, and deformation in the Purkinje cells of cerebellum in single and double deficient mice. Neuronal degeneration, glycoconjugate accumulation and demyelination was indicated in GM3S-/- mice and more dramatically Neu1-/- and Neu1-/-GM3S-/- mice. Immunohistochemistry analysis revealed the presence of oligodendrocyte and neuron loss derived from Neu1 and GM3S genes deficiencies in older mice, however the more deleterious impact of Neu1 deficiency can be concluded compared to GM3S deficiency. Additionally, the most dramatic structural changes, neuronal degeneration, oligodendrocyte loss was notified in the older Neu1-/- GM3S-/- mice. On the other hand, several behavioral analysis indicated impairments in neuropsychological behaviors depending on Neu1 and GM3S gene deficiencies, and the most impact of gene deficiencies was observed in double gene deficient mice. Impairments in behavioral analysis can be derived from the structural abnormalities, glycoconjugate accumulation, neuronal loss and demyelination due to oligodendrocytes loss in specific brain sections of single and double gene deficient mice.

Urinary oligosaccharide TLC findings demonstrated age dependent manner for accumulation of oligosaccharides in double gene deficient mice. At the same time, higher oligosaccharide accumulation in both young and older Neu1-/-GM3S-/- mice was notified when mice were compared to age matched Neu1-/- littermates, implying more impact of double gene deficiency in the oligosaccharide accumulation. In the line of with previous studies, it may be said that higher accumulation of oligosaccharides in Neu1-/-GM3S-/- mice compared to Neu1-/- mice can be due to elimination of complex gangliosides (-a and -b series) and highly expression of -o series gangliosides in double knock-out mice.

Additionally, worse symptoms in Neu1-/-GM3S-/- mice can be caused by complex gangliosides deficiency, which causes high sensitivity of oligosaccharide accumulation.

All of these comparisons demonstrated the effect of lysosomal Neu1 sialidase alone and combined with GM3S enzyme on glycolipid metabolism, several cellular processes including ER stress, oxidative stress and apoptosis, neuropsychological behaviors depending on brain structural alterations, neuronal vulnerability.

5.1 Future Directions

As a future investigation, glycolipid metabolism in brain can be further studied by mass spectrophotometry method in addition to thin layer chromatography. In this way, unknown lipids and compounds that could not be detected by thin layer chromatography can be identified by mass spectrophotometry, thereby the effect of Neu1 sialidase on the glycolipid metabolism in brain may be further understood. Additionally, the elderly Neu1-/- mice instead of 5-month-old Neu1-/- mice may be used for investigation of Neu1 sialidase effect on the brain gangliosides.

Sialidosis is a systematic disorder caused by the lysosomal Neu1 sialidase deficiency (d'Azzo et al. 2002), therefore, several tissues are affected in bodies of patients such as spleen, kidney, liver in addition to brain. Because of that, the glycolipid metabolism in the other tissues including spleen, liver, kidney can be analyzed in detail by thin layer chromatography and mass spectrophotometry methods besides brain tissue. In addition to effect of Neu1 sialidase on the glycolipid metabolism of other tissues, combined role of Neu1 sialidase and GM3S enzyme can be also investigated in other tissues. Together, structural changes such as vacuole formation and cellular alterations such as oxidative stress, ER stress and apoptosis may be understood in these tissues in the case of deficiency Neu1 alone and together with GM3S gene. Additionally, thalamus tissue of differently genotyped mice (WT, Neu1-/-, GM3S-/- and Neu1-/-GM3S-/-) can be analyzed as a further investigation because it has been showed the different ganglioside pattern in distinct brain sections including cortex and cerebellum tissues according to our results.

Oligosaccharide accumulation was only analyzed in the urine samples of mice, however, complex oligosaccharide accumulation can be understood in the other tissues of Neu1-/-GM3S-/- mice in order to investigate the effect of ganglioside deficiency on

the oligosaccharide accumulation in brain and other tissues by using anti-oligosaccharide antibody. In this way, the effect of accumulated oligosaccharides on the neurological and behavioral abnormalities in double knock-out mice can be investigated.

In utero or neonatal mice could be used for effect of these enzymes on developmental stage. Fibroblast cell cultures and serum plasma of mice models could be further analysed

Activity of other sialidases in the case of Neu1 sialidase deficiency can be analyzed in single and double knock-out mice in order to understand the presence of any compensatory mechanism.

The detail understanding of Neu1 effect on glycolipid metabolism in the brain and other tissues may help in order to develop new therapeutic agents that targets glycolipid pathways, thereby cure can be supplied for sialidosis patients.

REFERENCES

Aerts, Johannes M.F.G., Chi-Lin Kuo, Lindsey T. Lelieveld, Daphne E.C. Boer, Martijn J.C. van der Lienden, Herman S. Overkleeft, and Marta Artola. (2019). "Glycosphingolipids and Lysosomal Storage Disorders as Illustrated by Gaucher Disease." Current Opinion in Chemical Biology 53: 204–15.

Ando, Susumu, Nan-Chen Chang, and Robert K. Yu. (1978). "High-Performance Thin-Layer Chromatography and Densitometric Determination of Brain Ganglioside Compositions of Several Species." Analytical Biochemistry 89 (2): 437–50.

Annunziata, Ida, Annette Patterson, Danielle Helton, Huimin Hu, Simon Moshiach, Elida Gomero, Ralph Nixon, and Alessandra d'Azzo. (2013). "Lysosomal NEU1 Deficiency Affects Amyloid Precursor Protein Levels and Amyloid-β Secretion via Deregulated Lysosomal Exocytosis." Nature Communications 4 (1).

Aoki, Kazuhiro, Adam D. Heaps, Kevin A. Strauss, and Michael Tiemeyer. (2019). "Mass Spectrometric Quantification of Plasma Glycosphingolipids in Human GM3 Ganglioside Deficiency." Clinical Mass Spectrometry 14 (November): 106–14.

Boccuto, L., Aoki, K., Flanagan-Steet, H., Chen, C. F., Fan, X., Bartel, F., ... & Alexov, E. 2014. A mutation in a ganglioside biosynthetic enzyme, ST3GAL5, results in salt & pepper syndrome, a neurocutaneous disorder with altered glycolipid and glycoprotein glycosylation. Human molecular genetics, 23(2), 418-433.

Bonten, E, A van der Spoel, M Fornerod, G Grosveld, and A d'Azzo. (1996). "Characterization of Human Lysosomal Neuraminidase Defines the Molecular Basis of the Metabolic Storage Disorder Sialidosis." Genes & Development 10 (24): 3156–69.

Borodzicz, Sonia, Katarzyna Czarzasta, Marek Kuch, and Agnieszka Cudnoch-Jedrzejewska. (2015). "Sphingolipids in Cardiovascular Diseases and Metabolic Disorders." Lipids in Health and Disease 14 (1).

Bostwick, David G., Erik E. Alexander, Rohini Singh, Ailin Shan, Junqi Qian, Regina M. Santella, Larry W. Oberley, et al. (2000). "Antioxidant Enzyme Expression and Reactive Oxygen Species Damage in Prostatic Intraepithelial Neoplasia and Cancer." Cancer 89 (1): 123–34.

Boustany, Rose-Mary Naaman. (2013). “Lysosomal Storage Diseases—the Horizon Expands.” Nature Reviews Neurology 9 (10): 583–98.

Brandenburg, K., & Holst, O. (2015). “Glycolipids: Distribution and Biological Function.“ In eLS (pp. 1–10).

Breiden, Bernadette, and Konrad Sandhoff. (2020). “Mechanism of Secondary Ganglioside and Lipid Accumulation in Lysosomal Disease.” International Journal of Molecular Sciences 21 (7): 2566.

Carter, H. E., Haines, W. J., Ledyard, W. E., & Norris, W. P. 1947. Biochemistry of the sphingolipides I. Preparation of sphingolipides from beef brain and spinal cord. Journal of Biological Chemistry, 169(1), 77-82.

Chen, X. P., Enioutina, E. Y., & Daynes, R. A. (1997). “The Control of IL-4 Gene Expression in Activated Murine T Lymphocytes: A Novel Role for Neu-1 Sialidase. “ The Journal of Immunology, 158(7), 3070-3080.

Chen, Guo-Yun, Nicholas K Brown, Wei Wu, Zahra Khedri, Hai Yu, Xi Chen, Diantha van de Vlekkert, Alessandra D’Azzo, Pan Zheng, and Yang Liu. (2014). “Broad and Direct Interaction between TLR and Siglec Families of Pattern Recognition Receptors and Its Regulation by Neu1.” ELife 3 (September).

Coet, Timothy, Kunihiko Suzuki, Brian Popko, Kunihiko Suzuki, Brian Popko, Kunihiko Suzuki, and Brian Popko. (1998). “New Perspectives on the Function of Myelin Galactolipids.” Trends in Neurosciences 21 (3): 126–30.

Conzelmann, E., and K. Sandhoff. (1983). “Partial Enzyme Deficiencies: Residual Activities and the Development of Neurological Disorders.” Developmental Neuroscience 6 (1): 58–71. https://doi.org/10.1159/000112332.

D’Azzo, Alessandra, Eda Machado, and Ida Annunziata. (2015). “Pathogenesis, Emerging Therapeutic Targets and Treatment in Sialidosis.” Expert Opinion on Orphan Drugs 3 (5): 491–504.

D'Azzo, A., A. Hoogeveen, A. J. Reuser, D. Robinson, and H. Galjaard. (1982). "Molecular Defect in Combined Beta-Galactosidase and Neuraminidase Deficiency in Man." Proceedings of the National Academy of Sciences 79 (15): 4535–39.

Geest, N. de. (2002). "Systemic and Neurologic Abnormalities Distinguish the Lysosomal Disorders Sialidosis and Galactosialidosis in Mice." Human Molecular Genetics 11 (12): 1455–64.

Donida, B., Marchetti, D. P., Biancini, G. B., Deon, M., Manini, P. R., da Rosa, H. T., ... & Coitinho, A. S. (2015). Oxidative stress and inflammation in mucopolysaccharidosis type IVA patients treated with enzyme replacement therapy. Biochimica et Biophysica Acta (BBA)-Molecular Basis of Disease, 1852(5), 1012-1019

Dridi, L., V. Seyrantepe, A. Fougerat, X. Pan, E. Bonneil, P. Thibault, A. Moreau, et al. (2013). "Positive Regulation of Insulin Signaling by Neuraminidase 1." Diabetes 62 (7): 2338–46.

Elmore, Susan. (2007). "Apoptosis: A Review of Programmed Cell Death." Toxicologic Pathology 35 (4): 495–516.

Ferreira, Carlos R., and William A. Gahl. (2017). "Lysosomal Storage Diseases." Translational Science of Rare Diseases 2 (1–2): 1–71.

Fingerhut, Ralph, Gijsbertus T. J. Horst, Frans W. Verheuen, and Ernst Conzelmann. (1992). "Degradation of Gangliosides by the Lysosomal Sialidase Requires an Activator Protein." European Journal of Biochemistry 208 (3): 623–29.

Fletcher, Jessica L., Gauthami S. Kondagari, Charles H. Vite, Peter Williamson, and Rosanne M. Taylor. (2014). "Oligodendrocyte Loss During the Disease Course in a Canine Model of the Lysosomal Storage Disease Fucosidosis." Journal of Neuropathology & Experimental Neurology 73 (6): 536–47.

Folkerth, Rebecca D., Joseph Alroy, Ina Bhan, and Edward M. Kaye. (2000). "Infantile G M1 Gangliosidosis: Complete Morphology and Histochemistry of Two Autopsy Cases, with Particular Reference to Delayed Central Nervous System Myelination." Pediatric and Developmental Pathology 3 (1): 73–86.

Fragaki, Konstantina, Samira Ait-El-Mkadem, Annabelle Chaussenot, Catherine Gire, Raymond Mengual, Laurent Bonesso, Marie Bénéteau, et al. (2012). “Refractory Epilepsy and Mitochondrial Dysfunction Due to GM3 Synthase Deficiency.” European Journal of Human Genetics 21 (5): 528–34.

Frisch, Amos, and Elizabeth F. Neufeld. (1979). “A Rapid and Sensitive Assay for Neuraminidase: Application to Cultured Flbroblasts.” Analytical Biochemistry 95 (1): 222–27.

Furukawa K., Ohmi, Y., Ohkawa, Y., Tajima, O., & Furukawa, K.. (2014). “Glycosphingolipids in the Regulation of the Nervous System. “ Advances in Neurobiology 9, 307–20.

Futerman, A. H., & Van Meer, G. (2004). “The Cell Biology of Lysosomal Storage Disorders. “ Nature Reviews Molecular Cell Biology, 5(7), 554-565.

Geboes, Lies, Laure Dumoutier, Hilde Kelchtermans, Evelien Schurgers, Tania Mitera, Jean-Christophe Renauld, and Patrick Matthys. (2009). “Proinflammatory Role of the Th17 Cytokine Interleukin-22 in Collagen-Induced Arthritis in C57BL/6 Mice.” Arthritis & Rheumatism 60 (2): 390–95.

Giussani, Paola, Cristina Tringali, Laura Riboni, Paola Viani, and Bruno Venerando. (2014). “Sphingolipids: Key Regulators of Apoptosis and Pivotal Players in Cancer Drug Resistance.” International Journal of Molecular Sciences 15 (3): 4356–92.

Gordon-Lipkin, Eliza, Julie S. Cohen, Siddharth Srivastava, Bruno P. Soares, Eric Levey, and Ali Fatemi. (2018). “ST3GAL5-Related Disorders: A Deficiency in Ganglioside Metabolism and a Genetic Cause of Intellectual Disability and Choreoathetosis.” Journal of Child Neurology 33 (13): 825–31.

Gusel’nikova, V. V., and D. E. Korzhevskiy. (2015). “NeuN As a Neuronal Nuclear Antigen and Neuron Differentiation Marker.” Acta Naturae 7 (2): 42–47.

Hill, A. S., Sahay, A., & Hen, R. 2015. Increasing adult hippocampal neurogenesis is sufficient to reduce anxiety and depression-like behaviors. Neuropsychopharmacology, 40(10), 2368-2378.

Hinek, Aleksander, Alexey V. Pshezhetsky, Mark von Itzstein, and Barry Starcher. (2005). “Lysosomal Sialidase (Neuraminidase-1) Is Targeted to the Cell Surface in a Multiprotein Complex That Facilitates Elastic Fiber Assembly.” Journal of Biological Chemistry 281 (6): 3698–3710.

Hiraoka, Miki, Ei Ohkawa, Akira Abe, Masaki Murata, Shinji Go, Jin-ichi Inokuchi, and Hiroshi Ohguro. (2019). “Visual Function in Mice Lacking GM3 Synthase.” Current Eye Research 44 (6): 664–70.

Ho, Nurulain, Chengchao Xu, and Guillaume Thibault. (2018). “From the Unfolded Protein Response to Metabolic Diseases – Lipids under the Spotlight.” Journal of Cell Science 131 (3): jcs199307.

Huang, J. Q., J. M. Trasler, S. Igdoura, J. Michaud, N. Hanal, and R. A. Gravel. (1997). “Apoptotic Cell Death in Mouse Models of GM2 Gangliosidosis and Observations on Human Tay-Sachs and Sandhoff Diseases.” Human Molecular Genetics 6 (11): 1879–1885.

Igdoura, S. A., C. Gafuik, C. Mertineit, F. Saberi, A. V. Pshezhetsky, M. Potier, J. M. Trasler, and R. A. Gravel. (1998). “Cloning of the CDNA and Gene Encoding Mouse Lysosomal Sialidase and Correction of Sialidase Deficiency in Human Sialidosis and Mouse SM/J Fibroblasts.” Human Molecular Genetics 7 (1): 115–20.

Iqbal, Jahangir, Meghan T. Walsh, Samar M. Hammad, and M. Mahmood Hussain. (2017). “Sphingolipids and Lipoproteins in Health and Metabolic Disorders.” Trends in Endocrinology & Metabolism 28 (7): 506–18.

Kakugawa, Y., T. Wada, K. Yamaguchi, H. Yamanami, K. Ouchi, I. Sato, and T. Miyagi. (2002). “Up-Regulation of Plasma Membrane-Associated Ganglioside Sialidase (Neu3) in Human Colon Cancer and Its Involvement in Apoptosis Suppression.” Proceedings of the National Academy of Sciences 99 (16): 10718–23.

Kamphoven, Joep H.J, Martijn M de Ruiter, Leon P.F Winkel, Hannerieke M.P Van den Hout, Jan Bijman, Chris I De Zeeuw, Hans L Hoeve, Bert A Van Zanten, Ans T Van der Ploeg, and Arnold J.J Reuser. (2004). “Hearing Loss in Infantile Pompe’s Disease and Determination of Underlying Pathology in the Knockout Mouse.” Neurobiology of Disease 16 (1): 14–20.

Kaye, Edward M., Joseph Alroy, Srinivasa S. Raghavan, Gerald A. Schwarting, Lester S. Adelman, Val Runge, Dafna Gelblum, Johann G. Thalhammer, and Gonzalo Zuniga. (1992). "Dysmyelinogenesis in Animal Model of GM1 Gangliosidosis." Pediatric Neurology 8 (4): 255–61.

Kiguchi, Kaoru, Cynthia B. Henning-Chubb, and Eliezer Huberman. (1990). "Glycosphingolipid Patterns of Peripheral Blood Lymphocytes, Monocytes, and Granulocytes Are Cell Specific1." The Journal of Biochemistry 107 (1): 8–14.

Kleizen, Bertrand, and Ineke Braakman. (2004). "Protein Folding and Quality Control in the Endoplasmic Reticulum." Current Opinion in Cell Biology 16 (5): 597.

Kolter, Thomas. (2012). "Ganglioside Biochemistry." ISRN Biochemistry 2012: 1–36.

Kolter, Thomas, and Konrad Sandhoff. (2009). "Lysosomal Degradation of Membrane Lipids." FEBS Letters 584 (9): 1700–1712.

Lee, Jae-Min, Chang-Ju Kim, Jong-Min Park, Min Song, and Youn-Jung Kim. (2018). "Effect of Treadmill Exercise on Spatial Navigation Impairment Associated with Cerebellar Purkinje Cell Loss Following Chronic Cerebral Hypoperfusion." Molecular Medicine Reports, April.

Liu, Yujing, Ryuichi Wada, Hiromichi Kawai, Kazunori Sango, Chuxia Deng, Tadashi Tai, Michael P. McDonald, et al. (1999). "A Genetic Model of Substrate Deprivation Therapy for a Glycosphingolipid Storage Disorder." Journal of Clinical Investigation 103 (4): 497–505.

Liu, Y., A. Hoffmann, A. Grinberg, H. Westphal, M. P. McDonald, K. M. Miller, J. N. Crawley, K. Sandhoff, K. Suzuki, and R. L. Proia. (1997). "Mouse Model of GM2 Activator Deficiency Manifests Cerebellar Pathology and Motor Impairment." Proceedings of the National Academy of Sciences 94 (15): 8138–43.

Mah, Linda, Claudia Szabuniewicz, and Alexandra J. Fiocco. (2016). "Can Anxiety Damage the Brain?" Current Opinion in Psychiatry 29 (1): 56–63.

Malhotra, Renuka. (2012). "Membrane Glycolipids: Functional Heterogeneity: A Review." Biochemistry & Analytical Biochemistry 1 (2).

Miyagi, Taeko, Junji Sagawa, Kimio Konno, and Shigeru Tsuiki. (1990). “Immunological Discrimination of Intralysosomal, Cytosolic, and Two Membrane Sialidases Present in Rat Tissues1.” The Journal of Biochemistry 107 (5): 794–98.

Miyagi T, Yamaguchi K. 2007. Sialic Acids. In: Kamerling JP, Ed. Comprehensive Glycoscience: From Chemistry to Systems Biology: Elsevier Ltd. pp. 297-323.

Miyagi, Taeko. (1990). “Multiple Forms of Mammalian Sialidase. Altered Expression in Carcinogenesis.” The Tohoku Journal of Experimental Medicine 168 (2): 223–29.

Miyagi, Taeko, and Shigeru Tsuiki. (1985). “Rat-Liver Lysosomal Sialidase. Solubilization, Substrate Specificity and Comparison with the Cytosolic Sialidase.” European Journal of Biochemistry 141 (1): 75–81.

Miyagi, Taeko., and K. Yamaguchi. (2012). “Mammalian Sialidases: Physiological and Pathological Roles in Cellular Functions.” Glycobiology 22 (7): 880–96.

Monti, E., Preti, A., Venerando, B., & Borsani, G. 2002. Recent development in mammalian sialidase molecular biology. Neurochemical research, 27(7-8), 649-663.

Mütze, Ulrike, Friederike Bürger, Jessica Hoffmann, Helmut Tegetmeyer, Jens Heichel, Petra Nickel, Johannes R Lemke, Steffen Syrbe, and Skadi Beblo. (2017). “Multigene Panel next Generation Sequencing in a Patient with Cherry Red Macular Spot: Identification of Two Novel Mutations in NEU1 Gene Causing Sialidosis Type I Associated with Mild to Unspecific Biochemical and Enzymatic Findings.” Molecular Genetics and Metabolism Reports 10 (March): 1–4.

Nakamura, K., Koike, M., Shitara, K., Kuwana, Y., Kiuragi, K., Igarashi, S., ... & Hanai, N. 1994. Chimeric anti-ganglioside GM2 antibody with antitumor activity. Cancer research, 54(6), 1511-1516.

Nakamura, Hideo, Takahiro Maeda, Tomoko Kohno, Naoki Sadamori, and Michito Ichimaru. (1991). “Hypoplastic Acute Leukemia Associated with Inv(16)(P13q22).” Cancer Genetics and Cytogenetics 51 (1): 63–66.

Nampoothiri, Sreekala, and Rajanikant G. K. (2017). “Evaluating Rodent Aerobics For Preclinical Ischemic Stroke Intervention Assessments.” Science Trends, February.

Nan, Xinli, Ivan Carubelli, and Nicholas M. Stamatos. (2006). “Sialidase Expression in Activated Human T Lymphocytes Influences Production of IFN-γ.” Journal of Leukocyte Biology 81 (1): 284–96.

Nath, Shalini, Chhabinath Mandal, Uttara Chatterjee, and Chitra Mandal. (2018). “Association of Cytosolic Sialidase Neu2 with Plasma Membrane Enhances Fas-Mediated Apoptosis by Impairing PI3K-Akt/MTOR-Mediated Pathway in Pancreatic Cancer Cells.” Cell Death & Disease 9 (2).

Neufeld, Elizabeth F. (1991). “Lysosomal Storage Diseases.” Annual Review of Biochemistry 60 (1): 257–80.

Niimi, Kimie, Chieko Nishioka, Tomomi Miyamoto, Eiki Takahashi, Ichiro Miyoshi, Chitoshi Itakura, and Tadashi Yamashita. (2011). “Impairment of Neuropsychological Behaviors in Ganglioside GM3-Knockout Mice.” Biochemical and Biophysical Research Communications 406 (4): 524–28.

Onyenwoke, Rob U., and Jay E. Brenman. (2015). “Lysosomal Storage Diseases-Regulating Neurodegeneration.” Journal of Experimental Neuroscience 9s2 (January): JEN.S25475.

Olsen, Anne S. B., and Nils J. Færgeman. (2017). “Sphingolipids: Membrane Microdomains in Brain Development, Function and Neurological Diseases.” Open Biology 7 (5): 170069.

Palmano, Kate, Angela Rowan, Rozey Guillermo, Jian Guan, and Paul McJarrow. (2015). “The Role of Gangliosides in Neurodevelopment.” Nutrients 7 (5): 3891–3913.

Pan, Xuefang, Camila De Britto Pará De Aragão, Juan P. Velasco-Martin, David A. Priestman, Harry Y. Wu, Kohta Takahashi, Kazunori Yamaguchi, et al. (2017). “Neuraminidases 3 and 4 Regulate Neuronal Function by Catabolizing Brain Gangliosides.” The FASEB Journal 31 (8): 3467–83.

Pasquel-Davila Daniela, S., Yanez-Vaca Sabrina, A., Espinosa-Hidalgo Nicole, D., & Cuadros-Buenaventura Evelin, G. CS 2019.02. 01.28 Bionature Conference Series Vol.2 No.1. cancer, 7, 9.

Peferoen, Laura, Markus Kipp, Paul van der Valk, Johannes M. van Noort, and Sandra Amor. (2014). "Oligodendrocyte-Microglia Cross-Talk in the Central Nervous System." Immunology 141 (3): 302–13.

Platt, Frances M., Barry Boland, and Aarnoud C. van der Spoel. (2012). "Lysosomal Storage Disorders: The Cellular Impact of Lysosomal Dysfunction." The Journal of Cell Biology 199 (5): 723–34.

Plomp, Jaap J., and Hugh J. Willison. (2009). "Pathophysiological Actions of Neuropathy-Related Anti-Ganglioside Antibodies at the Neuromuscular Junction." The Journal of Physiology 587 (16): 3979–99.

Plotegher, Nicoletta, and Michael R. Duchen. (2017). "Mitochondrial Dysfunction and Neurodegeneration in Lysosomal Storage Disorders." Trends in Molecular Medicine 23 (2): 116–34.

Prokazova, N. V., N. N. Samovilova, E. V. Gracheva, and N. K. Golovanova. (2009). "Ganglioside GM3 and Its Biological Functions." Biochemistry (Moscow) 74 (3): 235–49.

Pshezhetsky, Alexey V., Catherine Richard, Lorraine Michaud, Suleiman Igdoura, Shupei Wang, Marc-André Elsliger, Jingyi Qu, et al. (1997). "Cloning, Expression and Chromosomal Mapping of Human Lysosomal Sialidase and Characterization of Mutations in Sialidosis." Nature Genetics 15 (3): 316–20.

Rama Rao, K.V., and T. Kielian. (2016). "Astrocytes and Lysosomal Storage Diseases." Neuroscience 323 (May): 195–206.

Ren, Li-rong, Li-ping Zhang, Shu-ying Huang, Yuan-fang Zhu, Wen-juan Li, Shan-yu Fang, Li Shen, and Yan-ling Gao. (2015). "Effects of Sialidase NEU1 SiRNA on Proliferation, Apoptosis, and Invasion in Human Ovarian Cancer." Molecular and Cellular Biochemistry 411 (1–2): 213–19.

Richardson, Katie, Achilleas Livieratos, Richard Dumbill, Steven Hughes, Gauri Ang, David A. Smith, Lauren Morris, et al. (2016). “Circadian Profiling in Two Mouse Models of Lysosomal Storage Disorders; Niemann Pick Type-C and Sandhoff Disease.” Behavioural Brain Research 297 (January): 213–23.

Risher, W. C., Patel, S., Kim, I. H., Uezu, A., Bhagat, S., Wilton, D. K., ... & Stevens, B. 2014. Astrocytes refine cortical connectivity at dendritic spines. Elife, 3, e04047.

Saher, Gesine, and Sina Kristin Stumpf. (2015). “Cholesterol in Myelin Biogenesis and Hypomyelinating Disorders.” Biochimica et Biophysica Acta (BBA) - Molecular and Cell Biology of Lipids 1851 (8): 1083–94.

Saito, Megumi, and Kiyoshi Sugiyama. (2002). “Characterization of Nuclear Gangliosides in Rat Brain: Concentration, Composition, and Developmental Changes.” Archives of Biochemistry and Biophysics 398 (2): 153–59.

Sandhoff, Roger, Stefan T. Hepbildikler, Richard Jennemann, Rudolf Geyer, Volkmar Gieselmann, Richard L. Proia, Herbert Wiegandt, and Hermann-Josef Gröne. (2002). “Kidney Sulfatides in Mouse Models of Inherited Glycosphingolipid Disorders.” Journal of Biological Chemistry 277 (23): 20386–98.

Sasazawa, F., T. Onodera, T. Yamashita, N. Seito, Y. Tsukuda, N. Fujitani, Y. Shinohara, and N. Iwasaki. (2014). “Depletion of Gangliosides Enhances Cartilage Degradation in Mice.” Osteoarthritis and Cartilage 22 (2): 313–22.

Schengrund, Cara-Lynne. (2015). “Gangliosides: Glycosphingolipids Essential for Normal Neural Development and Function.” Trends in Biochemical Sciences 40 (7): 397–406.

Schnaar, Ronald L. (2009). “Brain Gangliosides in Axon-Myelin Stability and Axon Regeneration.” FEBS Letters 584 (9): 1741–47.

Schneider Gasser, Edith M, Carolin J Straub, Patrizia Panzanelli, Oliver Weinmann, Marco Sassoè-Pognetto, and Jean-Marc Fritschy. (2006). “Immunofluorescence in Brain Sections: Simultaneous Detection of Presynaptic and Postsynaptic Proteins in Identified Neurons.” Nature Protocols 1 (4): 1887–97.

Schneider-Jakob, Helge Renate, and Michael CANTZ. (1991). “Lysosomal and Plasma Membrane Ganglioside GM3 Sialidases of Cultured Human Fibroblasts. Differentiation by Detergents and Inhibitors.” Biological Chemistry Hoppe-Seyler 372 (1): 443–50.

Seibenhener, Michael L., and Michael C. Wooten. (2015). “Use of the Open Field Maze to Measure Locomotor and Anxiety-like Behavior in Mice.” Journal of Visualized Experiments, no. 96 (February).

Sekijima, Yoshiki, Katsuya Nakamura, Dai Kishida, Aya Narita, Kaori Adachi, Kosaku Ohno, Eiji Nanba, and Shu-ichi Ikeda. (2013). “Clinical and Serial MRI Findings of a Sialidosis Type I Patient with a Novel Missense Mutation in the NEU1 Gene.” Internal Medicine 52 (1): 119–24

Seyrantepe, Volkan, Alexandre Iannello, Feng Liang, Evgeny Kanshin, Preethi Jayanth, Suzanne Samarani, Myron R. Szewczuk, Ali Ahmad, and Alexey V. Pshezhetsky. (2010). “Regulation of Phagocytosis in Macrophages by Neuraminidase 1.” Journal of Biological Chemistry 285 (1): 206–15.

Seyrantepe, Volkan, Helena Poupetova, Roseline Froissart, Marie-Thrse Zabot, Irane Maire, and Alexey V. Pshezhetsky. (2003). “Molecular Pathology of NEU1 Gene in Sialidosis.” Human Mutation 22 (5): 343–52.

Seyrantepe, Volkan, Maryssa Canuel, Stéphane Carpentier, Karine Landry, Stéphanie Durand, Feng Liang, Jibin Zeng, et al. (2008). “Mice Deficient in Neu4 Sialidase Exhibit Abnormal Ganglioside Catabolism and Lysosomal Storage.” Human Molecular Genetics 17 (11): 1556–68.

Seyrantepe, Volkan, Secil Akyildiz Demir, Zehra Kevser Timur, Johanna Von Gerichten, Christian Marsching, Esra Erdemli, Emin Oztas, et al. (2018). “Murine Sialidase Neu3 Facilitates GM2 Degradation and Bypass in Mouse Model of Tay-Sachs Disease.” Experimental Neurology 299 (Pt A): 26–41.

Seyrantepe, Volkan, Karine Landry, Stéphanie Trudel, Jacob A. Hassan, Carlos R. Morales, and Alexey V. Pshezhetsky. (2004). “Neu4, a Novel Human Lysosomal Lumen Sialidase, Confers Normal Phenotype to Sialidosis and Galactosialidosis Cells.” Journal of Biological Chemistry 279 (35): 37021–29.

Simpson, Michael A, Harold Cross, Christos Proukakis, David A Priestman, David C A Neville, Gabriele Reinkensmeier, Heng Wang, et al. (2004). "Infantile-Onset Symptomatic Epilepsy Syndrome Caused by a Homozygous Loss-of-Function Mutation of GM3 Synthase." Nature Genetics 36 (11): 1225–29.

Stewart, B. W. (1994). "Mechanisms of Apoptosis: Integration of Genetic, Biochemical, and Cellular Indicators." JNCI Journal of the National Cancer Institute 86 (17): 1286–96.

Tardy, Claudine, Nathalie Andrieu-Abadie, Robert Salvayre, and Thierry Levade. (2004). "Lysosomal Storage Diseases: Is Impaired Apoptosis a Pathogenic Mechanism?" Neurochemical Research 29 (5): 871–80.

Tourtellotte, W. W. (1965). "Tay-Sachs' Disease." Archives of Neurology 13 (4): 452–53.

Tessitore, Alessandra, Maria del P. Martin, Renata Sano, Yanjun Ma, Linda Mann, Angela Ingrassia, Eric D. Laywell, Dennis A. Steindler, Linda M. Hendershot, and Alessandra d'Azzo. (2004). "GM1-Ganglioside-Mediated Activation of the Unfolded Protein Response Causes Neuronal Death in a Neurodegenerative Gangliosidosis." Molecular Cell 15 (5): 753–66.

Thulasiraman, Padmamalini, Kelbie Kerr, Kathleen McAlister, Samantha Hardisty, Albany Wistner, and Ian McCullough. (2019). "Neuraminidase 1 Regulates Proliferation, Apoptosis and the Expression of Cadherins in Mammary Carcinoma Cells." Molecular and Cellular Biochemistry 462 (1–2): 207–15.

Tsay, Grace Chen, and Glyn Dawson. (1976). "Oligosaccharide storage in brains from patients wıth fucosidosis, GM1-gangliosidosis and GM2-gangliosidosis (sandhoff's dısease)." Journal of Neurochemistry 27 (3): 733–40.

Uemura, T, K Shiozaki, K Yamaguchi, S Miyazaki, S Satomi, K Kato, H Sakuraba, and T Miyagi. (2009). "Contribution of Sialidase NEU1 to Suppression of Metastasis of Human Colon Cancer Cells through Desialylation of Integrin B4." Oncogene 28 (9): 1218–29.

Van der Horst, G. T., Galjart, N. J., d'Azzo, A., Galjaard, H., & Verheijen, F. W. 1989. Identification and in vitro reconstitution of lysosomal neuraminidase from human placenta. Journal of Biological Chemistry, 264(2), 1317-1322.

Pelt, Johannes, Danielle G. J. L. BILSEN, Johannis P. KamerlİNg, and Johannes F. G. Vlıegenthart. (1988). "Structural Analysis of O-Glycosidic Type of Sialyloligosaccharide-Alditols Derived from Urinary Glycopeptides of a Sialidosis Patient." European Journal of Biochemistry 174 (1): 183–87.

Vidal-Donet, José Manuel, Jaime Cárcel-Trullols, Bonaventura Casanova, Carmen Aguado, and Erwin Knecht. (2013). "Alterations in ROS Activity and Lysosomal PH Account for Distinct Patterns of Macroautophagy in LINCL and JNCL Fibroblasts." Edited by Anthony Robert White. PLoS ONE 8 (2): e55526.

Vilaça, Rita, Elísio Silva, André Nadais, Vítor Teixeira, Nabil Matmati, Joana Gaifem, Yusuf A. Hannun, Maria Clara Sá Miranda, and Vítor Costa. (2014). "Sphingolipid Signalling Mediates Mitochondrial Dysfunctions and Reduced Chronological Lifespan in the Yeast Model of Niemann-Pick Type C1." Molecular Microbiology 91 (3): 438–51.

Walter, P., and D. Ron. (2011). "The Unfolded Protein Response: From Stress Pathway to Homeostatic Regulation." Science 334 (6059): 1081–86.

Wei, Hui, Sung-Jo Kim, Zhongjian Zhang, Pei-Chih Tsai, Krystyna E. Wisniewski, and Anil B. Mukherjee. (2007). "ER and Oxidative Stresses Are Common Mediators of Apoptosis in Both Neurodegenerative and Non-Neurodegenerative Lysosomal Storage Disorders and Are Alleviated by Chemical Chaperones." Human Molecular Genetics 17 (4): 469–77.

Woods, Amina S., Benoit Colsch, Shelley N. Jackson, Jeremy Post, Kathrine Baldwin, Aurelie Roux, Barry Hoffer, et al. (2013). "Gangliosides and Ceramides Change in a Mouse Model of Blast Induced Traumatic Brain Injury." ACS Chemical Neuroscience 4 (4): 594–600.

Woś, Marcin, Joanna Szczepanowska, Sławomir Pikuła, Anna Tylki-Szymańska, Krzysztof Zabłocki, and Joanna Bandorowicz-Pikuła. (2016). "Mitochondrial Dysfunction in Fibroblasts Derived from Patients with Niemann-Pick Type C Disease." Archives of Biochemistry and Biophysics 593 (March): 50–59.

Wraith, Ed. (2009). “New Therapies in the Management of Niemann-Pick Type C Disease: Clinical Utility of Miglustat.” Therapeutics and Clinical Risk Management, November, 877.

Wu, Xudong, Katherine A. Steigelman, Erik Bonten, Huimin Hu, Wenxuan He, Tianying Ren, Jian Zuo, and Alessandra d’Azzo. (2010). “Vacuolization and Alterations of Lysosomal Membrane Proteins in Cochlear Marginal Cells Contribute to Hearing Loss in Neuraminidase 1-Deficient Mice.” Biochimica et Biophysica Acta (BBA) - Molecular Basis of Disease 1802 (2): 259–68.

Xia, Baoyun, Ghazia Asif, Leonard Arthur, Muhammad A Pervaiz, Xueli Li, Renpeng Liu, Richard D Cummings, and Miao He. (2013). “Oligosaccharide Analysis in Urine by MALDI-TOF Mass Spectrometry for the Diagnosis of Lysosomal Storage Diseases.” Clinical Chemistry 59 (9): 1357–68.

Yamaguchi, Kazunori, Keiko Hata, Koichi Koseki, Kazuhiro Shiozaki, Hirotoshi Akita, Tadashi Wada, Setsuko Moriya, and Taeko Miyagi. (2005). “Evidence for Mitochondrial Localization of a Novel Human Sialidase (NEU4).” Biochemical Journal 390 (1): 85–93.

Yamanaka, S., M. D. Johnson, A. Grinberg, H. Westphal, J. N. Crawley, M. Taniike, K. Suzuki, and R. L. Proia. (1994). “Targeted Disruption of the Hexa Gene Results in Mice with Biochemical and Pathologic Features of Tay-Sachs Disease.” Proceedings of the National Academy of Sciences 91 (21): 9975–79.

Yamashita, T., A. Hashiramoto, M. Haluzik, H. Mizukami, S. Beck, A. Norton, M. Kono, et al. (2003). “Enhanced Insulin Sensitivity in Mice Lacking Ganglioside GM3.” Proceedings of the National Academy of Sciences 100 (6): 3445–49.

Yao, Denggao, Rhona McGonigal, Jennifer A. Barrie, Joanna Cappell, Madeleine E. Cunningham, Gavin R. Meehan, Simon N. Fewou, et al. (2014). “Neuronal Expression of GalNAc Transferase Is Sufficient to Prevent the Age-Related Neurodegenerative Phenotype of Complex Ganglioside-Deficient Mice.” The Journal of Neuroscience 34 (3): 880–91.

Yogalingam, Gouri, Erik J. Bonten, Diantha van de Vlekkert, Huimin Hu, Simon Moshiach, Samuel A. Connell, and Alessandra d'Azzo. (2008). "Neuraminidase 1 Is a Negative Regulator of Lysosomal Exocytosis." Developmental Cell 15 (1): 74–86. Yoo, Soojin, and June-Bum Kim. (2015). "Anti-Apoptotic and Beneficial Metabolic Activities of Resveratrol in Type II Gaucher Disease." Biological & Pharmaceutical Bulletin 38 (6): 913–18.

Yoshikawa, M., S. Go, S.-i. Suzuki, A. Suzuki, Y. Katori, T. Morlet, S. M. Gottlieb, et al. (2015). "Ganglioside GM3 Is Essential for the Structural Integrity and Function of Cochlear Hair Cells." Human Molecular Genetics 24 (10): 2796–2807.

Yoshikawa, M., S. Go, K. Takasaki, Y. Kakazu, M. Ohashi, M. Nagafuku, K. Kabayama, et al. (2009). "Mice Lacking Ganglioside GM3 Synthase Exhibit Complete Hearing Loss Due to Selective Degeneration of the Organ of Corti." Proceedings of the National Academy of Sciences 106 (23): 9483–88.

Yu, Robert K, Yi-Tzang Tsai, Toshio Ariga, and Makoto Yanagisawa. (2011). "Structures, Biosynthesis, and Functions of Gangliosides--an Overview." Journal of Oleo Science 60 (10): 537–44.

Zammarchi, Enrico, Maria Alice Donati, Amelia Morrone, Gian Paolo Donzelli, Xiao Yan Zhou, and Alessandra D'Azzo. (1996). "Early-Infantile Galactosialidosis: Clinical, Biochemical, and Molecular Observations in a New Patient." American Journal of Medical Genetics 64 (3): 453–58.

Zanoteli, Edmar, Diantha van de Vlekkert, Erik J. Bonten, Huimin Hu, Linda Mann, Elida M. Gomero, A. John Harris, Giulio Ghersi, and Alessandra d'Azzo. (2010). "Muscle Degeneration in Neuraminidase 1-Deficient Mice Results from Infiltration of the Muscle Fibers by Expanded Connective Tissue." Biochimica et Biophysica Acta (BBA) - Molecular Basis of Disease 1802 (7–8): 659–72.

Zhang, Zhongjian, Yi-Ching Lee, Sung-Jo Kim, Moonsuk S. Choi, Pei-Chih Tsai, Yan Xu, Yi-Jin Xiao, Peng Zhang, Alison Heffer, and Anil B. Mukherjee. (2005). "Palmitoyl-Protein Thioesterase-1 Deficiency Mediates the Activation of the Unfolded Protein Response and Neuronal Apoptosis in INCL." Human Molecular Genetics 15 (2): 337–46.